Research on novel lattice fermions toward efficient QCD simulations

Tatsuhiro Misumi

Abstract

Numerical lattice simulations have been contributing to understanding of hadron physics, physics of quark-gluon-plasma and flavor physics. However, the fermion doubling problem still prevents us from performing lattice simulations efficiently. In this thesis we investigate new types of lattice fermions which can reduce numerical expense in lattice simulations. We pay attention to two classes of new fermion formulations; 1. Generalized Wilson and overlap fermions (based on naive fermions) and 2. Staggered-Wilson and staggered-overlap fermions (based on staggered fermions). In particular in the latter case, the matrix size of fermion propagators in staggered fermions is much smaller than the other lattice fermions and the numerical cost could be reduced greatly. We show that these new fermions are constructed by introducing generalized Wilson terms called "flavored-mass terms" into naive and staggered fermions. To give a theoretical foundation to them, we numerically show that the index theorem holds and correctly detects the topology of gauge configurations in the lattice gauge theory with these fermions. Our discovery of a variety of overlap fermions is quite significant from the theoretical viewpoint since the overlap formulation which satisfies the Ginsparg-Wilson relation is the only known theoretical solution to the doubling problem. We next show the applicability of these fermions to numerical QCD simulations by studying discrete symmetries and phase structure. We show that they have basic discrete symmetries, which, we expect, are to be promoted to essential symmetries of QCD such as the euclidean rotational symmetry (Lorentz symmetry), C, P and T symmetries. By investigating the Gross-Neveu model and the strong-coupling lattice QCD with the generalized Wilson and staggered-Wilson fermions, we find the parity-broken phase (Aoki phase) and the second-order phase transition. Since the chiral limit and the PCAC relation are acquired by tuning a mass parameter to second-order critical lines in lattice QCD with Wilson-type fermions, our result indicates that we can simulate QCD by using these new types of Wilson fermions. This also indicates the applicability of the generalized overlap and staggered-overlap fermions which are constructed from the generalized Wilson and staggered-Wilson fermions through the overlap formula. We expect that efficient lattice simulations with these new lattice fermions contribute largely to research on hadron physics and other related topics.

Contents

Chapter 1

Introduction

The lattice discretization of the field theory [1] is one of the most powerful tools to elaborate non-perturbative aspects of quantum gauge theories such as Quantum Chromo Dynamics (QCD). In the lattice field theory fields are defined on the discrete euclidean spacetime with a lattice spacing a, and the degrees of freedom (d.o.f.) become countably infinite while those in the continuum field theory are uncountably infinite. When we consider the finite volume of the lattice spacetime, the d.o.f. are finite and the path integral becomes calculable. In such a mathematically well-defined theory, we can calculate quantities in a non-perturbatively way and we are free from the divergence appearing in the continuum theory. One of outstanding advantages in the lattice field theory is that the gauge field is quantized in a gauge-invariant way: The gauge field on the lattice, which is called a link variable, is defined on the link of lattice sites as an element of the gauge group. The gauge-symmetric action is defined as a closed loop called a plaquette action. By performing the finite-dimensional path integral and taking an infinite volume limit and the continuum limit $a \to 0$, we can quantize the field theory through a mathematically safe procedure.

In principle we can calculate any physical quantities by performing the path integral numerically. They are calculated by a stochastic integral technique such as the Monte Carlo method [2]. Here the gauge field configuration is stochastically generated according to the weight in the partition function (e^{-S} for the pure gauge theory). We obtain a result by calculating the quantity of interest for as many configurations as possible and averaging it. After this computation, we need to take an infinite volume limit and a continuum limit. The infinite volume limit is equivalent to the thermodynamics limit in the statistical mechanics. To take the continuum limit, we can utilize the relation between the lattice spacing and the gauge coupling: The bare gauge coupling has one-to-one correspondence with the lattice spacing, for example the zero lattice spacing corresponds to the zero bare gauge coupling for asymptotic-free theories such as QCD, which corresponds to a ultraviolet (Gaussian) fixed point in the renormalization group. Thus we can obtain physical quantities for the continuum theory by calculating them for several bare gauge coupling and extrapolating results to the zero bare-coupling limit.

The lattice gauge simulation may at first seem to be a perfect and easy method to study non-perturbative aspects of the gauge theories. But it is true if and only if we consider the pure gauge theory: It is not straightforward to construct lattice field theories

with fermion fields. There is a notorious difficulty, called "Fermion doubling problem" [3]. The chirally-symmetric fermion action on the lattice inevitably acquires degenerate degrees of freedom in a multiple number of two if we impose basic presuppositions as locality, translation symmetry and hermiticity. For example, for the Lorentz-symmetric fermion action with chiral symmetry on the d-dimensional hypercubic lattice, 2^d poles of the fermion propagator appear within the Brillouin zone, which is a restricted momentum space $|p| < \pi/a$ due to the lattice discretization. Since all the fermionic modes in this restricted momentum space contribute to the continuum theory, the one lattice fermion field describes 2^d fermions in the continuum. We call these multiple fermions "species" while the unnecessary $2^d - 1$ species are called "doublers". Since we can obtain a doubler-less lattice fermion if we throw away the chiral symmetry, we can schematically state that the doubling problem is a confilict between chiral symmetry and elimination of doublers. This multiplicity of fermions on the lattice originates not only from the lattice discretization but also from the fact that the boundary condition for the finite volume lattice should be taken to be a periodic one, which leads to the d-dimensional toric spacetime. The no-go theorem by Nielsen and Ninomiya [4] uncovers the background of this multiplicity by relating the Dirac operator of lattice fermions to the Poincare-Hopf theorem [5], which shows the relation between the Euler number $\chi(M)$ of the compact and orientable differentiable manifold M and the index of the vector function defined on M. In the case of lattice fermions, the Dirac operator in the momentum space can be regarded as a vector function defined on the torus up to the γ-matrix where the Euler number is zero ($n = 0$). The index here stands for the net number of zeros of the vector function, counted with signs $\pm$ depending on the slope of the zero crossing. For the Dirac operator this index is identified as the chiral charge for each species, which means the sign in front of γ_5 differently assigned to each zero. A conclusion from the Poincare-Hopf theorem is that the index should be zero for the zero Euler number $n = 0$ This means that the number of zeros of the Dirac operator with a positive chiral charge should be equal to the number of zeros with a negative chiral charge. Lattice fermions should therefore appear in a multiple number of two, half of which have a positive chiral charge or chirality and the others have a negative charge. If we impose the Lorentz symmetry on the theory in addition to the presuppositions of this no-go theorem, there emerge 2^d fermions.

The doubling problem yields two serious difficulties: Firstly we cannot describe the chiral lattice gauge theory in which a left or right chiral fermion couples to gauge fields. Therefore it seems impossible to construct a lattice field theory describing the weak sector in the standard model. Secondly we have no control on the number of fermions on the lattice: Because of the doubling problem, we cannot choose the number of quarks freely in the lattice field theory. Thus, even if a theory of interest is vector-like with an even number of quarks, it is sometimes difficult to construct it on the lattice. Indeed, although the strong sector in the standard model or QCD contains a even number of fermions or six quarks, 16 species in the naive lattice fermion action is incompatible with it. In fact, six quarks have different masses and the contribution to the physics from them depends on the energy scale. For example, to study non-perturbative phenomena in QCD such as confinement and spontaneous chiral symmetry breaking, we need three quarks (up, down and strange) at low energy below the typical QCD scale < 1GeV. More precisely, we need two light quarks for up and down and one heavier quark for strange on the lattice. As

long as we work on naive lattice fermions, it seems impossible to describe QCD on the lattice. After all, in order to realize QCD on the lattice, we need to obtain a doubler-less lattice fermion by breaking the chiral symmetry at first. However, in such a case, since the chiral symmetry is broken even in the massless limit, the mass of fermions suffers from $O(1/a)$ additive renormalization and the PCAC (Partially Conserved Axialvector Current) relation is spoiled for general values of parameters. Thus lattice fermions with chiral symmetry breaking cannot reproduce spontaneous chiral symmetry breaking, small pion mass and other essential phenomena. As seen from this, it is not easy to simulate gauge theories with a phenomenologically desirable number of fermions. In this thesis I concentrate on this second difficulty inherent to lattice QCD simulations.

By now, several lattice fermion formulations bypassing the doubling problem have been proposed in order to perform QCD simulations. The key point is how to deal with the chiral symmetry in lattice fermion actions. There are roughly two approaches for this purpose, which we call "A" and "B" in Fig. 1.1.

The route A is to break the chiral symmetry first in order to obtain a doubler-less lattice fermion, and offset the symmetry breaking later in some way: The simplest formulation in this direction is the Wilson fermion [6, 7]. In this formulation we add a chiral symmetry breaking term called the Wilson term to the naive fermion action, which assigns $O(1/a)$ mass to doublers. In the classical continuum limit we acquire a single fermion mode because doublers are decoupled with infinite mass. However the explicit chiral symmetry breaking yields an additive mass renormalization as we mentioned above. For QCD simulations with this fermion we need to take a massless or physical quark-mass limit called "chiral limit" by fine tuning a counter term to compensate for the renormalized large mass, . In fact it is known that the PCAC relation is recovered by tuning a mass parameter. By starting from this Wilson formulation, we can construct another beautiful solution in which the exact chiral symmetry exists. The overlap fermion [8, 9] is essentially composed of a sign function of the hermitian Dirac kernel of the Wilson fermion, which again breaks chiral symmetry and decouples doublers in the $a \to 0$ limit. However, it instead possesses the $O(a)$-modified chiral symmetry, called Ginsparg-Wilson symmetry [8], which results in the usual chiral symmetry in the continuum limit. The point is that this symmetry forbids the additive mass renormalization and we no longer need fine-tuning. This solution indicates that the definition of chiral symmetry should be modified on the lattice in a way compatible with lattice discretization. Although the overlap formulation is a brilliant solution to the doubling problem from the theoretical viewpoint, the sign function in the overlap formulation requires terribly expensive numerical cost. Thus it has not yet been applied to numerical simulations extensively.

We have another formulation based on Wilson fermions. The domain-wall fermion [10, 11, 12] is essentially equivalent to the overlap fermion, which starts from the 5-dimensional Wilson fermion with a mass domain-wall in the 5th direction. A single chiral fermion emerges at this domain-wall, which ends up as a single Dirac fermion by combining with a chiral fermion with the opposite chirality emerging at the boundary. In the infinite volume limit of the 5th direction, the chiral symmetry of this Dirac fermion becomes exact since there is no overlap between the wave functions of left and right chiral fermions in this limit. (It is not inconsistent with the no-go theorem since locality is not exact in this case.) However it is certainly impossible to prepare an infinite 5th volume

in practical lattice simulation, and we cannot have exact chiral symmetry in the domain-wall formulation practically. We are again required to tune a mass parameter to restore the chiral symmetry although the additive mass renormalization is drastically reduced in this case compared to the Wilson fermion. In addition the non-exact locality requires a numerically expensive algorithm for simulations. We note, if we perform the Pauli-Villars regularization in the domain-wall fermion to decouple the 5-dimensional doublers and restore exact locality, the chiral symmetry is translated into the exact Ginsparg-Wilson symmetry of the overlap fermion. Thus the two formulations get equivalent in this limit and this regularization scheme. We note these approaches, Wilson, overlap and domain-wall fermions, attempt to realize single fermionic degrees of freedom by breaking the presuppositions of the no-go theorem.

On the other hand, there is another route to approach numerical simulations, which we call a route B. As we have mentioned already [3], the hypercubic symmetry results in 2^d species of fermions in d dimensions. Thus it is potentially possible to reduce the number of species by breaking hypercubic symmetry properly. The staggered fermion is obtained by decomposing the naivee fermion into four equivalent one-spinor fermions by the method called "spin diagonalization". By reconstructing the Dirac fermion out of one-spinors on different sites in the hypercubic block, we obtain four species of Dirac fermions, which is 1/4 of the original number of species. This staggered fermion approach [13, 14, 15] possesses a flavored-hypercubic symmetry instead of the original hypercubic symmetry. The notable advantage of this formalism is reduction of the numerical cost due to the exact chiral symmetry and the small matrix size of the Dirac operator. However, in order to reduce 4 species to 2 or 1 for physical 2 or $(2+1)$-flavor QCD simulations, it requires a quite dangerous technique called a "rooting procedure", which is known to mutilate certain processes. An interesting goal of this direction is a fermion action with only 2 species, the minimal number required by the no-go theorem. Such minimally doubled fermions were proposed in ref. [16, 17, 18, 19, 20]. They all possess one exact chiral symmetry and exact locality. However it has been shown in [21, 22, 23] that we need to fine-tune several parameters to reach a continuum limit with these actions. This is because they lack sufficient discrete symmetries such as a hypercubic symmetry to prohibit redundant operators from being generated through loop corrections [24, 25, 26, 27, 28]. Thus the minimally doubled fermions have not been extensively used so far.

As we have seen so far, all the known solutions to the doubling problem have their individual shortcomings. In this thesis, we investigate new fermion formulations which can reduce numerical costs for lattice QCD greatly. We pay special attention to the theoretical foundation and applicability to numerical simulations. We will mainly study two types of new lattice fermions; generalized Wilson fermions and staggered-Wilson fermions:

One purpose of this thesis is to generalize usual Wilson and overlap fermions to lattice fermions with any number of flavor based on Ref. [29]. We will show that the Wilson term in the Wilson fermion is just one example of more general chiral-symmetry-breaking terms called "flavored-mass terms", which work to lift the degeneracy of 16 species of a naive fermion. In the case of the usual Wilson fermion, the Wilson term splits 16 degenerate eigenvalues of the Dirac operator into 5 branches with 1, 4, 6, 4 and 1 fermion modes, as shown in Fig. 2.3. Since we can utilize only the left or right branches in practical simulations, we usually obtain a single fermion from the Wilson fermion. However we

will show that we can realize various ways of species splitting by using the generalized Wilson terms, or the flavored-mass terms in Chap. 3. By adding a desirable type of flavored-mass terms to naive fermions, we can construct "generalized Wilson fermions" with any number of flavors, from which the generalized overlap and domain-wall fermions are also constructed as shown Chap. 4. It is possible to simulate the physical two-flavor QCD by using only one generalized Wilson fermion. We will numerically show that these generalized Wilson fermions correctly detect the gauge topology through the index of the Dirac zero modes in Chap. 5. This result not only gives a theoretical foundation to these lattice formulations but also indicates that the index theorem holds for them.

Th other purpose of this thesis is to show the practical applicability of the staggered versions of Wilson and overlap fermions to lattice simulations based on [33]. Since a naive lattice fermion has equivalence to four staggered fermions, it is natural to consider a generalization of the flavored-mass terms to staggered fermions. If it is possible, we can construct staggered-Wilson or staggered-overlap fermions. It has recently been shown that the flavored-mass terms for staggered fermions can be constructed in Ref. [30, 31, 32]. These results show that we can formulate new types of Wilson fermions, which we call "staggered-Wilson" and "staggered-overlap" fermions. One potential advantage of these fermions is reduction in the matrix sizes of Dirac propagators, which contributes to reduction of numerical cost in lattice simulations. We will first give a theoretical foundation to these new fermions by pointing out that the flavored-mass terms for staggered fermions are related through the spin diagonalization to those for the naive fermions in Chapters. 3 and 5. In Chap. 4 we will investigate symmetries of the staggered-Wilson fermions. We will show that they have basic discrete symmetries, which, we expect, are to be promoted to essential symmetries of QCD such as the euclidean rotational symmetry (Lorentz symmetry), C, P and T symmetries. We will next show the applicability of the new staggered-Wilson fermions to lattice QCD simulations in Chap. 6 and 7. Here we make use of a characteristic property about the parity broken phase in Wilson-type fermions. In lattice QCD with usual Wilson fermions there appears the parity broken phase with the second-order phase transition [35, 36, 37, 38, 39, 40, 41, 42, 43, 44, 45]. "Taking a chiral limit" in Wilson-type fermions is equivalent to "tuning a mass parameter to the second-order critical line" in this phase diagram since the pion becomes massless or the PCAC relation is recovered due to the critical behavior of the correlation length near the second-order critical line [46, 47, 48]. To show that the parity phase structure with the second-order phase transition exists for the staggered-Wilson fermions, we study the Gross-Neveu model and the strong-coupling lattice QCD. It strongly suggests that we can apply the staggered-Wilson fermions to lattice QCD by tuning a mass parameter to take a chiral limit. We will indeed show that the chiral and continuum limit can be taken within the model study of the Gross-Neveu model. Since the parity phase structure also indicates applicability of overlap fermions, we can expect both staggered-Wilson and staggered-overlap fermions are applied to lattice QCD and reduce the numerical expense greatly. We note the numerical advantage in the staggered overlap fermion have been partly shown in the recent work [49].

We depict a variety of lattice fermions in Fig. 1.1. (only Lorentz-symmetric fermions) It is clear that we have a hopeful frontier of the lattice fermions as the generalized-Wilson fermion and staggered-based Wilson and overlap fermions. The flavored-mass

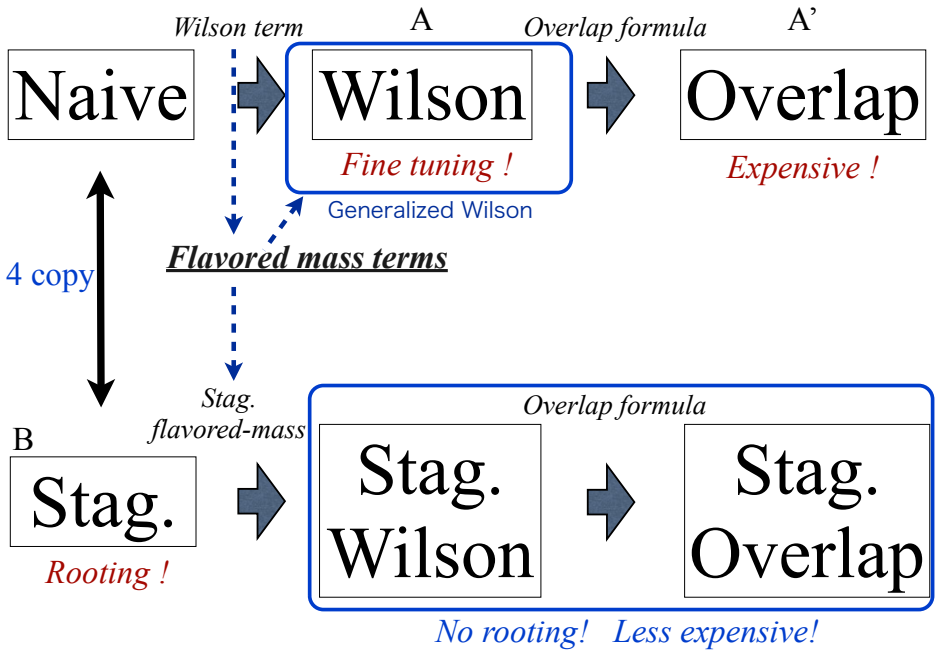

Figure 1.1: A variety of lattice fermions. By using the flavored-mass terms, we can generalize the Wilson fermion to the generalized one enclosed by the blue line. By generalizing the flavored-mass terms to the staggered fermion, we obtain the staggered-Wilson and staggered-overlap fermions which are also enclosed by the blue line. These novel fermions are the main theme of this thesis.

terms enable us to obtain these new lattice fermions. In the next chapter we begin with reviewing the lattice gauge theory and several lattice fermion formulations from the viewpoint of symmetries, the number of doubling species and the spectrum of Dirac eigenvalues.

Chapter 2

A variety of lattice fermions

2.1 Lattice field theory

Lattice discretization regularizes euclidean field theories by introducing a minimum length a or equivalently a momentum cutoff $\Lambda \sim 1/a$ [1]. For d dimensional lattice theories d-dimensional cubic lattice is usually adopted. Its sites are represented by d integer numbers as $n = (n_1, n_2, ..., n_d)$. We here term the object between the nearest lattice sites in the μ direction ($\mu = 1, 2, ..., d$) as "μ-link". An advantage in the lattice field theory is that the gauge field is quantized in a gauge-invariant way: The gauge field on the lattice, which is called a link variable, is defined on the link of lattice sites as an element of the compact gauge group. It is given by $U_{n,\mu} = \exp(iagA_\mu(n))$ where $A_\mu = A^a_\mu(n)T^a$ and T^a (a=0,1,2,3...) is a generator associated with gauge group of interest. Bosonic and fermionic fields are defined as site variables ϕ_n, ψ_n which are defined on the lattice sites. Here we introduce the gauge coupling g and the corresponding gauge field $A_\mu(n)$ in the continuum. We note that $U_{n,\mu}$ has indices of colors depending the gauge group as $U^{ab}_{n,\mu}$.

From now, we concentrate on the 4-dimensional lattice theory where the fermions and bosons are in the fundamental representation of the gauge group. We also consider compact gauge group such as $SU(N)$. We note that $U_{n,\mu}$ has no mass dimension while ϕ_n has a mass dimension 1 and ψ_n has a mass dimension 3/2 as in the usual 4-dimensional field theory. Then the lattice action for the gauge theory coupled with bosons and fermions is in general given by

$$S_L = S_G + S_B + S_F, \tag{2.1}$$

with

$$S_G = -\frac{1}{g^2}\sum_{n,\mu} \mathrm{Tr}[U_{n,\mu}U_{n+\mu,\nu}U^\dagger_{n+\nu,\mu}U^\dagger_{n,\nu}], \tag{2.2}$$

$$S_B = a^4 \sum_{n,\mu} \phi^\dagger_n \frac{U_{n,\mu}\phi_{n+\mu} + U^\dagger_{n-\mu,\mu}\phi_{n-\mu} - 2\phi_n}{2a^2} + \frac{a^4}{2}\sum_n m_{\mathrm{b}}\phi^\dagger_n\phi_n, \tag{2.3}$$

$$S_F = a^4 \sum_{n,\mu} \bar{\psi}_n\gamma_\mu \frac{U_{n,\mu}\psi_{n+\mu} - U^\dagger_{n-\mu,\mu}\psi_{n-\mu}}{2a} + a^4\sum_n m_{\mathrm{f}}\bar{\psi}_n\psi_n, \tag{2.4}$$

where we introduce mass $m_{\rm b}$ for bosons and $m_{\rm f}$ for fermions with a dimension $1/a$. We hide the color indices and flavor indices as $U^{ab}_{n,\mu} \to U_{n,\mu}$, $\phi^{a,f}_n \to \phi_n$ and $\psi^{a,f}_n \to \psi_n$ for now. Since we work on the path integral quantization, we treat $\bar{\psi}$ as an independent field although the on-shell condition of course gives $\bar{\psi} = \psi^\dagger \gamma_4$. It is obvious that in the classical continuum the actions result in the well-known continuum forms as,

$$S_G \ \to \ \int d^4x F_{\mu\nu}(x) F_{\mu\nu}(x) + O(a), \tag{2.5}$$

$$S_B \ \to \ \int d^4x \frac{1}{2}\phi^\dagger(x)(D_\mu^2 + m)\phi(x) + O(a), \tag{2.6}$$

$$S_F \ \to \ \int d^4x \bar{\psi}(x)(\gamma_\mu D_\mu + m)\psi(x) + O(a), \tag{2.7}$$

where $x \equiv na$ and $D_\mu = \partial_\mu + igA_\mu(x)$. Here let us go back to the lattice actions (2.2), (2.3) and (2.4). In lattice field theory we can nondimensionalize boson and fermion actions by redefining fields and mass as $a\phi_n \to \psi_n$, $a^{3/2}\psi_n \to \psi_n$ and $ma \to m$. The dimensionless actions are given by

$$S_B = \frac{1}{2}\sum_{n,\mu} \phi^\dagger_n (U_{n,\mu}\phi_{n+\mu} + U^\dagger_{n-\mu,\mu}\phi_{n-\mu} - 2\phi_n) + \frac{1}{2}\sum_n m_{\rm b}\phi^\dagger_n\phi_n, \tag{2.8}$$

$$S_F = \frac{1}{2}\sum_{n,\mu} \bar{\psi}_n \gamma_\mu (U_{n,\mu}\psi_{n+\mu} - U^\dagger_{n-\mu,\mu}\psi_{n-\mu}) + \sum_n m_{\rm f}\bar{\psi}_n\psi_n, \tag{2.9}$$

where all the fields and parameters are dimensionless. This action is a starting point of lattice simulations. In this thesis we will use this form of the action and fields except for a special care required.

The goal of lattice simulations is to calculate correlation functions for operators of interest or thermodynamical quantities from the partition function. Here we consider a QCD-type theory, in which a gauge field is coupled to fermion fields in the fundamental representation. The partition function for this theory is given by

$$Z = \int \mathcal{D}U \, \mathcal{D}\psi \, \exp[-S_U - S_F]. \tag{2.10}$$

We usually integrate out fermion fields into the fermion determinant . Thus the action is rewritten as

$$Z = \int \mathcal{D}U \det D(U) \exp[-S_U], \tag{2.11}$$

where we define the Dirac operator of the lattice fermion as

$$D(U)_{nm} = \gamma_\mu (U_{n,\mu}\delta_{n+\mu,m} - U^\dagger_{n-\mu,\mu}\delta_{n-\mu,m}) + m\delta_{n,m}. \tag{2.12}$$

Now we can write correlation functions for any operator in the path integral form. For example, the 2-point correlation function of the pion operator $\pi^a = \bar{\psi}\gamma_5\tau^a\psi$ in the 2-flavor case (τ_a stands for the Pauli matrix) is given by

$$\begin{aligned}\langle \pi^a_n \pi^b_m \rangle = \int \mathcal{D}U \, \det D(U) e^{-S_U} (&\delta_{ab}{\rm Tr}[\gamma_5 D^{-1}(U)_{nm}\gamma_5 D^{-1}(U)_{mn}] \\ &+\delta_{a0}{\rm Tr}[\gamma_5 D^{-1}(U)_{nn}]{\rm Tr}[\gamma_5 D^{-1}_{mm}]),\end{aligned} \tag{2.13}$$

where Tr stands for trace for color and spinor indices. In Monte Carlo simulations the gauge field configuration is stochastically generated according to the weight in the partition function as $D(U)e^{-S_U}$. By summing up results for as many configurations as possible and averaging them, we derive results for the finite lattice spacing. By taking a infinite volume limit and a continuum limit, we derive results for the continuum theory. Since the continuum limit is defined at the ultraviolet fixed point which corresponds to a $g \to 0$ limit in QCD, we can obtain physical quantities by extrapolating results for different bare couplings to zero bare coupling. This is a basic process in the lattice simulations [2]. However this process itself does not cost much in numerical simulations. What cost the most is calculation of the fermion propagator and its determinant. To perform the full lattice simulations, we need to solve a large-size linear equation for a Dirac operator matrix including the space-time coordinate, Dirac spinor, flavor and color indices for each gauge configuration. In particular the numerical cost for the fermion propagator soars for smaller mass and we cannot simulate QCD with practical quark mass. It is because the number of conditions in the conjugate gradient process, which is usually used for solution of a large linear equation, are determined by the minimum eigenvalue of the Dirac operator, which is related to fermion mass: However the most serious problem for lattice QCD with fermions is not this: It is a notorious problem called a "doubling problem" [3]. Let us look into this by rewriting a free lattice fermion action in the momentum expression with the lattice spacing being explicit as

$$S_F = \int_{-\pi/a}^{\pi/a} d^4p\bar{\psi}(ap)(\frac{i}{a}\gamma_\mu \sin ap_\mu + m)\psi(ap), \tag{2.14}$$

where we define the 4-vector momentum as p_μ ($\mu = 1, 2, 3, 4$). Discretization of spacetime results in restriction of the euclidean momentum space as $-\pi/a < p_\mu \leq \pi/a$, which is called the Brillouin zone. The zero point of the Dirac operator or the pole of the propagator in the momentum space $D(p) = \frac{i}{a}\sin ap_\mu + m = 0$ corresponds fermion degrees of freedom. What is notable here is that this Dirac operator has 16 zeros within the Brillouin zone for a massless case as

$$\tilde{p}_\mu = 0, \ \text{ or } \ \pi/a, \tag{2.15}$$

where $\tilde{p}_\mu$ takes 0 or π/a thus the total number of zeros is sixteen. Let us look into it in details for general dimensions. The naive lattice fermion propagator for d dimensions is given by

$$D^{-1}(pa) = \frac{-i\gamma_\mu \sin ap_\mu + am}{\sin^2 ap_\mu + a^2m^2}, \tag{2.16}$$

with $\mu = 1, 2, 3, ..., d$. The pole of the fermion propagator

$$\sin^2 ap_\mu + a^2m^2 = 0, \tag{2.17}$$

indicates existence of particles and their dispersion relations. In a classical continuum limit $a \to 0$, the sine function is expanded as

$$\sin p_\mu a \ \sim \ \hat{p}_\mu a \ + \ O(a^2), \tag{2.18}$$

for $p_\mu = \hat{p}_\mu$ and

$$\sin p_\mu a \ \sim \ -\hat{p}_\mu a \ + \ O(a^2), \tag{2.19}$$

for $p_\mu = \hat{p}_\mu + \pi/a$ ($\hat{p}_\mu \ll 1/a$). Thus the propagator in the continuum limit is given by

$$D^{-1}(pa) \ \rightarrow \ \frac{1}{a} \sum_{p_\mu = 0, \pi/a} \frac{-i(-1)^{\delta_\mu} \gamma_\mu \hat{p}_\mu + m}{\hat{p}_\mu^2 + m^2}, \tag{2.20}$$

where $\delta_\mu = 0$ for $p_\mu = 0$ and $\delta_\mu = 1$ for $p_\mu = \pi/a$ respectively. This expression clearly uncovers that the naive fermion describes 2^d Dirac fermion modes. This multiple emergence of fermion degrees of freedom, which we call species or doublers, is a generic and inevitable property of the lattice fermion action. It is summarized in the famous no-go theorem, Nielsen-Ninomiya's theorem [4]. This theorem states that the lattice fermion action with chiral symmetry, locality and hermitcity should acquire fermions in multiple number of two. As shown in [3] intuitively, although the sine function is consistent with the the physical continuum dispersion for the zero at $\tilde{p} = (0, 0, 0, 0)$, its periodicity results in another zero at a different momentum point such as $\tilde{p} = (\pi, 0, 0, 0)$. Thus we have one pair of zeros per one dimension, leading to16 fermion modes in a 4 dimensional theory with the hypercubic symmetry. Unfortunately the pairs have opposite chiral charges ($\gamma_5 \leftrightarrow -\gamma_5$), thus left-chirality modes are always paired by right-chirality modes. It means that we cannot formulate the chiral gauge theory such as the Weak- interaction sector in the standard model, at least by using this naive discretization of the fermion action. On the other hand, we can formulate a vector-type gauge theory, but there are 16 fermions contributing to the continuum limit. Thus we cannot describe quarks in QCD. Since we need to break chiral symmetry explicitly to obtain doubler-less lattice fermions, the doubling problem in lattice QCD can be called as a conflict of "chiral symmetry vs doubler-less lattice fermion".

As we have seen, the formulation of lattice fermions has difficulty to match phenomenological theories. From the next section, we will look into a variety of lattice fermion actions, some of which bypass the no-go theorem by breaking the presuppositions of the no-go theorem appropriately.

2.2 Naive fermion

In this section we review the naive lattice fermion from the viewpoint of the symmetry and the Dirac eigenvalues. Symmetries of the naive lattice fermion can be classified into two types; discrete symmetries and continuous symmetries. Discrete symmetries include the hypercubic symmetry, C, P and T invariance. The hypercubic symmetry results in the Euclidean rotational symmetry in the continuum limit. These symmetries are phenomenologically desiarble. On the other hand, continuous symmetries are affected by the flavor structure of lattice species. The continuous symmetries include flavor and chiral symmetry. Since the naive fermion contains 16 species, we expect that the theory has $U(16) \times SU(16)$ symmetry in the continuum limit. However the lattice discretization errors break it to $U(4) \times U(4)$ at finite lattice spacing, which is an anomaly-free subgroup of the continuum $U(16) \times SU(16)$. In this section we first show that the kinetic term of

the naive fermion has the U(4)×U(4) symmetry at a finite lattice spacing. In the presence of the mass term or the chiral condensate, this symmetry is explicitly or spontaneously broken down to the diagonal U(4). Note this section is not only a review of the old papers in [50, 51, 52, 53, 54, 55, 56], but also contains study on the algebra of the symmetries of naive fermions from the original work by the present authors [57].

We here concentrate on a free case, but the symmetries we show here still hold in the presence of the link variables. We again write the dimensionless free action of the naive fermion as,

$$S_{\rm nf} = \frac{1}{2}\sum_{n,\mu}(\bar{\psi}_n\gamma_\mu\psi_{n+\hat{\mu}} - \bar{\psi}_{n+\hat{\mu}}\gamma_\mu\psi_n) + m\sum_n \bar{\psi}_n\psi_n\,. \tag{2.21}$$

The kinetic term of the above action obviously has the vector and axial-vector U(1) symmetry as does the action of the continuum theory,

$$\mathrm{U}(1)_V \;:\; \psi_n \to \psi'_n = \exp(\mathrm{i}\theta)\psi_n\,, \quad \bar{\psi}_n \to \bar{\psi}'_n = \exp(-\mathrm{i}\theta)\bar{\psi}_n\,, \tag{2.22}$$

$$\mathrm{U}(1)_A \;:\; \psi_n \to \psi'_n = \exp(\mathrm{i}\theta\gamma_5)\psi_n\,, \quad \bar{\psi}_n \to \bar{\psi}'_n = \bar{\psi}_n\exp(\mathrm{i}\theta\gamma_5)\,. \tag{2.23}$$

In addition to these well-known symmetries, the lattice kinetic term has other symmetries which include site-dependent prefactors. For instance, there is a site-dependent version of $\mathrm{U}(1)_V$, which is given by

$$\psi_n \to \psi'_n = \exp\left[\mathrm{i}(-1)^{n_1+\ldots+n_4}\theta\right]\psi_n\,, \quad \bar{\psi}_n \to \bar{\psi}'_n = \exp\left[\mathrm{i}(-1)^{n_1+\ldots+n_4}\theta\right]\bar{\psi}_n\,. \tag{2.24}$$

There is also a site-dependent version of $\mathrm{U}(1)_A$ given by

$$\psi_n \to \psi'_n = \exp\left[\mathrm{i}(-1)^{n_1+\ldots+n_4}\theta\gamma_5\right]\psi_n\,, \quad \bar{\psi}_n \to \bar{\psi}'_n = \bar{\psi}_n\exp\left[-\mathrm{i}(-1)^{n_1+\ldots+n_4}\theta\gamma_5\right]\,. \tag{2.25}$$

Note that the transformation laws of $\bar{\psi}_n$ are determined so that they preserve the link reflection positivity. In other words, we require the transformations to commute with the following anti-linear operation Θ.

$$\Theta[\psi_n] = \bar{\psi}_{n_i,-n_4+1}\,\gamma_4\,, \quad \Theta[\bar{\psi}_n] = \gamma_4\psi_{n_i,-n_4+1}\,. \tag{2.26}$$

More generally, the kinetic term is invariant under the following transformations,

$$\psi_n \to \psi'_n = \exp\left[\mathrm{i}\,T^{(+)} + \mathrm{i}\,T^{(-)}\right]\psi_n\,, \quad \bar{\psi}_n \to \bar{\psi}'_n = \bar{\psi}_n\exp\left[-\mathrm{i}\,T^{(+)} + \mathrm{i}\,T^{(-)}\right]\,. \tag{2.27}$$

Here, $T^{(+)}$ and $T^{(-)}$ are site-dependent 4×4 matrices: $T^{(+)}\in\mathcal{M}^+$, $T^{(-)}\in\mathcal{M}^-$ with

$$\mathcal{M}^+ = \mathrm{span}\left\{\mathbf{1}_4\,,\ (-1)^{n_1+\ldots+n_4}\gamma_5\,,\ (-1)^{\check{n}_\mu}\gamma_\mu\,,\ (-1)^{n_\mu}\mathrm{i}\gamma_\mu\gamma_5\,,\ (-1)^{n_{\mu,\nu}}\frac{\mathrm{i}\,[\gamma_\mu\,,\gamma_\nu]}{2}\right\}\,, \tag{2.28}$$

$$\mathcal{M}^- = \mathrm{span}\left\{(-1)^{n_1+\ldots+n_4}\mathbf{1}_4\,,\ \gamma_5\,,\ (-1)^{n_\mu}\gamma_\mu\,,\ (-1)^{\check{n}_\mu}\mathrm{i}\gamma_\mu\gamma_5\,,\ (-1)^{\check{n}_{\mu,\nu}}\frac{\mathrm{i}\,[\gamma_\mu\,,\gamma_\nu]}{2}\right\}\,, \tag{2.29}$$

where $\check{n}_\mu = \sum_{\rho\neq\mu} n_\rho$, $n_{\mu,\nu} = n_\mu + n_\nu$ and $\check{n}_{\mu,\nu} = \sum_{\rho\neq\mu,\nu} n_\rho$. Let us now take a closer look at the algebraic structure of the above symmetries. First we instantly notice that

the elements of $\mathcal{M}^+$ and $\mathcal{M}^-$ are 4×4 Hermitian matrices up to site-dependent signs. In addition, we also notice that they have the following $\mathbb{Z}_2$-grading structure:

$$[\mathcal{M}^+,\mathcal{M}^+]=\mathcal{M}^+\,,\quad [\mathcal{M}^+,\mathcal{M}^-]=\mathcal{M}^-\,,\quad [\mathcal{M}^-,\mathcal{M}^-]=\mathcal{M}^+\,. \tag{2.30}$$

These features imply that $\mathcal{M}^+$ generates a U(4) subgroup of the whole symmetry group, which we call $\mathrm{U}(4)^+$. Furthermore, by taking linear combinations of $\mathcal{M}^+$ and $\mathcal{M}^-$ appropriately, we can obtain two mutually decoupled U(4) symmetries, which are generated by $\mathcal{M}^R$ and $\mathcal{M}^L$.

$$\mathcal{M}^R \;=\; \mathrm{span}\left\{\frac{1+(-1)^{n_1+\ldots+n_4}}{2}\mathcal{M}\right\},\quad \mathcal{M}^L=\mathrm{span}\left\{\frac{1-(-1)^{n_1+\ldots+n_4}}{2}\mathcal{M}\right\},$$

where

$$\mathcal{M} \;=\; \left\{(-1)^{n_1+\ldots+n_4}\,\mathbf{1}_4\,,\;\gamma_5\,,\;(-1)^{n_\mu}\,\gamma_\mu\,,(-1)^{\check{n}_\mu}\,\mathrm{i}\gamma_\mu\gamma_5\,,\;(-1)^{\check{n}_{\mu,\nu}}\,\frac{\mathrm{i}\,[\gamma_\mu\,,\gamma_\nu]}{2}\right\}. \tag{2.31}$$

Therefore, we conclude that the kinetic term of the naive fermion has $\mathrm{U}(4)\times\mathrm{U}(4)$ symmetry. Note that this $\mathrm{U}(4)\times\mathrm{U}(4)$ symmetry can be interpreted as a symmetry among four copies of staggered fermions which we will discuss in the next section.

So far we have not included the mass term in our analysis. In the presence of the mass term, it is readily seen from (2.27) that the original $\mathrm{U}(4)\times\mathrm{U}(4)$ symmetry is explicitly broken down to $\mathrm{U}(4)^+$ symmetry. On the other hand, in the presence of the chiral condensate, the original $\mathrm{U}(4)\times\mathrm{U}(4)$ symmetry spontaneously breaks down to $\mathrm{U}(4)^+$ producing sixteen Nambu-Goldstone bosons (NG bosons), which correspond to sixteen generators contained in $\mathcal{M}^-$. One of the notable features of these NG bosons is that they include the site-dependent signs in their definitions, $\bar{\psi}_n\mathcal{M}^-\psi_n$. These site-dependent signs have the effect of shifting momenta by π. For instance, if we Fourier-transform $\bar{\psi}_n\left((-1)^{n_1+\ldots+n_4}\right)\mathbf{1}_4\psi_n$, we obtain a meson with shifted momenta, $\left(\bar{\psi}\psi\right)(p_\mu+\pi)$.

Finally let us look into eigenvalues of the Dirac operator of the naive lattice fermion. The dimensionful Dirac operator in the position space is given by

$$D_{nm}=\frac{\gamma_\mu}{2a}(U_{n,\mu}\delta_{n+\mu,m}-U^\dagger_{n-\mu,\mu}\delta_{n-\mu,m})+m\delta_{n,m}. \tag{2.32}$$

From now we concentrate on the free ($U_{n,\mu}=0$) and massless ($m=0$) We also write a form of the momentum space as

$$D(p)=\frac{i}{a}\gamma_\mu\sin ap_\mu+m. \tag{2.33}$$

What we want to emphasize is that they are anti-hermitian for a massless case as $D^\dagger=-D$. For a free and massless case, we can easily calculate the eigenvalues of these Dirac operators. We depict the results in Fig. 2.1. All the eigenvalues are on the imaginary axis, reflecting the anti-hermiticity of the Dirac operator. As is well-known, the Dirac operator of the continuum theory gives the pure-imaginary eigenvalues except for zero modes. Thus we expect that the lattice fermion theory with the imaginary Dirac spectrum results in the correct continuum theory, and this carry over in the case with nonzero mass and

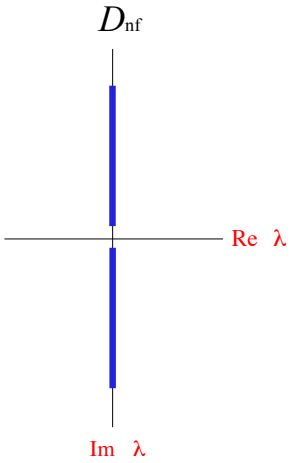

Figure 2.1: The complex Dirac spectrum for the free case of the massless naive lattice fermion. All the eigenvalues have pure-imaginary values because of the anti hermiticity of the massless Dirac operator. We note this spectrum is 16-fold degenerate reflecting the 16 species.

the gauge fields. However the spectrum on the imaginary axis is 16-degenerate, which reflects the 16 species in the lattice fermion. We can show the degeneracy by introducing flavored-mass terms which we will discuss later. We note that the naive Dirac operator satisfies γ_5 hermiticity, which means a property of the Dirac operator as

$$D^\dagger = \gamma_5 D \gamma_5, \tag{2.34}$$

This translates into the hermiticity of the operator $\gamma_5 D = H$ as,

$$(\gamma_5 D)^\dagger = \gamma_5 D. \tag{2.35}$$

This property "γ_5-hermiticity" is a necessary condition for a physical euclidean theory. Due to this property, eigenvalues except for zero modes appear in complex pairs as

$$D\phi = \lambda\phi \quad \rightarrow \quad D(\gamma_5\phi) = \bar{\lambda}(\gamma_5\phi), \tag{2.36}$$

where ϕ is an eigenfunction of D and λ is an associated eigenvalue. The pairing of the complex eigenvalues leads to the real and positive determinant of the Dirac operator. It is essential for the path integral formulation of the euclidean theory. From this property and chiral symmetry, we can analytically reconfirm that the massless Dirac spectrum of naive lattice fermions is pure-imaginary as

$$\gamma_5 D + D\gamma_5 = 0, \quad D^\dagger = \gamma_5 D \gamma_5 \rightarrow \; D + D^\dagger = 0.$$

As seen from the study in this section, the naive lattice fermion possesses $U(4) \times U(4)$ symmetries originating from the 16 species. The other symmetries and the appearance of the Dirac spectrum are consistent with the continuum theory, but we cannot avoid the species doublers in this fermion formalism.

2.3 Staggered fermions

In this section we translate the naive fermion into staggered fermions using the spin diagonalzation. This section is a review based on [13, 14, 15, 58, 59, 60, 61, 62, 63]. Using the field χ_n defined by

$$\chi_n = \gamma_4^{n_4}\gamma_3^{n_3}\gamma_2^{n_2}\gamma_1^{n_1}\psi_n, \quad \bar{\chi}_n = \bar{\psi}_n\gamma_1^{n_1}\gamma_2^{n_2}\gamma_3^{n_3}\gamma_4^{n_4}\,, \tag{2.37}$$

the naive fermion action (2.21) can be represented as follows:

$$S_{\rm nf} = 4S_{\rm st} = 4[\frac{1}{2}\sum_{n,\mu}\eta_\mu(n)\bar{\chi}_n\left(\chi_{n+\hat{\mu}} - \chi_{n-\hat{\mu}}\right) + \frac{m}{2}\sum_n \bar{\chi}_n\chi_n] \quad \text{with} \quad \eta_\mu(n) = (-1)^{\sum_{\nu<\mu} n_\nu}\,. \tag{2.38}$$

This action is called the staggered fermion action. One naive fermion is equal to four staggered fermions. However there are several significant differences: Firstly, in this formalism, the fermion is defined as an one spinor on each lattice site, not a four-spinor. Thus the four-spinor Dirac fermions can be reconstructed from the 16 spinors in the hypercubic block, which results in the 4 flavor (taste) Dirac fermions. In this case a physical lattice spacing is not a, but $2a$. We note that spinor indices and taste indices are related in a complicated way in this formulation. Therefore the transformation about the space-time is combined with the flavor rotation. Let us look into this formulation in details. We define $\Psi(N)$ as Dirac fermion fields defined on the lattice sites N, which defined as $n = 2N + A$ where n is the original staggered lattice sites and N is the physical sites for the Dirac fermion with A being the 4 vector whose components takes 0 or 1. $\Psi(N)$ is given by

$$\Psi(N)_{\alpha,\,f} = \sum_A \left(\frac{\gamma_A}{2}\right)_{\alpha,\,f}\chi_A(N)\,, \quad \bar{\Psi}(N)_{\alpha,\,f_1,\,f_2} = \sum_A \left(\frac{\bar{\gamma}_A}{2}\right)_{\alpha,\,f}\bar{\chi}_A(N)\,, \tag{2.39}$$

where $A_\mu = 0$ or 1, $\chi_A(N) = \chi_{2N+A}$, $\gamma_A = \gamma_1^{A_1}\gamma_2^{A_2}\gamma_3^{A_3}\gamma_4^{A_4}$, and $\bar{\gamma}_A$ denotes the complex conjugate of γ_A. In terms of $\Psi(N)$, the staggered fermion action can be written as

$$\begin{aligned} S_{\rm st} &= \frac{1}{2}\sum_{N,\mu}\left[\bar{\Psi}(N)\left(\gamma_\mu\otimes\mathbf{1}_4\right)\nabla_\mu\Psi(N) + \bar{\Psi}(N)\left(\gamma_5\otimes\gamma_\mu^{\rm T}\gamma_5^{\rm T}\right)\nabla_\mu^2\Psi(N)\right] \\ &\quad + m\sum_N \bar{\Psi}(N)\left(\mathbf{1}_4\otimes\mathbf{1}_4\right)\Psi(N)\,, \end{aligned} \tag{2.40}$$

where

$$\bar{\Psi}(A\otimes B)\Psi = \sum_{\alpha,\,\alpha',\,f,\,f'}\bar{\Psi}_{\alpha,f}\left(A\right)_{\alpha\alpha'}\left(B\right)_{ff'}\Psi_{\alpha',f'}\,, \tag{2.41}$$

$$\nabla_\mu\Psi(N) = \frac{\Psi(N+\hat{\mu}) - \Psi(N-\hat{\mu})}{2}\,, \tag{2.42}$$

$$\nabla_\mu^2\Psi(N) = \frac{\Psi(N+\hat{\mu}) - 2\Psi(N) + \Psi(N-\hat{\mu})}{2}\,, \tag{2.43}$$

and the superscript T denotes transposition. We call the representation as the spin-flavor or spin-taste representation since the spinor and taste structure is manifest in this

representation. It is obvious that this fermion action works as four Dirac fermions with the discretization error terms. We note that the four flavors is consistent with the no-go theorem. By restoring a lattice spacing the second term in the action (2.40) is expressed by

$$S_{\rm st}^{(2)} \;=\; a\cdot\frac{a^4}{2}\sum_{N,\mu}\bar{\Psi}(N)\left(\gamma_5\otimes\gamma_\mu^{\rm T}\gamma_5^{\rm T}\right)\frac{\Psi(N+\hat{\mu})-2\Psi(N)+\Psi(N-\hat{\mu})}{2a^2}, \tag{2.44}$$

where $\Psi(N)$ has a mass dimension 3/2. Since $\bar{\Psi}\nabla^2\Psi$ is the dimension 5 operator, we usually call this kind of terms a dimension 5 term. Near the classical continuum it turns out to be a O(a) term as

$$S_{st}^{(2)} \;\rightarrow\; a\int dx\bar{\Psi}(x)\partial_\mu^2\Psi(x), \tag{2.45}$$

which disappears in the classical continuum. We note this term breaks flavor and chiral symmetry to $U(1)_V\times U(1)_A$. The $U(1)_V$ is given by the transformation as

$$U(1)_V \;:\; e^{\theta}\chi_n \;\sim\; e^{i\theta(\mathbf{1}_4\otimes\mathbf{1}_4)}\Psi(N), \tag{2.46}$$

while the $U(1)_A$ is given by

$$U(1)_A \;:\; e^{\epsilon(n)}\chi_n \;\sim\; e^{i\theta(\gamma_5\otimes\gamma_5)}\Psi(N), \tag{2.47}$$

where we define $\epsilon(n)=(-1)^{n_1+n_2+n_3+n_4}$, which is translated into the $\Gamma_{55}=\gamma_5\otimes\gamma_5$ in the spin-flavor representation. As with the naive fermion, the residual chiral symmetry is flavored one, which has nothing to do with the flavor-singlet $U_A(1)$ anomaly. Since the naive fermion can be seen as four copies of the staggered fermions, it is now clear why the naive fermion possesses $U(4)\times U(4)$ symmetry. We next discuss the discrete symmetry of the staggered fermions [59, 61]. One of the characteristic symmetries is the shift symmetry as

$$\mathcal{S}_\rho:\;\chi_n\rightarrow\zeta_\rho(n)\chi_{n+\hat{\rho}},\quad \bar{\chi}_n\rightarrow\zeta_\rho(n)\bar{\chi}_{n+\hat{\rho}},\quad U_{\mu,n}\rightarrow U_{\mu,n+\hat{\rho}}, \tag{2.48}$$

with $\zeta_1(n)=(-1)^{n_2+n_3+n_4}$, $\zeta_2(n)=(-1)^{n_3+n_4}$, $\zeta_3(n)=(-1)^{n_4}$ and $\zeta_4(n)=1$. The axis reversal is also symmetry, whose transformation is given by,

$$\mathcal{I}_\rho:\;\chi_n\rightarrow(-1)^{n_\rho}\chi_{In},\quad \bar{\chi}_n\rightarrow(-1)^{n_\rho}\bar{\chi}_{In},\quad U_{\mu,n}\rightarrow U_{\mu,In}, \tag{2.49}$$

with $I=I^\rho$ is the axis reversal $n_\rho\rightarrow -n_\rho$, $n_\tau\rightarrow n_\tau$, $\tau\neq\rho$. The staggered rotational transformation is given by

$$\mathcal{R}_{\rho\sigma}:\;\chi_n\rightarrow S_R(R^{-1}n)\chi_{R^{-1}n},\quad \bar{\chi_n}\rightarrow S_R(R^{-1}n)\bar{\chi}_{R^{-1}n},\quad U_{\mu,n}\rightarrow U_{\mu,Rn}, \tag{2.50}$$

where $R_{\rho\sigma}$ is the rotation $n_\rho\rightarrow n_\sigma$, $n_\sigma\rightarrow -n_\rho$, $n_\tau\rightarrow n_\tau$, $\tau\neq\rho,\sigma$ and $S_R(n)=\frac{1}{2}[1\pm\eta_\rho(n)\eta_\sigma(n)\mp\zeta_\rho(n)\zeta_\sigma(n)+\eta_\rho(n)\eta_\sigma(n)\zeta_\rho(n)\zeta_\sigma(n)]$ with $\rho\lesseqgtr\sigma$. The staggered fermion has invariance under the charge conjugation transformation, which is given by

$$\mathcal{C}:\;\chi_n\rightarrow\epsilon_n\bar{\chi}_n^T,\;\bar{\chi}_n\rightarrow-\epsilon_n\chi_n^T,\;U_{\mu,n}\rightarrow U_{\mu,n}^*. \tag{2.51}$$

As shown in [59, 60], these transformations produce rotations in both spinor and flavor spaces. Here we use the momentum space method shown in [59, 60] to identify the spinor and flavor labels in these: We first define the 16 species-fields in the momentum space as $\phi(p)_A \equiv \chi(p+\pi_A)$ $(-\pi/2 \leq p_\mu < \pi/2)$ where π_A $(A = 1, 2, ..., 16)$ being 4-dim vectors whose components take 0 or π. We use a dimensionless form of the momentum redefined as $p_\mu a \to p_\mu$. For convenience, we here consider a 16-multiplet field as $\phi(p) = (\phi(p)_1, \phi(p)_2, \cdots, \phi(p)_{16})^T$. As this 16-multiplet field has both the spinor(space-time) and the flavor(taste) indices, we can construct the two sets of generators acting on the spinor and flavor spaces as 16×16 matrices respectively. Here we denote them as Γ_μ and Ξ_μ acting on the spinor and flavor spaces respectively. We note they possess properties as $\{\Gamma_\mu, \Gamma_\nu\} = 2\delta_{\mu\nu}$, $\{\Xi_\mu, \Xi_\nu\} = 2\delta_{\mu\nu}$ and $\{\Gamma_\mu, \Xi_\nu\} = 0$. By rewriting staggered fermions in the spin-flavor representation, they can be represented as gamma matrices for Dirac fermion. By using these definitions we show the shift transformation gives flavor rotation, which is schematically given by

$$\mathcal{S}_\mu : \ \phi(p) \ \to \ \exp(ip_\mu)\Xi_\mu \, \phi(p). \tag{2.52}$$

The axis reversal gives spinor and flavor rotations as

$$\mathcal{I}_\rho : \phi(p) \ \to \ \Gamma_\rho\Gamma_5\Xi_\rho\Xi_5 \, \phi(Ip). \tag{2.53}$$

The rotational transformation is given by the spinor and flavor rotations as

$$\mathcal{R}_{\rho\sigma} : \ \phi(p) \ \to \ \exp(\frac{\pi}{4}\Gamma_\rho\Gamma_\sigma) \exp(\frac{\pi}{4}\Xi_\rho\Xi_\sigma) \, \phi(R^{-1}p). \tag{2.54}$$

We note that the rotational symmetry followed by the axis reversal forms the staggered hypercubic symmetry, which is a combined symmetry between the spacetime and flavor space. In the continuum limit the space-time and flavor rotation decouples to the Lorentz symmetry and the flavor symmetry. The parity symmetry is encoded as the 4th-direction shift with spatial axis reversal,

$$\mathcal{I}_s\mathcal{S}_4 \sim \exp(ip_4)\Gamma_1\Gamma_2\Gamma_3\Gamma_5 \, \phi(-\mathbf{p}, p_4) \sim \exp(ip_4)\Gamma_4 \, \phi(-\mathbf{p}, p_4), \tag{2.55}$$

with $\mathcal{I}_s \equiv \mathcal{I}_1\mathcal{I}_2\mathcal{I}_3$. By following the arguments in [61, 63], it is easily shown that the present actions are invariant even under $\mathcal{I}_s\Xi_4\phi(-\mathbf{p}, p_4) = \Gamma_4\phi(-\mathbf{p}, p_4)$. Thus we conclude the fermion actions possess physically well-defined parity symmetry. The charge conjugation can be also shown to be symmetry of these fermions [59]. We now expect that this fermion formulation is promoted to be a correct continuum theory except for the multiplicity of four species.

The spectrum of Dirac eigenvalues in this case is essentially similar to the naive fermion. The dimensionful Dirac operator in this case is given by

$$D_{nm} = \frac{\eta_\mu}{2a}(U_{n,\mu}\delta_{n+\mu,m} - U^\dagger_{n-\mu,\mu}\delta_{n-\mu,m}) + m\delta_{n,m}, \tag{2.56}$$

which is again anti-hermitian for a massless case as $D^\dagger = -D$. For a free and massless case, the spectrum of these Dirac operators is depicted as Fig. 2.2 All the eigenvalues are on the imaginary axis as with the continuum theory, which resulte from the anti-hermiticity of

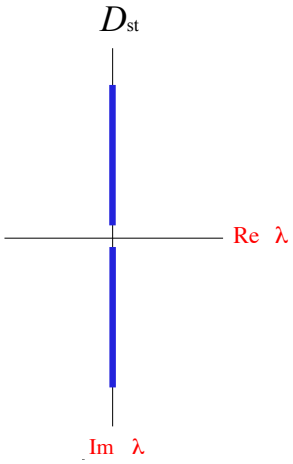

Figure 2.2: The complex Dirac spectrum for the free case of the massless staggered fermion. All the eigenvalues have pure-imaginary values because of the anti-hermiticity of the massless Dirac operator.

the Dirac operator. However the spectrum on the imaginary axis is 4-degenerate, which reflects 4 doubling species. The γ_5 hermiticity

$$D^\dagger = \gamma_5 D \gamma_5, \tag{2.57}$$

again indicates the pairing of the complex eigenvalues, which leads to a real and positive determinant of the Dirac operator. To summarize this section, the staggered lattice fermion possesses $U_V(1) \times U_A(1)$ symmetry and the other basic symmetries. We expect that the $U_V(1) \times U_A(1)$ symmetry is promoted to $U(4) \times SU(4)$ symmetry in the continuum limit and it describes a four-flavor continuum theory. However four degenerate quarks are inconsistent with the physical QCD.

2.4 Wilson fermion

In this section we will discuss the Wilson fermion [6, 7]. This section is mostly devoted to a review on the Wilson fermion, but also contains a new result on the symmetry enhancement of the Wilson fermion at the special value of the mass parameter form the study [57] by the present author. The Wilson fermion lifts degeneracy of sixteen species into five branches by introducing the species-splitting term called the Wilson term, which breaks the chiral symmetry explicitly. The free action for Wilson fermion [6, 7] is given by

$$S = S_{\rm nf} + S_W \quad \text{with} \quad S_W = -\frac{ar}{2} \sum_{n,\mu} a^4 \bar{\psi}_n \frac{(\psi_{n+\hat{\mu}} - 2\psi_n + \psi_{n-\hat{\mu}})}{a^2}, \tag{2.58}$$

where S_{nf} is the naive lattice fermion action and S_W is the Wilson term. One of the criterions for constructing lattice fermion actions is to modify the naive action so that it results in the correct continuum form (2.7) in a classical continuum limit. In fact the Wilson term turns out to be the second-derivative term proportional to a near a continuum limit as

$$S_W \to a \int dx \bar{\psi}(x) \partial_\mu^2 \psi(x), \tag{2.59}$$

whose influence seems to disappear in the classical continuum limit. From now we use a dimensionless form of the Wilson action as

$$\begin{aligned} S_W = & \frac{1}{2} \sum_{n,\mu} (\bar{\psi}_n \gamma_\mu \psi_{n+\hat{\mu}} - \bar{\psi}_{n+\hat{\mu}} \gamma_\mu \psi_n) + m \sum_n \bar{\psi}_n \psi_n \\ & - \frac{r}{2} \sum_{n,\mu} \bar{\psi}_n \left(\psi_{n+\hat{\mu}} - 2\psi_n + \psi_{n-\hat{\mu}} \right) . \end{aligned} \tag{2.60}$$

In the momentum space the free action with $m = 0$ and $r = 1$ is given by

$$S_W = \int_{-\pi}^{\pi} dp \bar{\psi}(p) \sum_\mu [i\gamma_\mu \sin p_\mu + (1 - \cos p_\mu)] \psi(p), \tag{2.61}$$

where the zero of the Dirac operator only appears at $p = (0, 0, 0, 0)$ while the other species have infinite mass and decouple in the continuum limit. This is clearly seen from the Dirac operator near the continuum. If we restore the lattice spacing as $p \to ap$ and take the classical continuum limit, the Dirac operator is given by

$$D(p)/a = i\gamma_\mu p_\mu + O(a), \tag{2.62}$$

for $p = (0, 0, 0, 0)$, and

$$D(p)/a = i\gamma'_\mu p_\mu + \frac{2}{a} + O(a), \tag{2.63}$$

for $p = (\pi, 0, 0, 0)$ where we define $\gamma'_1 = -\gamma_1$ and $\gamma'_j = \gamma_j$ for $j = 2, 3, 4$. Now we obtain a single flavor fermion or doublerless fermion at the price of the chiral symmetry. However note that, if we take $m = -2$ with $r = 1$, the Dirac operator is given by

$$D(p) = \sum_\mu (i\gamma_\mu \sin p_\mu + (1 - \cos p_\mu) - 2, \tag{2.64}$$

which have zeros at $p = (\pi, 0, 0, 0)$, $(0, \pi, 0, 0)$, $(0, 0, \pi, 0)$, $(0, 0, 0, \pi)$. This choice of the mass parameter describe four fermions at least classically. Besides, for $m = -4$ we have six modes while we have four modes for $m = -6$. For $m = -8$ we again have a single mode. The sum of them are sixteen. Thus the fermion modes which we obtain from the Wilson fermion depends on the choice of the mass parameter. We call these five choices of the mass parameter "branches" (the meaning of branches will be clear in the Dirac spectrum in Fig. 2.3). However it is practically difficult to utilize branches other than $m = 0$ or $m = -8$ due to the phase structure shown later.

Among the $U(4)\times U(4)$ flavor and chiral symmetries in naive fermions shown in Sec.2.2, only the $U(1)$ vector invariance remain for general values of the parameters m and r in the Wilson fermion as,

$$\psi_n \to \psi'_n = e^{\mathrm{i}\theta}\psi_n\,, \quad \bar{\psi}_n \to \bar{\psi}'_n = e^{-\mathrm{i}\theta}\bar{\psi}_n\,, \tag{2.65}$$

Since the chiral symmetry is broken, there is no symmetry to prohibit the mass term generated through radiative corrections. This is why we need to take the chiral limit by tuning a mass parameter in QCD simulations with this fermion. Let us look into this in details.

The complex spectrum of the Dirac operator eigenvalues for the Wilson fermion is depicted in Fig. 2.3. Here the imaginary spectrum of the naive fermion is split into the complex spectrum where the five branches appear. 1, 4, 6, 4 and 1 fermion modes exist on these five branches. For example the mode at $\tilde{p} = (0, 0, 0, 0)$ corresponds to the most left branch, which is called a "physical branch", while the mode at $\tilde{p} = (\pi, 0, 0, 0)$ forms the next branch with other three species. In Fig. 2.3, the mass parameter m stands for the crossing point of the physical branch with the real axis, which stands for the mass of the mode at $p = (0, 0, 0, 0)$. Thus the figure corresponds to a case for negative mass m. As long as we keep $m = 0$, the physical branch stays at the origin and other branches cross the real axis at the scale of $O(1/a)$ (if we restore the lattice spacing). Thus, if we take the continuum limit $a \to 0$ with keeping $m = 0$, the spectrum around the physical branch gets close to the imaginary axis while crossings of other branches go to infinity as shown in Fig. 2.4. Since the continuum fermion in the euclidean theory has pure imaginary Dirac eigenvalues, this limit describes a single fermion with the doublers decoupled. However, in the presence of the link variables, the whole spectrum can move to left or right depending on gauge configurations because there is nothing to prohibit the additive $O(1/a)$ mass renormalization due to the chiral symmetry breaking. This results in the necessity of tuning the mass parameter m for a massless limit or a physical quark-mass limit of the physical branch. This fine-tuning process, which is called the chiral limit, costs much in practical simulations. Besides, even if we want to study the spontaneous symmetry breaking in QCD, this fermion formulation gives no information since there is no chiral symmetry in the first place and we instead just mimic the QCD by tuning a mass parameter.

The surprising property of QCD with the Wilson fermion is a parity-broken phase structure called the "Aoki phase" [35, 44, 45]: In the mass and gauge-coupling plane, the pion condensate becomes nonzero in some parameter region. The order of phase transition is in general second. We depict the schematic figure of the parity phase diagram in Fig. 2.5. We define a new mass parameter M as $M = m + 4r$. Here it is shown that the phase diagram reflects the species-splitting of the Wilson Dirac spectrum. Near the continuum limit or in the weak-coupling region, the phase diagram is affected by the structure of doublers while in the strong-coupling region there are only two critical lines. It is because the strong coupling corresponds to the large lattice spacing where doublers can be neglected. From the viewpoint of this phase diagram, taking the chiral limit means tuning the mass parameter to the second-order critical line near the physical branch while the continuum limit means tuning the gauge coupling to zero along with this critical line [46, 47, 48]. Here we show the PCAC relation is recovered near the critical line. In

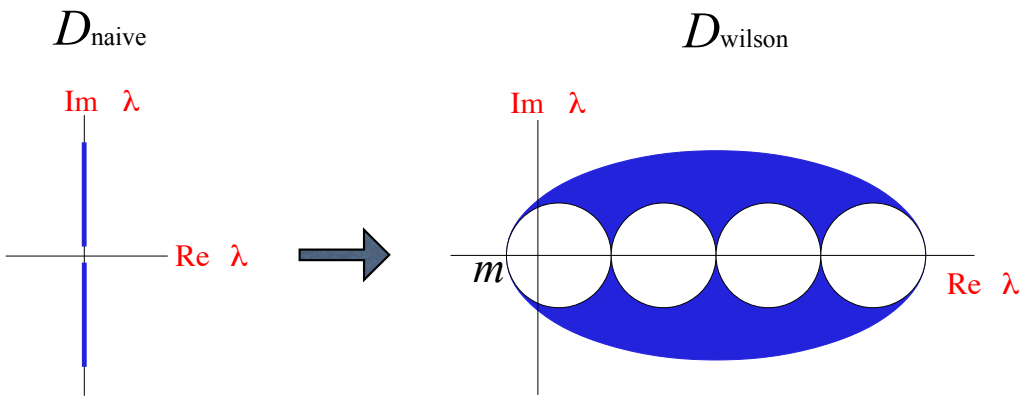

Figure 2.3: The complex Dirac spectrum for the free case. There are five branches where 1, 4, 6, 4 and 1 fermion modes correspond. The most left branch is called a physical branch. We denote m as the crossing point of this branch with the real axis, which indicates the mass of the corresponding fermion mode. By tuning this mass as $m = 0$, the physical branch produces a single massless mode. We note the scale of the crossing points of the other branches are $O(1/a)$ when we restore the lattice spacing.

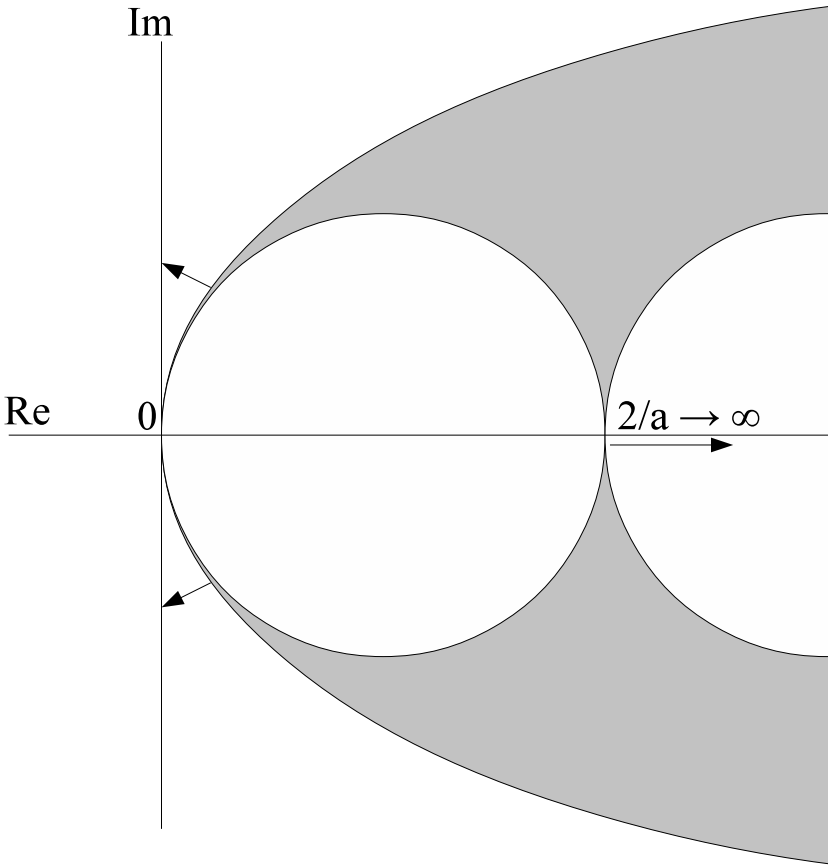

Figure 2.4: When we take the continuum limit $a \to 0$ with keeping $m = 0$, the spectrum around the physical branch gets close to the imaginary axis while the crossings of the other branches go to infinity.

this case, the correlation length ξ corresponds to inverse of the pion mass m_π. Near the second-order critical line, the correlation length is given by

$$\xi \sim |M - M_c|^{-\nu}, \tag{2.66}$$

where we define M_c as a critical mass parameter and ν as a critical exponent. Thus the square pion mass m_π^2 is given by

$$m_\pi^2 \sim |M - M_c|^{2\nu}. \tag{2.67}$$

Since the field theory of pions is four-dimensional bosonic theory, the critical exponent is given by the mean-field approximation as $\nu = 1/2$. We here redefine $|M - M_c|$ as a quark mass m_q. By using this critical exponent, we obtain the relation between the pion mass and the quark mass as

$$m_\pi^2 = C m_q, \tag{2.68}$$

where C is a constant depending on the lattice spacing or the bare gauge coupling. In the continuum limit this constant correctly produces the pion decay constant. It is surprising that we obtain the PCAC relation without using chiral symmetry. Thus the existence of the Aoki phase diagram and the second-order phase transition clearly indicates the applicability of Wilson-type fermions to lattice QCD simulations. This fact will become quite important in chapter 6 where we will discuss application of new lattice fermions.

Now we follow the process of derivation of the hadron mass in lattice QCD simulations with this fermion [64, 65]. There are two processes we need to take; one is the chiral limit and the other is the continuum limit. The goal is to derive the hadron mass for the light quark mass limit $m_q = m_l$ and the continuum limit $a \to 0$ or $g_0 \to 0$. To take the two limits, we need two physical quantities as input parameters. We here choose the pion mass m_π and the rho meson mass m_ρ. We first take an arbitrary value of the bare coupling g_0, for example, $g_0^2 = 1$, which corresponds to a certain value of the lattice spacing a. The first thing we need to do is tune the quark mass parameter so that it gives the physical ratio of the two mesons $m_\pi a / m_\rho a = 0.135/0.770 = 0.18$. Practically we extrapolate calculated results of the hadron mass to this physical point. Here the quark mass parameter is defined as $m_q a = M - M_c$ as we have discussed in (2.68). Note that we restore the lattice coupling here. If we compute the pion mass for several m_q near $m_q = 0$, we find the PCAC relation up to the quadratic and higher corrections as

$$(m_\pi a)^2 = A_\pi m_q a + B_\pi (m_q a)^2 + ... \tag{2.69}$$

Here we consider a fitting function up to the second order. Fitting parameters A_π and B_π are derived by fitting computed results to this equation. For the rho meson mass, we can also have a fitting function of the quark mass parameter as

$$m_\rho a = A_\rho + B_\rho (m_q a) + ... \tag{2.70}$$

A_ρ and B_ρ are also obtained by fitting. Then the square ratio of them is given by

$$\frac{(m_\pi a)^2}{(m_\rho a)^2} = \frac{135^2}{770^2} = \frac{A_\pi m_q a + B_\pi (m_q a)^2}{(A_\rho + B_\rho (m_q a))^2}. \tag{2.71}$$

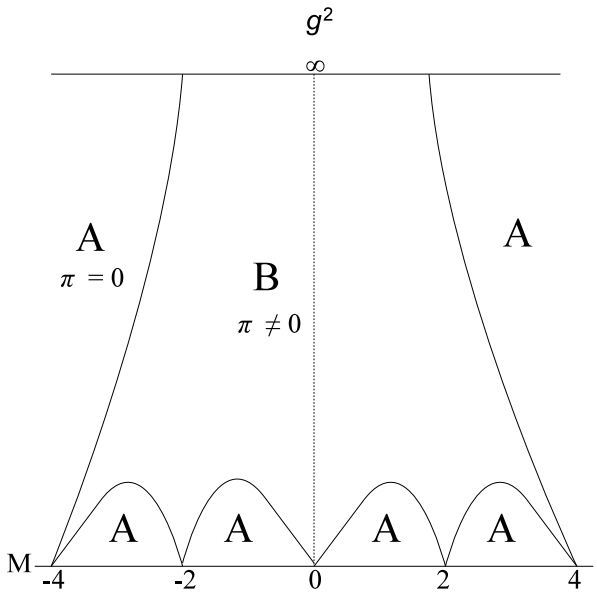

Figure 2.5: The parity phase structure for the Wilson fermion (Aoki phase) in ref.[35]. B corresponds to the parity-broken phase where the pion condensate is nonzero as $\langle\bar{\psi}\gamma_5\psi\rangle \neq 0$. We define M as $\mathrm{M} = m + 4r$. There are five cusps corresponding 1, 4, 6, 4 and 1 fermion branches in the Dirac spectrum. The usual chiral limit is taken by tuning the mass parameter to the rightest critical line.

This is just a quadratic equation of $m_q a$. By solving this equation we derive the light quark mass limit. In the study by the CP-PACS collaboration [64, 65], the light quark mass limit is given by $m_q a = m_l a = 0.0015$. We now figure out the lattice coupling a for $g_0^2 = 1$. By using the fitting equation for the rho meson mass and $m_l a = 0.0015$, we derive the lattice spacing as

$$a = \frac{A_\rho + B_\rho (m_l a)}{770[\mathrm{MeV}]}. \tag{2.72}$$

In the above study, it is given by $a = 0.387[\mathrm{GeV}^{-1}]$. We have finished the preparation. Let us predict the neutron mass $m_N a$ from the lattice simulation. The neutron mass is also fit by an appropriate function as

$$m_N a = A_N + B_N m_q a + C_N (m_q a)^2. \tag{2.73}$$

Here the three fitting parameters A_N, B_N and C_N are determined by fitting. Then the neutron mass in the light quark mass limit is given by

$$m_N = \frac{A_N + B_N m_l a + C_N (m_l a)^2}{a}, \tag{2.74}$$

with $m_l a = 0.0015$. We borrow the result $m_N = 989[\mathrm{MeV}]$ from [64, 65]. The next step is to take a continuum limit $a \to 0$. By repeating the process of the chiral limit for several values of the bare gauge coupling g_0^2, we obtain the fitting function of the lattice spacing as

$$m_N(a) = m_N(0) + C_1 a + C_2 a^2 + ..., \tag{2.75}$$

where C_1 and C_2 are fitting parameters. Finally we extrapolate the results to the $a \to 0$ limit, and we obtain a result of the neutron mass in the continuum limit. The references [64, 65] shows $m_N(a \to 0) \sim 930\mathrm{MeV}$, which is consistent with the experimental value. Here we omit the process of the infinite volume limit and evaluation of errors. What we want to emphasize here is we can perform lattice QCD with the Wilson fermion, although the chiral limit process requires much numerical cost. One of the main theme of this thesis is to improve this simulations by introducing new types of Wilson fermions.

In the end of this section, we note the additional $\mathrm{U}(1)_V^-$ symmetry appears if m and r satisfy $m + 4r = 0$, at which the on-site terms cancel out between the mass term and the Wilson term [57]. The site-dependent U(1) vector transformation, $\mathrm{U}(1)_V^-$, defined by

$$\psi_n \to \psi'_n = e^{\mathrm{i}(-1)^{n_1+\ldots+n_4}\theta}\psi_n\,, \quad \bar{\psi}_n \to \bar{\psi}'_n = e^{\mathrm{i}(-1)^{n_1+\ldots+n_4}\theta}\bar{\psi}_n\,. \tag{2.76}$$

This choice of the mass parameter $m + 4r = 0$ corresponds to the central cusp in the Aoki phase Fig. 2.5, to which the six fermion modes corresponds. As shown in [57] by the present author, this symmetry is spontaneously broken by the pion condensate, $\langle\bar{\psi}\gamma_5\psi\rangle$ where the associated NG boson appears. The six-flavor and 12-flavor QCD can be simulated with this parameter choice in the Wilson fermion.It has possibility to contribute to recent searches for the conformal window [66, 68, 69, 71, 72, 73, 74].

2.5 Overlap fermion

The overlap and Domain-wall fermions are constructed from the Wilson fermion. As we discussed in the introduction in 1, the domain-wall fermion becomes equivalent to the overlap fermion in the large 5th-volume limit. Thus we here concentrate only on the overlap fermion. Since we will argue new types of overlap fermions in chapter 5 in details. we here discuss the overlap Dirac operator for later convenience. We just note that symmetries of the overlap fermion are the same with the Wilson fermion except the Ginsparg-Wilson relation, which we will discuss later. The overlap formula is essentially given by the sign function of the Wilson Dirac kernel with appropriate negative mass as

$$D_{ov} = 1 + \gamma_5 \frac{H_W(m)}{\sqrt{H_W^2(m)}} = 1 + \frac{D_W(m)}{\sqrt{D_W^\dagger(m) D_W(m)}}, \tag{2.77}$$

where the mass parameter should be negative in the range as $-2 < m < 0$. We define the Wilson Dirac operator for $r = 1$ as

$$D_W(m)_{xy} = \frac{1}{2}\gamma_\mu (V_\mu - V_\mu^\dagger) + \frac{1}{2}\sum_\mu (2\delta_{xy} - V_\mu - V_\mu^\dagger) + m\delta_{xy}, \tag{2.78}$$

with $(V_\mu)_{xy} = U_{\mu,x}\delta_{y,x+\mu}$ in the presence of the link variables. $H_W(m)$ is a hermitean version of the Dirac operator defined as

$$H_W(m)_{xy} = \gamma_5 D_W(m)_{xy}. \tag{2.79}$$

Fermion modes with negative mass in D_W translate into massless modes in the overlap formula in (2.77) since the sign function gives -1 for the negative-mass mode while it gives $+1$ for the positive-mass mode near the zero momentum $p = 0$. If we set the mass parameter as $-2 < m < 0$, only the physical branch in the Dirac spectrum crosses the real axis at a negative value, which corresponds to the negative mass, while the other doubler branches crosses at the positive points. This situation is depicted as Fig. 2.3 where only the left branch crosses the real axis at a negative point. Then we obtain one massless mode from the overlap formula with the Wilson kernel. What is outstanding in this formalism is that the overlap fermion possesses a kind of exact chiral symmetry, which is a modified chiral symmetry compatible with the lattice discretization. It is given by the anti-commutation relation of the overlap Dirac operator with γ_5 as

$$\{\gamma_5, D_{ov}\} = a D_{ov}\gamma_5 D_{ov}, \tag{2.80}$$

where we tentatively restore the lattice spacing. This relation is called the Ginsparg-Wilson relation, which results in the usual chiral symmetry in the continuum limit. Although it is a modified chiral symmetry, it works as the chiral symmetry, for example, to prevent the mass term from being generated by quantum corrections. We can also translate this symmetry as a modification of γ_5 to $\gamma_5(1 - aD_{ov})$. Since the usual chiral symmetry is broken explicitly, this is not inconsistent with the no-go theorem [4]. We note that this lattice formulation is a theoretical solution to the doubling problem.

Here we look into the eigenvalue spectrum of the overlap Dirac operator where we still consider the negative mass in the range $-2 < m < 0$. We first note the overlap Dirac operator again satisfies γ_5 hermiticity as $\gamma_5 D_{ov}\gamma_5 = D_{ov}^\dagger$ We define ϕ and λ as an eigenfunction and an eigenvalue of D_{ov} as $D_{ov}\phi = \lambda\phi$. By considering the complex conjugate of this equation, we have $\phi^\dagger D_{ov}^\dagger = \phi^\dagger\bar{\lambda}$ where $\bar{\lambda}$ is defined as the complex conjugate of λ. We now rewrite the Ginsparg-Wilson relation (2.80) into an equation for eigenvalues by using γ_5 hermiticity as

$$\begin{aligned} & D_{ov} + \gamma_5 D_{ov}\gamma_5 = a\gamma_5 D_{ov}\gamma_5 D_{ov}, \\ \rightarrow \quad & D_{ov} + D_{ov}^\dagger = a D_{ov}^\dagger D_{ov}, \\ \rightarrow \quad & \phi^\dagger(\lambda + \bar{\lambda})\phi = \phi^\dagger a\bar{\lambda}\lambda\phi\,. \end{aligned} \tag{2.81}$$

We separate the eigenvalue λ as $\lambda = x + iy$, then we find

$$(x - \frac{1}{a})^2 + y^2 = \left(\frac{1}{a}\right)^2, \tag{2.82}$$

which is depicted as Fig. 2.6. The spectrum is perfectly circle-shape at least for the free case. The eigenvalues around $\lambda = 0$ corresponds to the physical massless mode while the eigenvalues around $\lambda = 2/a$ correspond to the doubler modes with $O(1/a)$ mass. This is because the the Dirac operator in (2.77) gives a eigenvalue 0 for the negative mass mode while it gives $2/a$ for the positive mass mode in the zero momentum case when the lattice spacing is manifest. In the continuum limit ($a \rightarrow 0$), the spectrum around $\lambda = 0$ gets sticked to the imaginary axis. It indicates that this spectrum assimilate into spectrum of the continuum theory in the continuum limit. Since the Ginsparg-Wilson relation prohibits additive mass renormalization, this property of the spectrum around $\lambda = 0$ holds for the gauge theory. On the other hand, the doubler modes around $\lambda = 2/a$ decouple with infinite mass in $a \rightarrow 0$ limit. We end up obtaining one massless fermion in the continuum even if the link variable is intorduced.

The only but the worst disadvantage of this formulation is that it is unsuitable for the numerical calculation since the overlap Dirac operator includes the sign function. This kind of the discrete function is sensitive to the numerical errors related to gauge configurations, and it is difficult to calculate the fermion propagator in this case. There have been lots of attempts to improve lattice simulations with overlap fermions [88]. Due to these struggles people have recently succeeded to apply this fermion to lattice QCD calculations, which yields the outstanding success in the realization of spontaneous chiral symmetry breaking for the first time [89]. However what we can calculate with this formulation is still restricted to quantities requiring small numerical costs, although it is the most theoretically established fermion formulation on the lattice. What we need now is a new improved version of the overlap fermion requiring less numerical cost. From the next chapter we will show we are able to acquire such a formulation by using staggered fermions.

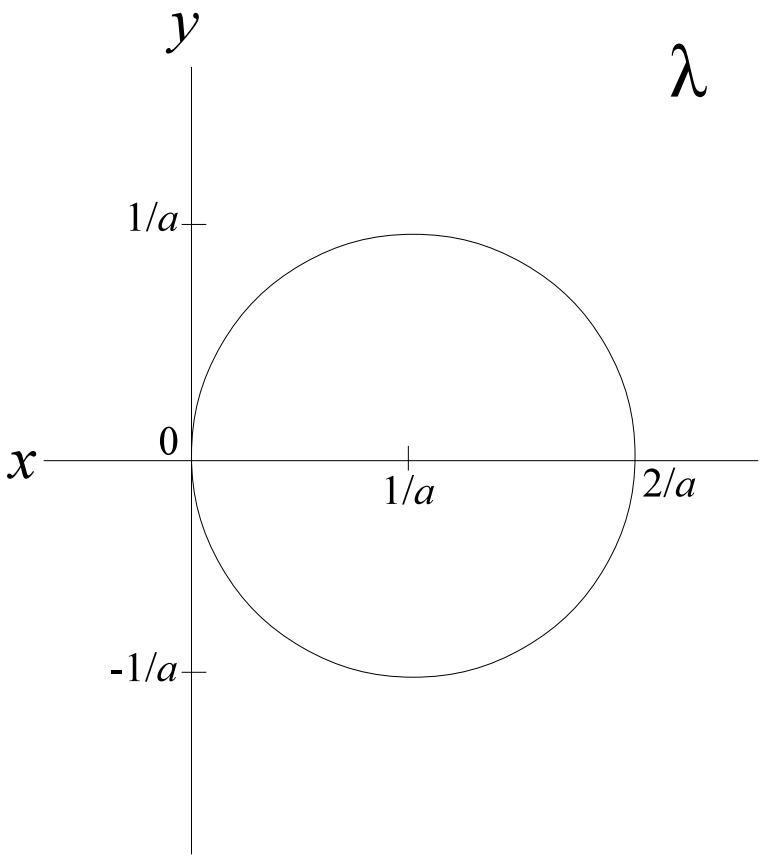

Figure 2.6: The complex Dirac spectrum for the free overlap fermion.

Chapter 3

Flavored mass terms

From this chapter we discuss a generalization of Wilson fermions, which yield a new class of the lattice fermions. The key for this goal is a species-splitting mass term or a "flavored-mass term". As we have shown in 2, the Wilson term lifts the degenerate mass of 16 species into the 5 branches, to which the 1, 4, 6, 4 and 1 fermion modes correspond respectively. In terms of the eigenvalue spectrum of the Dirac operator, the Wilson term split the 16 degenerate imaginary spectrum into 5 complex branches whose crossings with the real axis stand for their O(1/a) masses Fig. 2.3. In the practical lattice QCD, we need to tune the mass parameter so that one fermion mode at the most left branch has zero or O(1) quark mass while the other 15 fermion modes are decoupled with infinite mass in the $a \to 0$ limit. However we want to emphasize that there are more possibilities of the species-splitting ways other than the original one of the Wilson term. This is a starting point of the generalization of the Wilson term to the flavored-mass terms, which gives us a wide class of lattice fermions.

We note the "generalization" has the two-folded meanings: One is a generalization of the Wilson term within the naive fermion action, and the other is a generalization of the flavored-mass terms to staggered fermion actions. The former generalization leads to the generalized Wilson fermions with any number of flavors [29]. By this formulation, we are able to simulate two or three-flavor QCD with only one lattice fermion. There is also a possibility that we can study many-flavor QCD with these fermions. Not to mention, we can build the generalized overlap or domain-wall with any number of flavors from the generalized Wilson fermions. The latter gives us the staggered-based Wilson and overlap fermions, which we call the staggered-Wilson and staggered-overlap fermions [30, 31, 32]. As we will show, there are two types of the flavored-mass terms for the staggered fermions, where the four degenerate species are decomposed into $(2, 2)$ and $(1, 2, 1)$ branches respectively. By using them we can construct one-flavor and two-flavor staggered-Wilson fermions, by which we simulate the two or three-flavor QCD. One of the potential advantages of these formulations based on the staggered fermions is the reduction of the matrix of the Dirac operator, which leads to the reduction of the numerical costs. As we discussed in the previous chapter, the overlap formulation requires terribly expensive numerical tasks. The staggered-overlap fermion can improve this situation, or resolve the contradiction between the theoretical solution and the practical properties for computation.

In this chapter, we first consider a flavored-mass term for the minimally-doubled fermion as a toy model case. The minimally-doubled fermion [16, 17, 18, 20] is a well-known lattice fermion formulation which contains only two species, a minimal number allowed by the no-go theorem [4]. SInce these break Lorentz symmetry explicitly, they have not been applied to lattice QCD. However, the study on this fermion enables us to understand generic properties of the flavored-mass term since it possesses minimal species and the structure of doublers is simplest. After looking into the properties of the flavored-mass terms by the toy model, we move to the flavored-mass terms for the naive and staggered fermions.

Here let us roughly describe the method to construct the flavored-mass terms. If we have an independent field corresponding to each of species, in principle we can assign different masses to each of species. The method called "point-splitting" [90] enables us to treat species as independent fields. In this method we essentially divide the Brillouin zone into a number of momentum regions, each of which contains only one pole of the Dirac propagator. Then we define fermion fields corresponding species in accordance with the divided regions. Fortunately the staggered fermion has specie or tastes as different fields defined on different sites, thus we straightforwardly construct specie-fields in this case. However the species fields are actually not independent since they contain several chiral pairs in general. Thus, for the purpose of constructing the physical flavored-mass terms, we need to impose another condition. This is the γ_5 hermiticity: $(\gamma_5 D)^\dagger = \gamma_5 D$. This condition guarantees that the Dirac eigenvalues appear as the complex conjugate pair except the real eigenvalues, which results in the real and positive fermion determinant. The pairing of the Dirac eigenvalues and positivity of the determinant are essential properties for the path integral formulation of the euclidean field theory. The γ_5 hermiticity also works to eliminate the unphysical form of the flavored-mass terms since γ_5 respects the relation of the doubler pairs well. As such we obtain a proper flavored-mass term for the lattice fermions with the species-doublers. Note the results in this chapter are based on the original work by the present author in Ref. [29, 75]. However only the argument on the flavored-mass terms for the staggered fermions is based on Ref. [30, 31, 32].

We here remark on the notation of the lattice sites. From this chapter we basically use x instead of n to represent lattice sites since we need to use n for other indices sometimes. Of course, the lattice site x stands for d integer numbers for the d dimensional lattice.

3.1 Flavored mass for minimally doubled fermions

Here we introduce the point-splitting method [90] to obtain flavored mass terms in minimally doubled fermions. We begin with the introduction of minimally doubled fermions. The $d = 4$ Karsten-Wilczek action [16, 17] is obtained by introducing a Wilson-like term

proportional to $i\gamma_4$. Its position-space expression is

$$\begin{aligned} S_{\rm md} &= \sum_x \Bigg[\frac{1}{2}\sum_{\mu=1}^{3} \bar{\psi}_x \gamma_\mu \left(U_{x,\mu}\psi_{x+\mu} - U_{x,-\mu}\psi_{x-\mu} \right) \\ &\quad + \frac{i}{\sin\alpha} \left((\cos\alpha + 3)\bar{\psi}_x\gamma_4\psi_x - \frac{1}{2}\sum_{\mu=1}^{4} \bar{\psi}_x\gamma_4 \left(U_{x,\mu}\psi_{x+\mu} + U_{x,-\mu}\psi_{x-\mu} \right) \right) \Bigg], \end{aligned} \tag{3.1}$$

where the link variables satisfy $U_{x,\mu} = U^\dagger_{x+\mu,-\mu}$. For the free theory, the associated Dirac operator in momentum space is given by

$$D_{\rm md}(p) = i\sum_{\mu=1}^{3} \gamma_\mu \sin p_\mu + \frac{i\gamma_4}{\sin\alpha} \left(\cos\alpha + 3 - \sum_{\mu=1}^{4} \cos p_\mu \right), \tag{3.2}$$

where the parameter α adjusts the relative positions of zeros. It has only two zeros located at $p = (0, 0, 0, \pm\alpha)$. These two species are not equivalent since the gamma matrices are differently defined between them as $\gamma'_\mu = \Gamma^{-1}\gamma_\mu\Gamma$. In the above case the transformation matrix is given by $\Gamma = i\gamma_4\gamma_5$. This means the chiral symmetry possessed by this action is identified as a flavored one given by $\gamma_5 \otimes \tau_3$.

The point-splitting identifies these inequivalent species as independent flavors. In this method each flavor field is defined so that the associated propagator includes only a single pole. The simplest way of doing this is to define two independent fields in the two-divided Brillouin zones. However in this case the fields discretely disappear at the boundary of the two momentum regions. This definition in the momentum space result in the superposition of fermion fields defined on lots of different sites in the position space. On the other hand the point-splitting method enables us to define the species fields by using only the nearest-neighbor fields in the positions space. Let us look into the example: The point-split fields for this case is built by multiplying momentum functions removing another undesired pole in momentum space,

$$u(p - \alpha e_4) = \frac{1}{2}\left(1 + \frac{\sin p_4}{\sin\alpha} \right) \psi(p), \tag{3.3}$$

$$d(p + \alpha e_4) = \frac{1}{2}\Gamma\left(1 - \frac{\sin p_4}{\sin\alpha} \right) \psi(p). \tag{3.4}$$

Here $u(p - \alpha e_4)$ and $d(p + \alpha e_4)$ fields correspond to the poles at $p = (0, 0, 0, \alpha)$ and $(0, 0, 0, -\alpha)$, respectively. One of them becomes zero at the zero point of the other and vice-versa. Thus both of them yield single fermionic modes. Since there are no discrete definition in the momentum space, we remark the associated point-split fields in position space are composed of the original field and the two kinds of nearest neighbors [90]. With these flavor fields we obtain a flavor-multiplet field as following,

$$\Psi(p) = \begin{pmatrix} u(p - \alpha e_4) \\ d(p + \alpha e_4) \end{pmatrix}. \tag{3.5}$$

Here γ_5 multiplication on the original Dirac field is identified as

$$\gamma_5\psi(p) \quad \longrightarrow \quad \begin{pmatrix} +\gamma_5 & \\ & -\gamma_5 \end{pmatrix} \Psi(p) = (\gamma_5 \otimes \tau_3)\, \Psi(p). \tag{3.6}$$

Here we introduce a multiplet representation as a direct product of the Pauli matrix to express the 2-flavor structure. It means the flavored chiral symmetry generated by $\gamma_5 \otimes \tau_3$ is exactly preserved in terms of the flavor multiplet while the flavor singlet chiral symmetry given by $\gamma_5 \otimes \mathbf{1}$ is broken by discretization errors.

Now we can introduce a flavored mass term into minimally doubled fermions. We need to impose the γ_5 hermiticity for the Dirac operator with the flavored mass term, which leads to the γ_5 commutativity of the flavored-mass terms. Since γ_5 is here regarded as $\gamma_5 \otimes \tau_3$ in terms of the flavor multiplet as shown in (3.6)., the only possibility of the flavored mass to commute with γ_5 is

$$M_{\tau_3} \sim (\mathbf{1} \otimes \tau_3)\,. \tag{3.7}$$

It is quite natural that there is only one type of the flavored mass term for this fermion since there is only one possible mass splitting for two species. To implement this flavored mass term into the action, we rewrite it with the original Dirac field as

$$\bar{\Psi}(p)\,(\mathbf{1} \otimes \tau_3)\,\Psi(p) = \bar{u}u(p - \alpha e_4) - \bar{d}d(p + \alpha e_4) = \frac{\sin p_4}{\sin \alpha}\bar{\psi}(p)\psi(p). \tag{3.8}$$

It is straightforward to obtain the mass term in the position space with the link variables present,

$$M_{\tau_3} = \frac{m_{\tau_3}}{2i \sin \alpha}\bar{\psi}_x \left(U_{x,\hat{4}}\psi_{x+\hat{4}} - U_{x,-\hat{4}}\psi_{x-\hat{4}}\right). \tag{3.9}$$

where we introduce the parameter m_{τ_3}. The associated Dirac operator $D_{\mathrm{md}} - M_{\tau_3}$ is non-Hermitean, and when gauge fields are present the mass term does not commute with the kinetic term $[D_{\mathrm{md}}, M_{\tau_3}] \neq 0$. Thus the Dirac operator eigenvalues become complex. Indeed it is essential for the purpose to detect the index from the spectral flow of the Hermitean operator since it relies on real eigenvalues of the Dirac operator as will shown in 5.

In Fig. 3.1 we show a numerical result of complex eigenvalues of the Dirac operator for the $d = 2$ free case with a parameter $\alpha = \pi/2$. Here the low-lying spectrum is split into two branches crossing the real axis at the magnitude of the mass parameter $|m_{\tau_3}|$. It means that the flavored mass $-M_{\tau_3} = \mathrm{diag}(-m_{\tau_3}, +m_{\tau_3})$ assigns $-m_{\tau_3}(+m_{\tau_3})$ to modes depending on $+1(-1)$ chiral charges, or equivalently $+1(-1)$ eigenvalues for $\mathbf{1} \otimes \tau_3$. In other words the flavored mass term splits the minimally doubled fermion into two single Dirac fermions with $-m_{\tau_3}$ and $+m_{\tau_3}$. In Sec. 5.1 we will see this flavored mass gives the spectral flow of the Hermitean operator illustrating the correct index related to the gauge topology.

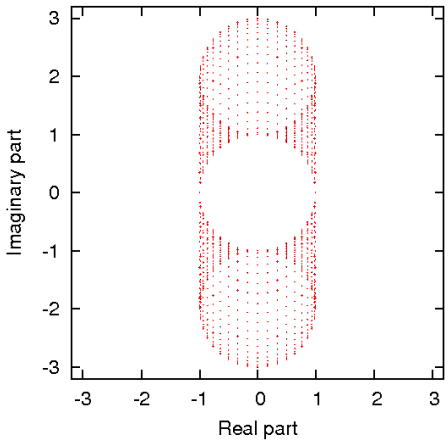

Figure 3.1: Complex spectrum of the free non-Hermitean Dirac operator $D_{\rm md} - M_{\tau_3}$ for the $d = 2$ free field case on a 36×36 lattice with a mass parameter $m_{\tau_3} = 1$. The spectrum is split into two branches crossing the real axis at $|m_{\tau_3}|$.

3.2 Flavored mass for Naive fermions

We can apply the same approach to the naive lattice fermion [1] to obtain proper flavored mass terms. The action of the naive fermions in general dimensions is simply given by

$$S_{\rm n} = \frac{1}{2} \sum_x \sum_{\mu=1}^{d} \bar{\psi}_x \gamma_\mu \left(U_{x,\mu} \psi_{x+\mu} - U_{x,-\mu} \psi_{x-\mu} \right). \tag{3.10}$$

For simplicity we first consider the $d = 2$ naive fermions. The Dirac operator has four zeros $(0,0)$, $(\pi,0)$, $(0,\pi)$ and (π,π) in momentum space, thus we introduce four associated point-split fields

$$\begin{aligned}
\psi_{(1)}(p - p_{(1)}) &= \frac{1}{4}(1+\cos p_1)(1+\cos p_2)\Gamma_{(1)}\psi(p), \\
\psi_{(2)}(p - p_{(2)}) &= \frac{1}{4}(1-\cos p_1)(1+\cos p_2)\Gamma_{(2)}\psi(p), \\
\psi_{(3)}(p - p_{(3)}) &= \frac{1}{4}(1+\cos p_1)(1-\cos p_2)\Gamma_{(3)}\psi(p), \\
\psi_{(4)}(p - p_{(4)}) &= \frac{1}{4}(1-\cos p_1)(1-\cos p_2)\Gamma_{(4)}\psi(p),
\end{aligned} \tag{3.11}$$

whose locations of zeros, chiral charges and transformation matrices Γ giving the corresponding set of gamma matrices, $\gamma_\mu^{(i)} = \Gamma_{(i)}^\dagger \gamma_\mu \Gamma_{(i)}$, are listed in Table 3.1. Although there is slight arbitrariness of choice of the point-splitting field, the difference only affect the $O(a)$ discretization errors which have no influence on the form of the flavored-mass terms.

label	position	χ charge	Γ
1	$(0,0)$	$+$	$\mathbf{1}$
2	$(\pi,0)$	$-$	$i\gamma_1\gamma_5$
3	$(0,\pi)$	$-$	$i\gamma_2\gamma_5$
4	(π,π)	$+$	γ_5

Table 3.1: Chiral charges and transformation matrices for each of zeros in the $d = 2$ naive fermions with $\gamma_1 = \sigma_1$, $\gamma_2 = \sigma_2$ and $\gamma_5 = \sigma_3$.

The flavor-multiplet field is given by

$$\Psi(p) = \begin{pmatrix} \psi_{(1)}(p - p_{(1)}) \\ \psi_{(2)}(p - p_{(2)}) \\ \psi_{(3)}(p - p_{(3)}) \\ \psi_{(4)}(p - p_{(4)}) \end{pmatrix}. \tag{3.12}$$

Here the operation of γ_5 on the original fermion field again means the flavored chiral transformation in the sense of the flavor multiplet as

$$\gamma_5\psi(p) \quad \longrightarrow \quad \begin{pmatrix} +\gamma_5 & & & \\ & -\gamma_5 & & \\ & & -\gamma_5 & \\ & & & +\gamma_5 \end{pmatrix} \Psi(p) = (\gamma_5 \otimes (\tau_3 \otimes \tau_3))\, \Psi(p). \tag{3.13}$$

Here we introduce a multiplet representation as two direct products of the Pauli matrix to express the 4-flavor structure. To obtain the flavored mass terms producing physical fermions, we again impose the γ_5 hermiticity of the Dirac operator with the flavored mass terms which yields only the flavored-mass terms respecting the relation of the doubler pairs. Thus we impose the γ_5 commutativity. Now γ_5 is expressed as $(\gamma_5 \otimes (\tau_3 \otimes \tau_3))$ in the flavor multiplet, there four possible flavored mass terms for the 2d naive fermion are given by

$$\bar{\Psi}(p)\, (\mathbf{1} \otimes (\tau_3 \otimes \tau_3))\, \Psi(p) = \cos p_1 \cos p_2 \bar{\psi}(p)\psi(p), \tag{3.14}$$

$$\bar{\Psi}(p)\, (\mathbf{1} \otimes (\tau_3 \otimes \mathbf{1}))\, \Psi(p) = \cos p_1 \bar{\psi}(p)\psi(p) + O(a), \tag{3.15}$$

$$\bar{\Psi}(p)\, (\mathbf{1} \otimes (\mathbf{1} \otimes \tau_3))\, \Psi(p) = \cos p_2 \bar{\psi}(p)\psi(p) + O(a), \tag{3.16}$$

$$\bar{\Psi}(p)\, (\mathbf{1} \otimes (\mathbf{1} \otimes \mathbf{1}))\, \Psi(p) = \bar{\psi}(p)\psi(p) + O(a). \tag{3.17}$$

Here the concrete form of $O(a)$ discretization errors depends on the choice of the point-splitting fields since the choice of the point-splitting fields have small arbitrariness as we have discussed in the previous section. If we choose the other form of the flavor multiplet, it is also possible to eliminate the errors. However our purpose is just to find a proper flavored-mass terms. Therefore, once we know the leading forms of the flavored-mass term, we do not need to care about the discretization errors. (Actually the Wilson term also contains this kind of the errors.) All of these mass terms are spread over several nearby sites, and therefore their position-space expressions include hopping terms

with associated gauge field matrices. It is convenient to introduce the usual translation operators $T_{\pm\mu}\psi_x = U_{x,\pm\mu}\psi_{x\pm\mu}$ and $C_\mu = (T_{+\mu} + T_{-\mu})/2$. Then the flavored mass for the index (3.14) is written in the position space as

$$M_{\tau_3\otimes\tau_3} = m_{\tau_3\otimes\tau_3}\sum_{sym.} C_1C_2 \equiv M_{\rm n}, \tag{3.18}$$

$$M_{\tau_3\otimes\mathbf{1}} = m_{\tau_3\otimes\mathbf{1}}C_2, \tag{3.19}$$

$$M_{\mathbf{1}\otimes\tau_3} = m_{\mathbf{1}\otimes\tau_3}C_1, \tag{3.20}$$

$$M_{\mathbf{1}\otimes\mathbf{1}} = m, \tag{3.21}$$

where $\sum_{sym.}$ stands for symmetric summation over the order of the factors C_1 and C_2, and $m_{\tau_3\otimes\tau_3}$, $m_{\tau_3\otimes\mathbf{1}}$, $m_{\mathbf{1}\otimes\tau_3}$ and m stand for flavored-mass parameters and a usual mass parameter. It is clear that if you use the second or third ones, we need to take a sum of them to restore the Lorentz symmetry the continuum limit. What we want to emphasize here is the non-trivial flavored-mass terms with a proper mass shift results in the second-derivative terms proportional to a. For example, we find

$$\sum_n \bar\psi_n(M_{\tau_3\otimes\tau_3} - 1)\psi_n \;\to\; -a\int d^2x\bar\psi(x)D_\mu^2\psi(x) + O(a^2), \tag{3.22}$$

for $m_{\tau_3\otimes\tau_3} = 0$. This irrelevant term disappears in the classical continuum limit. Thus our formulation of constructing the lattice fermion action is consistent with the criterion for the usual Wilson fermion. It is also the case with the sum of $2 - M_{\tau_3\otimes\mathbf{1}} + M_{\mathbf{1}\otimes\tau_3}$ with $m_{\tau_3\otimes\mathbf{1}} = m_{\mathbf{1}\otimes\tau_3} = 0$, which is exactly two-dimensional Wilson term. This results indicate the naive fermions with these flavored-mass terms work as the generalized Wilson fermions.

Now let us look into the eigenvalues of the $d = 2$ naive Dirac operator $D_{\rm n} - M_{\rm f}$ with the flavored-mass term. In Fig. 3.2 we show a numerical result of the complex eigenvalues for the case of $M_{\rm f} = M_{\tau_3\otimes\tau_3}$. Here the low-lying spectrum is again split into two branches crossing the real axis at the magnitude of the mass parameter $|m_f|$ where we redefine $m_{\tau_3\otimes\tau_3} \equiv m_f$. However in this case both of the two branches are doubled. (We will be convinced of this doubling in Fig. 5.4 where it is lifted by the other mass terms.) It means that the flavored mass term $-M_{\tau_3\otimes\tau_3} = \mathrm{diag}(-m_f, +m_f, +m_f, -m_f)$ assigns $-m_f(+m_f)$ to modes depending on $+1(-1)$ chiral charges, or $+1(-1)$ eigenvalues for $\mathbf{1}\otimes(\tau_3\otimes\tau_3)$. Thus the $d = 2$ naive fermion with 4 species is split into two pairs of Dirac fermions with $-m_f$ and $+m_f$. In 5 we will show the spectral flow of the associated Hermitean operator gives the correct index related to the gauge topology.

Now we move to the $d = 4$ case obtain In this case there are more possibilities for flavored mass. We introduce 16 point-split fields, corresponding to 16 species doublers of

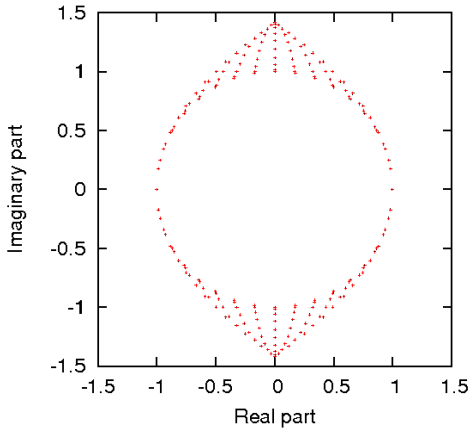

Figure 3.2: Complex spectra of non-Hermitean Dirac operator $D_{\rm f} - M_{\tau_3\otimes\tau_3}$ for the $d = 2$ free field case on a 36×36 lattice with mass parameter $m_{\tau_3\otimes\tau_3} = 1$.The spectrum is split into two doubled branches crossing the real axis at $|m_{\tau_3\otimes\tau_3}|$.

the $d = 4$ naive fermions,

$$\begin{aligned}
\psi_{(1)}(p - p_{(1)}) &= \frac{1}{2^4}(1+\cos p_1)(1+\cos p_2)(1+\cos p_3)(1+\cos p_4)\Gamma_{(1)}\psi(p), \\
\psi_{(2)}(p - p_{(2)}) &= \frac{1}{2^4}(1-\cos p_1)(1+\cos p_2)(1+\cos p_3)(1+\cos p_4)\Gamma_{(2)}\psi(p), \\
\psi_{(3)}(p - p_{(3)}) &= \frac{1}{2^4}(1+\cos p_1)(1-\cos p_2)(1+\cos p_3)(1+\cos p_4)\Gamma_{(3)}\psi(p), \\
&\vdots \\
\psi_{(16)}(p - p_{(16)}) &= \frac{1}{2^4}(1-\cos p_1)(1-\cos p_2)(1-\cos p_3)(1-\cos p_4)\Gamma_{(16)}\psi(p),
\end{aligned} \tag{3.23}$$

where the positions of zeros in the momentum space, chiral charges and definitions of transformation matrices $\Gamma_{(i)}$ are listed in Table 3.2. Here a set of gamma matrices $\gamma_\mu^{(i)}$ defined for each zero is given by this $\Gamma_{(i)}$ as $\Gamma_{(i)}^{-1}\gamma_\mu\Gamma_{(i)} = \gamma_\mu^{(i)}$. We classify these zeros depending on this $\Gamma_{(i)}$. For example we denote A: axial for the case of $\Gamma_{(2)} = i\gamma_1\gamma_5$ while we assign T: Tensor for $\Gamma_{(4)} = i\gamma_1\gamma_2$. We introduce a flavor multiplet field with 16 components as

$$\Psi(p) = \begin{pmatrix} \psi_{(1)}(p - p_{(1)}) \\ \psi_{(2)}(p - p_{(2)}) \\ \vdots \\ \psi_{(16)}(p - p_{(16)}) \end{pmatrix}. \tag{3.24}$$

In this representation the chiral transformation matrix γ_5 is converted to $\gamma_5\otimes(\tau_3\otimes\tau_3\otimes\tau_3\otimes\tau_3)$, under which the naive action is invariant. Here we introduce a multiplet representation as four direct products of the Pauli matrix to express the 16 flavor structure. By imposing

label	position	χ charge	Γ	type
1	$(0,0,0,0)$	$+$	$\mathbf{1}$	S
2	$(\pi,0,0,0)$	$-$	$i\gamma_1\gamma_5$	A
3	$(0,\pi,0,0)$	$-$	$i\gamma_2\gamma_5$	A
4	$(\pi,\pi,0,0)$	$+$	$i\gamma_1\gamma_2$	T
5	$(0,0,\pi,0)$	$-$	$i\gamma_3\gamma_5$	A
6	$(\pi,0,\pi,0)$	$+$	$i\gamma_1\gamma_3$	T
7	$(0,\pi,\pi,0)$	$+$	$i\gamma_2\gamma_3$	T
8	$(\pi,\pi,\pi,0)$	$-$	γ_4	V
9	$(0,0,0,\pi)$	$-$	$i\gamma_4\gamma_5$	A
10	$(\pi,0,0,\pi)$	$+$	$i\gamma_1\gamma_4$	T
11	$(0,\pi,0,\pi)$	$+$	$i\gamma_2\gamma_4$	T
12	$(\pi,\pi,0,\pi)$	$-$	γ_3	V
13	$(0,0,\pi,\pi)$	$+$	$i\gamma_3\gamma_4$	T
14	$(\pi,0,\pi,\pi)$	$-$	γ_2	V
15	$(0,\pi,\pi,\pi)$	$-$	γ_1	V
16	(π,π,π,π)	$+$	γ_5	P

Table 3.2: Positions of zeros, chiral charges and definitions of transformation matrices for the $d = 4$ naive fermions. Letters of S, V, T, V and P stand for Scalar, Vector, Tensor, Axial-vector and Pseudo-scalar, respectively.

the γ_5 commutativity, we find 5 possible types of flavored mass terms which are given by

$$
\begin{aligned}
\mathrm{S} &: \quad \bar{\Psi}\left(\mathbf{1}\otimes(\mathbf{1}\otimes\mathbf{1}\otimes\mathbf{1}\otimes\mathbf{1})\right)\Psi \;=\; \bar{\psi}\psi \\
\mathrm{V} &: \quad \bar{\Psi}\left(\mathbf{1}\otimes(\tau_3\otimes\mathbf{1}\otimes\mathbf{1}\otimes\mathbf{1})\right)\Psi \;=\; \cos p_1\,\bar{\psi}\psi \\
\mathrm{T} &: \quad \bar{\Psi}\left(\mathbf{1}\otimes(\tau_3\otimes\tau_3\otimes\mathbf{1}\otimes\mathbf{1})\right)\Psi \;=\; \cos p_1\cos p_2\,\bar{\psi}\psi \qquad \text{etc,} \\
\mathrm{A} &: \quad \bar{\Psi}\left(\mathbf{1}\otimes(\mathbf{1}\otimes\tau_3\otimes\tau_3\otimes\tau_3)\right)\Psi \;=\; \left(\prod_{\mu=2}^{4}\cos p_\mu\right)\bar{\psi}\psi \\
\mathrm{P} &: \quad \bar{\Psi}\left(\mathbf{1}\otimes(\tau_3\otimes\tau_3\otimes\tau_3\otimes\tau_3)\right)\Psi \;=\; \left(\prod_{\mu=1}^{4}\cos p_\mu\right)\bar{\psi}\psi
\end{aligned}
$$

where we omit the $O(a)$ discretization errors. Here the V-type includes 4 varieties while the T-type has 6 varieties and the A-type 4 varieties, giving then the total number as 16. Each of these varieties breaks the hypercubic symmetry of the lattice since their hoppings are anisotropic. Thus we need to take a proper combination of them in order to construct a flavored mass term with hypercubic symmetry. For example we need to take s sum of the 4-direction V-type terms with the same ratios as in the case of $d = 2$. It is also the case with the T- and A-types. Thus the 4 types of non-tirivial flavored masses with the

symmetry in terms of the original fermion field are given by

$$M_{\rm V} = \sum_{\mu} C_\mu, \tag{3.25}$$

$$M_{\rm T} = \sum_{perm.} \sum_{sym.} C_\mu C_\nu, \tag{3.26}$$

$$M_{\rm A} = \sum_{perm.} \sum_{sym.} \prod_{\nu} C_\nu, \tag{3.27}$$

$$M_{\rm P} = \sum_{sym.} \prod_{\mu=1}^{4} C_\mu, \tag{3.28}$$

where $\sum_{perm.}$ means summation over permutations of the space-time indices. Note we define $\sum_{perm.}$ and $\sum_{sym.}$ as containing factors, for example, 1/4! for $M_{\rm P}$. The vector type $M_{\rm V}$ is exactly the same as the usual Wilson term up to mass shift. It indicates that we successfully extend the Wilson terms to the more general terms, or flavored-mass terms. The species-splitting is different between these flavored-mass terms, which we will depict in the following figures, The tensor-type mass $M_{\rm T}$ can be decomposed into three parts as

$$M_{\rm T} = M_{\rm T}^{(1)} + M_{\rm T}^{(2)} + M_{\rm T}^{(3)}, \tag{3.29}$$

$$M_{\rm T}^{(1)} = \frac{1}{2}(C_1C_2 + C_2C_1) + \frac{1}{2}(C_3C_4 + C_4C_3), \tag{3.30}$$

$$M_{\rm T}^{(2)} = \frac{1}{2}(C_1C_3 + C_3C_1) + \frac{1}{2}(C_2C_4 + C_4C_2), \tag{3.31}$$

$$M_{\rm T}^{(3)} = \frac{1}{2}(C_1C_4 + C_4C_1) + \frac{1}{2}(C_2C_3 + C_3C_2). \tag{3.32}$$

These fractions of tensor flavored-mass terms are of great importance in research on the staggered-flavored mass from the next section.

Here we discuss on the discrete rotational symmetry of these flavored-mass terms. The whole hypercubic symmetry holds in M_V, M_T, M_A and M_P, which is expected to result in the Euclidean Lorentz symmetry in the continuum limit. However, In the three decomposed tensor-type flavored-mass terms (3.30)(3.31)(3.32), the rotational symmetry is broken to the double rotational symmetry as $x \to \mathcal{R}_{\mu\nu}\mathcal{R}_{\sigma\rho}x$ with (μ, ν, ρ, σ) being any permutation of $(1, 2, 3, 4)$. Although this symmetry prohibits the relevant and marginal operators being generated by quantum corrections, it is not obviously clear whether or not it leads to the euclidian rotational symmetry in the continuum. As we will discuss on staggered-Wilson symmetry in the next chapter, we will show that this symmetry seems to be large enough to result in the Lorentz symmetry in the continuum limit.

We show that the non-trivial flavored-mass terms with a proper mass shift result in the second-derivative terms proportional to a near the classical continuum limit as in the usual Wilson fermion. For example,

$$\sum_n \bar{\psi}_n (M_P - 1)\psi_n \;\to\; -a \int d^4x \bar{\psi}(x) D_\mu^2 \psi(x) + O(a^2), \tag{3.33}$$

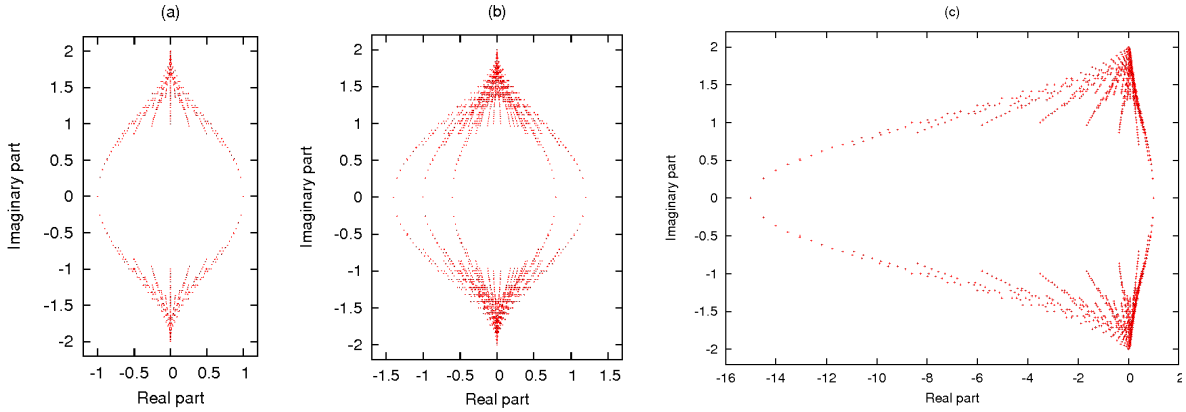

Figure 3.3: Complex spectra of non-Hermitean Dirac operators for the $d = 4$ free field case in momentum space with 16^4 grids of the brillouin zone. (a) $D_{\rm n} - M_{\rm P}$ with species split into $(8, 8)$. (b) $D_{\rm n} - (M_{\rm P} + 0.1M_{\rm A})$ with species split into $(2, 2, 4, 4, 4)$. (c) $D_{\rm n} - (M_{\rm P} + M_{\rm V} + M_{\rm T} + M_{\rm A})$ with species split into $(1, 15)$.

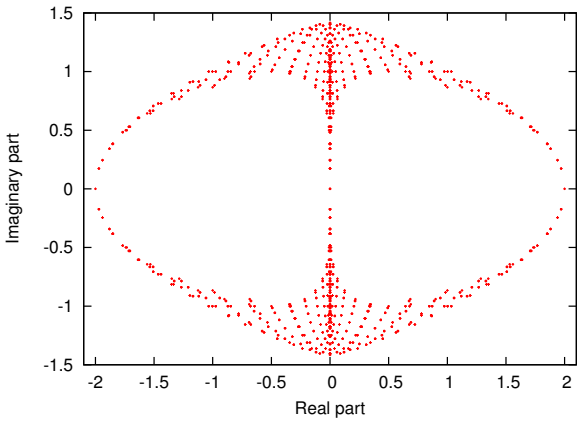

Figure 3.4: Complex spectra of non-Hermitean Dirac operators for the $d = 4$ free field case in momentum space with 16^4 grids of the brillouin zone for $D_{\rm n} - M_{\rm T}^{(i)}$ where $i = 1, 2, 3$. 16 species are split into $(4, 8, 4)$

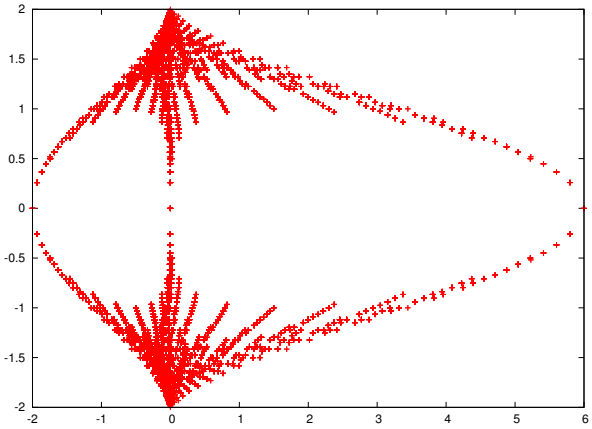

Figure 3.5: Complex spectra of non-Hermitean Dirac operators for the $d = 4$ free field case in momentum space with 16^4 grids of the brillouin zone for $D_{\rm n} - M_{\rm T}$ where $i = 1, 2, 3$. 16 species are split into $(6, 8, 2)$.

The other types including $M_{\rm T}^{(i)}$ $i = 1, 2, 3$ also satisfy this relation. It is consistent with the criterion for the Wilson fermion. The deviation from the usual Wilson fermion starts from $O(a^2)$ discretization errors. Thus, as long as we look at the physical branch, the difference of discretization errors between the generalized Wilson and the usual Wilson fermions is just $O(a^2)$. However the naive expansion about $a = 0$ is not valid for the other species. In fact the difference between the generalized and usual Wilson fermion is not negligible near zeros of doublers, which causes species splitting in a different way.

We note the vector type with the mass shift is exactly the Wilson term. We show the figure for eigenvalues of the free Dirac operator $D_{\rm n} - M_{\rm P}$ in Fig. 3.3(a). The mass term splits the modes into two branches, which are 8 fold degenerate. If we introduce other types of mass terms, the degeneracy is lifted as seen in Fig. 3.3(b). We also show the figure for eigenvalues of the free Dirac operator with the decomposed tensor flavored-mass terms $D_{\rm n} - M_{\rm T}^{(i)}$ in Fig. 3.4. The mass term splits the modes into three branches, which are 4, 8 and 4 fold degenerate. The Dirac spectrum with the summed tensor flavored-mass term $D_{\rm n} - M_{\rm T}^{(i)}$ in Fig. 3.5, where species are split into three branches with 6,8, and 2 fermion modes. We also consider the case of all the sum of them, which gives the one flavor branch as in in Fig. 3.3(c).

By using these flavored-mass terms, we obtain the generalized Wilson fermions with any flavor from one to sixteen. It is at least obvious that M_P gives 8-flavor Wilson fermions, $M_T^{(i)}$ gives 4-flavor fermions, M_T gives 2 and 6-flavor fermions, and $M_{V,A}$ gives 1-flavor fermions. Other flavor Wilson fermions can be obtained by combining more than two flavored- mass terms although we may need to care about potential renormalization of the rate of different types of flavored-mass terms. Possible applications are many-flavor QCD and the direct physical two- or three-flavor QCD. It also suggests the generalized overlap fermion is also constructed from these. Here we can obtain overlap fermions with any desirable flavors by letting the left branch contain a desirable flavor of species and shifting this branch to have the negative mass.

3.3 Flavored mass for staggered fermions

In this section we study staggered versions of the Wilson term, in which the flavored-mass terms lift the four degenerate tastes in a manner similar to the usual Wilson term. The concrete examples of the flavored-mass terms for the staggered fermions were first discussed in [59], and revisited in [30, 31, 32]. Thus the contents of this section are not a contribution from this thesis. However, as we will see later, I contribute much to this topic by studying the symmetries of them and the phase structure. Thus in this section we need to review details of this topic.

As we have seen, the Wilson term splits the degenerate 16 species into 5 branches where 1, 4, 6, 4 and 1 fermions live, which is just one example of the flavored-mass terms for the naive fermions [29, 75]. The significant condition for flavored-mass terms to yield physical fermions is that they should commute with γ_5 so that the Dirac operator satisfies the γ_5 hermiticity. We here note the natural definition of γ_5 in the naive fermion is flavored such as $\gamma_5 \otimes (\tau_3 \otimes \tau_3 \otimes \tau_3 \otimes \tau_3)$ in the spin-flavor representation. We have seen there are 4 types of non-trivial flavored-mass terms for the naive fermion which split species and satisfy γ_5 hermiticity. All these terms result in the same $O(a)$ form as $\sim a \int d^4x \bar{\psi} D_\mu^2 \psi$ near the continuum limit.

In a parallel way the staggered fermions also have non-trivial flavored-mass terms which split 4 tastes and commute with γ_5. In this case, the γ_5 is expressed in spin-taste representation as $\gamma_5 \otimes \gamma_5$, which we sometimes denote as Γ_{55}. Therefore we only have two choices of possible flavored-mass terms to satisfy the above conditions: $\mathbf{1} \otimes \gamma_5$ and $\mathbf{1} \otimes \sigma_{\mu\nu}$ ($\sigma_{\mu\nu} = i\gamma_\mu\gamma_\nu$). Actually these spin-flavor structures of flavored-mass terms are realized for one-component staggered fermions up to $O(a)$ discretization errors as

$$M_A = \epsilon \sum_{sym} \eta_1\eta_2\eta_3\eta_4 C_1C_2C_3C_4 = [\mathbf{1} \otimes \gamma_5] + O(a), \tag{3.34}$$

and

$$\begin{aligned} M_H &= M_H^{(1)} + M_H^{(2)} + M_H^{(3)}, \\ &= \frac{2}{\sqrt{3}}[\mathbf{1} \otimes (\sigma_{12} + \sigma_{34} + \sigma_{13} + \sigma_{42} + \sigma_{14} + \sigma_{23})] + O(a), \end{aligned} \tag{3.35}$$

$$M_H^{(1)} = \frac{i}{2\sqrt{3}}[\epsilon_{12}\eta_1\eta_2(C_1C_2 + C_2C_1) + \epsilon_{34}\eta_3\eta_4(C_3C_4 + C_4C_3)], \tag{3.36}$$

$$M_H^{(2)} = \frac{i}{2\sqrt{3}}[\epsilon_{13}\eta_1\eta_3(C_1C_3 + C_3C_1) + \epsilon_{42}\eta_4\eta_2(C_4C_2 + C_2C_4)], \tag{3.37}$$

$$M_H^{(3)} = \frac{i}{2\sqrt{3}}[\epsilon_{14}\eta_1\eta_4(C_1C_4 + C_4C_1) + \epsilon_{23}\eta_2\eta_3(C_2C_3 + C_3C_2)]. \tag{3.38}$$

where

$$C_\mu = (V_\mu + V_\mu^\dagger)/2, \tag{3.39}$$

$$(\eta_\mu)_{xy} = (-1)^{x_1+\ldots+x_{\nu-1}}\delta_{x,y}, \tag{3.40}$$

$$(\epsilon)_{xy} = (-1)^{x_1+\ldots+x_4}\delta_{x,y}, \tag{3.41}$$

$$(\epsilon_{\mu\nu})_{xy} = -(\epsilon_{\nu\mu})_{xy} = (-1)^{x_\mu+x_\nu}\delta_{x,y} \quad (\mu < \nu), \tag{3.42}$$

with $(V_\mu)_{xy} = U_{x,\mu}\delta_{y,x+\mu}$. Here ϵ is represented as $\Gamma_{55} = \gamma_5 \otimes \gamma_5$ in the spin-flavor representation while η_μ followed by the transporter C_μ is represented as $\gamma_\mu \otimes \mathbf{1}$ up to discretization errors, which we sometimes denote Γ_μ. Thus it is obvious that the M_A stands for $(\mathbf{1}\otimes\gamma_5)+O(a)$ while M_H stands for $(\mathbf{1}\otimes\sum\sigma_{\mu\nu})+O(a)$. We refer to M_A as the Adams-type [30] and M_H the Hoelbling-type [32]. By diagonalizing γ_5 or $\sum\sigma_{\mu\nu}$, we find that the Adams type splits 4 tastes into two branches with positive ($m = +1$) and the other two with negative($m = -1$) mass while the Hoelbling type splits them into three branches with positive($m = +2$), two with zero ($m = 0$) and the other one with negative mass($m = -2$). The divided Hoelbling flavored-mass terms (3.36)(3.37)(3.38) correspond to divided types in the tensor-types mass for naive fermions (3.30)(3.31)(3.32) . They have flavored structure as $\sim (\mathbf{1} \otimes (\sigma_{12} + \sigma_{34})) + O(a)$. By diagonalizing it, we find the flavor structure diag$[0, 0, -2, 2]$. They again split 4 taste into three branches with $(1, 2, 1)$ fermion modes. We will later discuss about whether these divided types have enough discrete symmetries to restore euclidian Lorentz symmetry in the continuum limit.

We here check all these staggered flavored-mass terms (3.34)(3.35)(3.36)(3.37)(3.38) lead to the second derivative terms proportional to a near the continuum. Near the classical continuum limit, these staggered flavored-mass terms M_f are given by

$$M_f \sim a \int d^4x \bar{\chi} D_\mu^2 \chi \, + \, O(a^2) \tag{3.43}$$

with proper mass shift. It is compatible with the criterion for the lattice fermion construction. We now can construct the two types of staggered-Wilson fermions with these flavored-mass terms which also lead to the staggered-overlap fermions.

Now let us compare these flavored-mass terms with the M_P and $M_T^{(i)}$ for the naive fermions in Fig. 3.6. It is obvious that the Adams-type flavored-mass term M_A corresponds to M_P while the divided Hoelbling-type terms $M_H^{(i)}$ corresponds to $M_T^{(i)}$. It is also possible to see that M_P and $M_T^{(i)}$ are decomposed into the Adams and the divided Hoelbling-type terms through the spin diagonalization which we discussed in chapter 2 as $\chi_x = \gamma_4^{x_4}\gamma_3^{x_3}\gamma_2^{x_2}\gamma_1^{x_1}\psi_x, \bar{\chi}_x = \bar{\psi}_x\gamma_1^{x_1}\gamma_2^{x_2}\gamma_3^{x_3}\gamma_4^{x_4}$. M_P is decomposed into M_A through this spin-diagonalization as

$$\bar{\psi}_x C_1C_2C_3C_4\psi_x \qquad \rightarrow \qquad \pm\bar{\chi}_x(\epsilon\eta_1\eta_2\eta_3\eta_4 C_1C_2C_3C_4)\chi_x.$$

Here the signs in front of $\bar{\chi}_x$ come from the residual γ_5 which remain in the process of the spin diagonalization of M_P. By diaonalizing γ_5, we find two Adams types terms with positive sign and two with negative signs. Such signs are not relevant for the species-splitting, and we can neglect them. $M_T^{(i)}$ is decomposed into $M_H^{(i)}$ through the spin-diagonalization. For example, $M_H^{(1)}$ is derived from $M_T^{(1)}$ as

$$\begin{aligned}\bar{\psi}_x[(C_1C_2 + C_2C_1) + (C_3C_4 + C_4C_3)]\psi_x \\ \rightarrow \quad \pm\bar{\chi}_x[i\epsilon_{12}\eta_1\eta_2(C_1C_2 + C_2C_1) \pm i\epsilon_{34}\eta_3\eta_4(C_3C_4 + C_4C_3)]\chi_x.\end{aligned} \tag{3.44}$$

The two types of signs come from $\sigma_{12} = \gamma_1\gamma_2$ and $\sigma_{34} = \gamma_3\gamma_4$, which remain after the usual spin diagonalization process. The point is that they commute with each other as $[\sigma_{12}, \sigma_{34}] = 0$, and they can be diagonalized simultaneously. If σ_{12} is diagonalized as

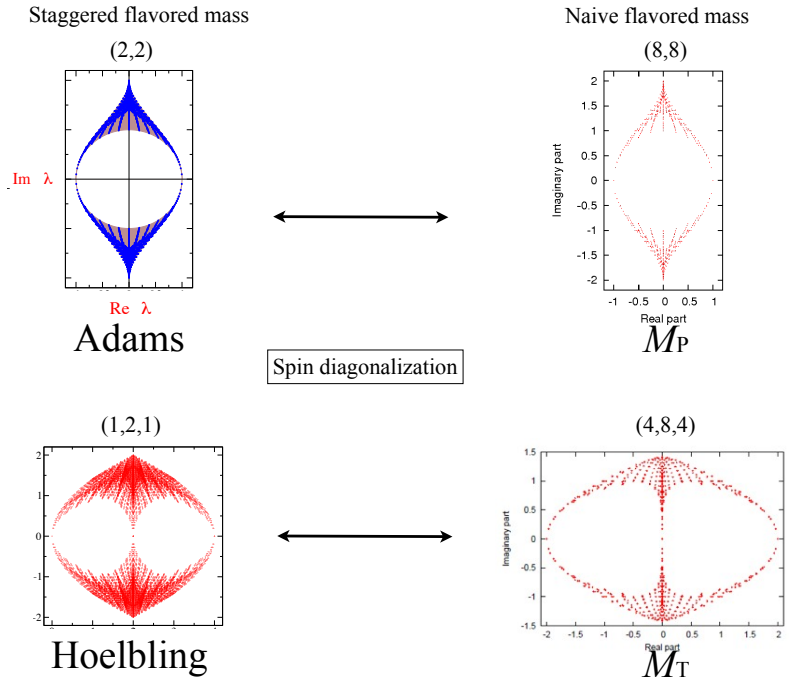

Figure 3.6: Comparison between the Adams-type flavored mass for staggered fermions [31, 49] and M_P for the naive fermion. Comparison between the divided Hoelbling-type flavored mass [32] and $M_T^{(i)}$.

diag.$[-1,1,-1,1]$, σ_{34} is diagonalized as diag.$[1,-1,-1,1]$. The above signs originate in these diagonalized gamma matrices. This spin diagonalization is applicable to $M_T^{(2)}$ and $M_T^{(3)}$, from which we derive $M_H^{(2)}$ and $M_H^{(3)}$ respectively. We in these cases utilize the commutation relations $[\sigma_{13},\sigma_{42}]=0$ and $[\sigma_{14},\sigma_{23}]=0$. We note that the full tensor-type flavored mass $M_T=\sum_{i=1,2,3}M_T^{(i)}$ (3.26) cannot be spin-diagonalized since the sigma matrices in different divided tensor-type masses cannot commute with each other as $[\sigma_{12},\sigma_{23}]\neq 0$. This means that The full Hoelbling term (3.35) cannot directly be derived from the flavored-mass terms for naive fermions through spin diagonalization. In this sense, the full Hoelbling term is peculiar to staggered fermions.

Finally, we conclude that the two types of the flavored mass terms for the staggered fermions M_A and $M_H^{(i)}$ are equivalent to the M_P and $M_T^{(i)}$ in the naive fermion. Since the spin diagonalization decomposes the action into four equivalent pieces, the only possible flavored-mass terms which can be decomposed are M_P, $M_T^{(i)}$ and their combinations since all the branches of them contains four or multiple of four fermion modes. (M_P has $(8,8)$ branches while $M_T^{(i)}$ has $(4,8,4)$ branches.)

Chapter 4

Novel lattice fermions

In this chapter, we summarize the novel lattice fermions, the generalized Wilson fermions and the staggered-Wilson fermions with emphasis on their symmetries. Here let us comment about the way of constructing the Wilson-type fermions from the flavored-mass terms. As we discussed in chapter 2 and we will discuss later in details in 6, the lattice QCD with the Wilson-type fermion should have the parity-broken phase as shown in Fig. 2.5. This phase structure gives a restriction on the way of taking the chiral limi for this fermion: It is difficult to take the chiral limit around the cusps except the most left or the rightest ones since most of the area around these cusps are surrounded by the parity-broken phase in Fig. 2.5. On the other hand, the edge cusps have enough area for the parity symmetric phase. Considering we need to take the chiral limit from the parity symmetric phase, the cusps we can use for the lattice QCD are practically restricted only to the edge cusps. These edge cusps correspond to the edge branch in the Dirac spectrum as shown in Fig. 2.3, thus we utilize them for the QCD simulation through the mass-parameter tuning. This is why the usual Wilson fermion, in which 1 fermion mode exists on the most left branch, is always used as an one-flavor lattice fermion. For the flavored-mass terms we show in the previous chapter, we shift the Dirac spectrum by introducing the usual mass term so that the most left branch comes to zero in the real axis. Note the results in this chapter including the generalized Wilson and the symmetries of the staggered-Wilson fermions are based on the original work by the present author in Ref. [34]. I only use the forms of the staggered-WIlson fermions from the references [31, 32].

4.1 Generalized Wilson fermions

By using the four non-trivial flavored-mass terms for the naive fermions, we can construct a variety of the generalized Wilson fermions. There are lots of possibilities, thus we only concentrate the characteristic cases here. The 8-flavor Wilson fermion is given by

$$S_{gW}^{(8)} = S_{nf} + r\sum_n \bar{\psi}_n(1 - M_P)\psi_n + m\sum_n \bar{\psi}_n\psi_n, \tag{4.1}$$

where we introduce the Wilson parameter r and the dimensionless mass parameter m with S_{nf} being the massless version of naive fermion action shown in (2.21). M_P is shown in

(3.28) and the associated Dirac spectrum is given in Fig. 3.3(a). As we have mentioned, we shift the flavored-mass term by $r\sum_n \bar{\psi}_n\psi_n$ to move the most left branch to massless point. This fermion action gives eight massless modes at least for the free case while the other eight species decouple in the continuum. If we substitute its Dirac kernel with the mass parameter $-2 < m < 0$ into the overlap formula, we obtain a 8-flavor overlap fermion. The 4-flavor Wilson fermion is given by

$$S_{gW}^{(4)} = S_{nf} \; + \; r\sum_n \bar{\psi}_n(2 - M_T^{(i)})\psi_n + m\sum_n \bar{\psi}_n\psi_n, \tag{4.2}$$

where 4 species become massless and other 12 decouple with inifinite mass for the free case. $M_T^{(i)}$ $(i = 1, 2, 3)$ is given by (3.30)(3.31)(3.32) and the figure 3.4 shows the splitting of the branches for this flavored-mass term. If we substitute its Dirac kernel with the mass parameter $-4 < m < 0$ into the overlap formula, we obtain a 4-flavor overlap fermion. The 2-flavor Wilson fermion is given by

$$S_{gW}^{(4)} = S_{nf} \; + \; r\sum_n \bar{\psi}_n(6 - M_T)\psi_n + m\sum_n \bar{\psi}_n\psi_n, \tag{4.3}$$

where 4 species become massless and other 12 decouple with inifinite mass for the free case. $M_T = \sum_{i=1,2,3} M_T^{(i)}$ is given by (3.26) and the figure 3.5 shows the splitting of the branches for this flavored-mass term. If we substitute its Dirac kernel with the mass parameter $-6 < m < 0$ into the overlap formula, we obtain a 2-flavor overlap fermion. Finally we show the usual Wilson fermion as

$$S_{gW}^{(4)} = S_{nf} \; + \; r\sum_n \bar{\psi}_n(4 - M_V)\psi_n + m\sum_n \bar{\psi}_n\psi_n, \tag{4.4}$$

where M_T is given by (3.25). This fermion is exactly the usual Wilson fermion, where the 16 species are decomposed into 5 branches with 1, 4, 6, 4 and 1 species. If we substitute its Dirac kernel with the mass parameter $-2 < m < 0$ into the overlap formula, we obtain 1-flavor usual overlap fermion. By combining these flavored-mass terms, we can derive the generalized Wilson and overlap fermions with any number of flavors, as shown in Fig. 3.3(a)(b) where for (a) we have two-flavor branch on the most left and for (b) we have 15-flavor branch on the rightest. As seen from these results, any-flavor Wilson and overlap fermions are available by combining the flavored-mass term for the naive fermions. Regarding the symmetries of the generalized Wilson fermion, as long as we take a sum for the space-time indices, there is no special symmetry breaking compared to the Wilson fermion: They possess $U(1)_V$ flavor symmetry, the hypercubic symmetry and other requisite symmetries as parity and charge conjugation. Only the divided tensor types $M_T^{(i)}$ have just the double rotational symmetry, but we can expect that it is sufficient symmetry for the restoration of the Lorentz symmetry from the argument in the next section.

In the end of this section, let us remind ourselves that one of the hardships from the doubling problem is that we cannot control the number of fermions on the lattice. This formulation brilliantly resolve this problem by using only one lattice fermion action.

4.2 Staggered Wilson fermions

To set the staggered-Wilson fermions in the same form as the usual Wilson fermion, we introduce the Wilson parameter $r = r\delta_{x,y}$ and shift the mass for the actions as with Wilson fermions. Then the Adams-type staggered-Wilson fermion action is given by

$$S_{\rm A} = \sum_{xy} \bar{\chi}_x [\eta_\mu D_\mu + r(1 + M_A) + M]_{xy} \chi_y, \tag{4.5}$$

with $D_\mu = \frac{1}{2}(V_\mu - V_{-\mu})$. Here M stands for the usual taste-singlet mass ($M = M\delta_{x,y}$). The Hoelbling-type staggered-Wilson fermion action is given by

$$S_{\rm H} = \sum_{xy} \bar{\chi}_x [\eta_\mu D_\mu + r(2 + M_H) + M]_{xy} \chi_y. \tag{4.6}$$

In the QCD simulation we will tune the mass parameter M to take a chiral limit. For some negative value of the mass parameter: $-1 < M < 0$ for $S_{\rm A}$ and $-2 < M < 0$ for $S_{\rm H}$ respectively, we obtain two-flavor and one-flavor overlap fermions respectively by using the overlap formula.

We here discuss the discrete symmetry of the staggered-Wilson fermions. Most of arguments here are re-interpretation of the work by Golterman and Smit [59]. As we have discussed in Sec. 2, the symmetries in usual staggered fermions were well investigated in [59, 63] by Golterman, Smit, Kilcup and Sharpe. The potential problem for staggered-Wilson fermions in lattice QCD is the discrete symmetry breaking. As discussed in [31, 32], the discrete symmetries possessed by the original staggered fermion is broken to their subgroups both in the Adams-type and Hoelbling-type actions. The shift symmetry in (4.7)

$$\mathcal{S}_\rho : \ \chi_x \to \zeta_\rho(x) \chi_{x+\hat{\rho}}, \quad \bar{\chi}_x \to \zeta_\rho(x) \bar{\chi}_{x+\hat{\rho}}, \quad U_{\mu,x} \to U_{\mu,x+\hat{\rho}}, \tag{4.7}$$

is broken into the two-direction subgroup as $x \to x + \hat{1} \pm \hat{\mu}$ in the Adams-tyep fermion while the Hoelbling-type fermions is invariant under the four-direction subgroup as $x \to x + \hat{1} \pm \hat{2} \pm \hat{3} \pm \hat{4}$. Note that these subgroups include the doubled shift $x \to x + 2\hat{\mu}$ as their subgroup. The axis reversal invariance in (4.8)

$$\mathcal{I}_\rho : \ \chi_x \to (-1)^{x_\rho} \chi_{Ix}, \quad \bar{\chi}_x \to (-1)^{x_\rho} \bar{\chi}_{Ix}, \quad U_{\mu,x} \to U_{\mu,Ix}, \tag{4.8}$$

is also broken to the subgroups in the both cases as we will show later. In addition, the Hoelbling-type fermion loses the original rotational symmetry of the staggered fermion (4.9)

$$\mathcal{R}_{\rho\sigma} : \ \chi_x \to S_R(R^{-1}x) \chi_{R^{-1}x}, \quad \bar{\chi}_x \to S_R(R^{-1}x) \bar{\chi}_{R^{-1}x}, \quad U_{\mu,x} \to U_{\mu,Rx}, \tag{4.9}$$

while it holds in the Adams-type fermion. The Hoelbling-type fermion also loses invariance under the charge conjugation transformation, which is given by

$$\mathcal{C} : \ \chi_x \to \epsilon_x \bar{\chi}_x^T, \ \bar{\chi}_x \to -\epsilon_x \chi_x^T, \ U_{\mu,x} \to U_{\mu,x}^*, \tag{4.10}$$

while the Adams-type holds it.

What we need to show here is whether the staggered-Wilson fermions possess essential subgroups of these symmetries: By "essential" symmetries we mean symmetries separated from the flavor rotations, which stand for the physical parity, charge conjugation and discrete rotational symmetry. Since the flavored-mass term for these cases obviously break the flavor rotation symmetries, it is natural that the above staggered discrete symmetries related to the flavor rotation are all broken to their subgroups. However, as long as the physical symmetries such as parity hold, we can expect the continuum limit with these lattice fermions gives a correct QCD or other continuous theories. To figure out these points we use the representation as shown in (4.11)(4.12)(4.13)

$$\mathcal{S}_\mu : \ \phi(p) \ \rightarrow \ \exp(ip_\mu)\Xi_\mu \, \phi(p), \tag{4.11}$$

$$\mathcal{I}_\rho : \phi(p) \ \rightarrow \ \Gamma_\rho\Gamma_5\Xi_\rho\Xi_5 \, \phi(Ip), \tag{4.12}$$

$$\mathcal{R}_{\rho\sigma} : \ \phi(p) \ \rightarrow \ \exp(\frac{\pi}{4}\Gamma_\rho\Gamma_\sigma) \exp(\frac{\pi}{4}\Xi_\rho\Xi_\sigma) \, \phi(R^{-1}p). \tag{4.13}$$

By using them we can clearly figure out the residual discrete symmetry of the staggered-Wilson fermions. Firstly the staggered-Wilson fermions are invariant under the essential subgroup of the combined transformations: Both the staggered-Wilson fermions are invariant under (4th-direction shift with spatial axis reversal) as

$$\mathcal{I}_s\mathcal{S}_4 \sim \exp(ip_4)\Gamma_1\Gamma_2\Gamma_3\Gamma_5 \, \phi(-\mathbf{p}, p_4) \sim \exp(ip_4)\Gamma_4 \, \phi(-\mathbf{p}, p_4), \tag{4.14}$$

with $\mathcal{I}_s \equiv \mathcal{I}_1\mathcal{I}_2\mathcal{I}_3$. This is essentially the parity transformation as shown in section 3 of the ref. [59]. In the continuum limit the phase factor disappears and it results in the continuum parity transformationas $\psi(p) \rightarrow \gamma_4\psi(-\mathbf{p}, p_4)$ for the Dirac fermion. Besides, by following the arguments in [61, 63], it is also possible to show the present actions are invariant even under $\mathcal{I}_s\Xi_4\phi(-\mathbf{p}, p_4) = \Gamma_4\phi(-\mathbf{p}, p_4)$. Thus we conclude these fermion actions possess physically well-defined parity symmetry. We here note the simple product of the μ-direction shift and the μ-direction axis reversal (shifted-axis reversal) is also symmetry of both the fermions. The charge conjugation can be also shown to be symmetry of these fermions by modifying the original charge conjugation transformation for the case with the flavored-mass terms [59].

As is well-known, the usual "staggered hypercubic symmetry" means invariance under the staggered rotation (4.9)(4.13) and the axis reversal (4.8)(4.12). Although both of the staggered-Wilson fermions themselves do not have this symmetry, we can show theories on the two- or one-flavor branches in these fermions are likely to recover the Lorentz symmetry in the continuum limit as following: Considering the Adams-type fermion possesses essential discrete symmetries as parity and charge conjugation symmetry as well as the staggered rotational symmetry [31], we can expect the discrete symmetry enhances to the requisite continuous symmetry in the continuum limit in the QCD with its two-flavor branch. Here the staggered rotational symmetry with the shifted axis reversal is expected to work as the hypercubic symmetry in the two-flavor branch.) On the other hand, the Hoelbling-type formulation breaks the staggered rotational symmetry to its subgroup while it also has parity and charge conjugation symmetry. However it is invariant under (μ, ν rotation), (ν, μ rotation), (μ shift) and (ν shift) as,

$$\mathcal{S}_\nu\mathcal{S}_\mu\mathcal{R}_{\nu\mu}\mathcal{R}_{\mu\nu} \sim \exp(ip_\mu + ip_\nu)\Gamma_\mu\Gamma_\nu \, \phi(\tilde{p}), \tag{4.15}$$

with $\tilde{p}_{\mu,\nu} = -p_{\mu,\nu}, \tilde{p}_\tau = p_\tau, \tau \neq \mu, \nu$. We call this transformation a shifted square rotation. It also possesses the doubled rotational symmetry [32] as

$$\mathcal{R}_{\rho\sigma}\mathcal{R}_{\mu\nu} \sim \exp[\frac{\pi}{4}(\Gamma_\rho\Gamma_\sigma + \Gamma_\mu\Gamma_\nu)] \exp[\frac{\pi}{4}(\Xi_\rho\Xi_\sigma + \Xi_\mu\Xi_\nu)]\, \phi(R^{-1}_{\rho\sigma}R^{-1}_{\mu\nu}p), \tag{4.16}$$

where (μ, ν, σ, ρ) is any permutation of $(1, 2, 3, 4)$. We note (4.15) gives the rotation purely in the spinor space, not including the flavor rotation. It is notable this discrete symmetry has the same form of the spinor rotation as the continuum Euclidean rotation. Thus we can speculate the theory on the one-flavor branch of the Hoelbling-type fermion would recover the pure-spacetime rotational symmetry without flavor rotation in the continuum. We also define the charge conjugation symmetry for the Hoelbling-type fermion by introducing the triple-rotation as

$$\mathcal{R}_{14}\mathcal{R}_{32}\mathcal{R}_{21}\mathcal{C}. \tag{4.17}$$

There are several possibilities for these three rotational combinations, thus it is not unique. However the point is that we can define the proper charge conjugation symmetry also for the Hoelbling-type fermion.

It is also suggested by the perturbative study that the staggered-Wilson fermions would possess sufficient discrete symmetry to result in the correct QCD in the continuum limit of lattice QCD with them. The ref. [59] clearly elaborated how the quantum corrections from the flavored-mass terms in the staggered fermions affect from the viewpoint of the perturbation theory. This kind of study has been also done in the recent revisiting [31, 32]. These perturbative studies indicate the breaking of the discrete symmetries generates only operators related with the taste structure, which just modify the particular linear combination of the 4 tastes and move the relative positions of the branches of the Dirac spectrum. As long as there is a clear separation between the branches, these modifications can be absorbed into the additive mass renormalization and does not carry any physical significance.

As seen from these arguments, it is likely that the staggered-Wilson fermions possesses sufficient discrete symmetries to recover the correct continuum theory with the Lorentz symmetry as well as the parity and charge conjugation. However, there has not yet been a consensus on whether it does harm to lattice QCD with staggered-Wilson fermions or whether these theories result in the correct QCD with the Lorentz symmetry and other requisite discrete symmetries. We can answer this question partly by studying the non-perturbative aspects of the gauge theories with these lattice fermions by looking into, for example, the index theorem or the parity phase structure since a clear symptom is expected to appear in these phenomena if the symmetry breaking ruins the essential properties of QCD. In chapter 5 and 6 we will find the situations about these topics in the staggered-Wilson fermion is qualitatively similar to the original Wilson case.

We here note that there emerges an extra symmetry only for the case of $M + 2r = 0$ in the Hoelbling-type fermion as

$$\tilde{\mathcal{C}} : \ \chi_x \to \bar{\chi}^T_x, \ \bar{\chi}_x \to \chi^T_x, \ U_{\mu,x} \to U^*_{\mu,x}. \tag{4.18}$$

The point is that the usual mass term $M\bar{\chi}_x\chi_x$ and the Adams-type flavored-mass term $\bar{\chi}_x M_{\mathcal{A}}\chi_x$ breaks this symmetry, thus they are prohibited to be generated by the quantum

corrections for this case: $M + 2r = 0$. This parameter choice corresponds to the central cusp in the Dirac spectrum of the Hoelbling fermion, where two fermion modes exist. It indicates that we can perform two-flavor lattice QCD simulation on this cusp without fine-tuning of the mass parameter as proposed in [33, 76]. We remind ourselves that, as we have shown for the Wilson fermion, the central cusp in the Wilson fermion has 6 flavors. From the viewpoint of the Aoki phase, this point is located in the parity broken phase (the except is only the continuum limit.). Thus the pion condensation breaks this discrete symmetry spontaneously in the Aoki phase. We expect that this spontaneous discrete symmetry breakdown leads to the continuum symmetry breakdown in the continuum, which can be regarded as SSB for the chiral symmetry in the twisted-mass QCD as in the central cusp for the Wilson fermion. We need further study for this cusp.

In the end of this section, we discuss on the divided Hoelbling actions, which are given by

$$S_{\rm H}^{(i)} = \sum_{xy} \bar{\chi}_x [\eta_\mu D_\mu + r(2 + M_H^{(i)}) + M]_{xy} \chi_y, \tag{4.19}$$

where $M_H^{(i)}$ are given by (3.36)(3.37)(3.38). As we discussed, these are derived from the tensor flavored mass for naive fermions $M_T^{(i)}$ while the full Hoelbling action cannot be derived from the naive fermion. We note that the symmetries we discussed above, including double shift, shifted axis reversal, shifted axis rotation, double rotation, hold also in divided Hoelbling-type fermions $S_{\rm H}^{(i)}$. There is thus possibility that we can also apply the divided Hoelbling fermions to lattice simulations although we need to study more on restoration of the euclidian Lorentz symmetry in the continuum.

Chapter 5

Index theorem and Overlap formulation

Lattice fermion actions without doublers do illustrate the index theorem nicely. For example, one old-fashioned way to study topology in QCD is to use Wilson fermion [1, 80], although it requires fine-tuning of a mass parameter because of explicit breaking of chiral symmetry. On the other hand, the index is hidden in lattice fermions with species doublers since the index effect cancels between doubling pairs. Although a theoretical approach to the index of the staggered fermions [13, 14, 15] were developed in [80, 81], it does not give an integer value from the beginning and requires a renormalization depending on the full ensemble of the gauge fields. Thus it is not easy to define the index theorem in naive, staggered and minimally-doubled fermions and thereby study topological effects. However if we use the flavored-mass terms, we expect we can easily detect the index since they properly lift the degeneracy in the fermion species and should reveal the hidden index among the species. In addition the correct index theorem for the lattice fermion means that this fermion correctly detects the topology of gauge theory. Thus we can show the practical applicability simulations of the novel fermions as the generalized Wilson and staggered-Wilson fermions to lattice QCD by showing the index theorem holds for them.. We again use a minimally doubled fermion as a toy model case since the simplicity of this fermion gives us insight into how our method works.

In this chapter we discuss the index theorem and overlap versions of the generalized Wilson fermion and staggered-Wilson fermions. Although the index theorem holds naive and staggered fermions with any type of flavored-mass terms as long as they lift the degeneracy of the species, we here concentrate on a pseudo-scalar type or Adams type of flavored mass terms to extract the index in the spectral flow of the associated Hermitean version of the Dirac operator. It is because such flavored-mass terms, which assigns positive and negative masses to species depending on their flavor-chiralities, removes the cancellation of the index between tastes perfectly. Thus, although we studied the several fermion actions for the generalized Wilson and staggered-Wilson fermions in the previous chapter, we here go back to 3 and consider only the Dirac operator with the form of $D_{nf} - M_P$ or $D_{st} - M_f^{(1)}$. Here we follow a parallel approach for identifying the would-be zero modes and their chiralities to that proposed in the Wilson case [77]: We identify the would-be zero modes and their chiralities with naive and staggered fermions away

from the continuum limit using the spectral flow of a certain Hermitean version of the Dirac operator. The integer index obtained here correctly illustrates the gauge topological charge up to a factor coming from species. Indeed we will show the spectral flow correctly illustrates the index determined by the gauge field topology in naive, minimally doubled and staggered fermions. In the end of this chapter we also present overlap versions built from the generalized Wilson and staggered-Wilson fermion kernels. It is a universal feature for fermions with species doublers that you can obtain the associated overlap fermion with a proper flavored mass term illustrating the correct index.

Note the results in this chapter are basically based on the original works [29, 75] by the present author. I also refer to the results on the index theorem in the staggered fermion in the reference [30].

5.1 Spectral flow and the index theorem

In this section we obtain the integer index related with gauge field topology for the minimally doubled, naive and staggered fermions with flavored-mass terms. As in the cases of Wilson [77] we utilize the spectral flow of the Hermitean operators. Here the would-be zero modes of the Dirac operators are identified as low-lying crossings of the eigenvalue flow of the Hermitean operators.

Let us begin with explaining what the spectral flow is. In the continuum field theory the index is defined as the difference between the numbers of zero modes of the massless Dirac operator with positive and negative chirality, n_+ and n_-. The statement of the index theorem is that the index is just equal to a topological charge Q of a background gauge configuration up to a sign factor depending on its dimensionality,

$$n_+ - n_- = (-1)^{d/2} Q. \tag{5.1}$$

Here the question is how to obtain the index of the Dirac operator. We can of course calculate the zero-mode chiralities straightforwardly, but there is a useful way called *spectral flow*. To introduce it we first introduce a certain Hermitean version of the Dirac operator

$$H(m) = \gamma_5 (D - m), \tag{5.2}$$

where any zero modes of the Dirac operator with $\pm$ chirality correspond to some eigenmodes of this Hermitean operator with eigenvalues $\lambda(m) = \mp m$. If we now consider the flow of the eigenvalues $\lambda(m)$ as the mass varies, those corresponding to zero modes will cross the origin with slopes ∓ 1 depending on their $\pm$ chirality. The non-zero eigenmodes of D, in contrast, occur in pairs which are mixed by H and cannot cross zero. Therefore the index of the Dirac operator is given by minus the spectral flow of the Hermitean operator, which stands for the net number of eigenvalues crossing the origin, counted with sign $\pm$ depending on the slope.

The index with lattice Wilson fermions [77] can similarly be obtained from the spectral flow, which in this case means the net number of eigenvalues crossing zero at low-lying values of m, counted with signs of the slopes. In the continuum limit, we are only interested in the crossings at small mass; the massive doublers also eventually cross zero,

but only for large values of m. Now we can symbolically write a formula for the index as

$$\text{Index}(D) = -\text{Spectral flow}(H). \tag{5.3}$$

It is quite natural to consider whether this formula is also available to detect the index of minimally doubled, naive and staggered fermions with the flavored mass terms we proposed. We will from now show this spectral flow method can be also applied to these cases. We first study the case for the minimally doubled and naive fermions. The associated Hermitean operators for minimally doubled and naive fermions are given by

$$H_{\text{md}}(m_{\tau_3}) = \gamma_5(D_{\text{md}} - M_{\tau_3}), \tag{5.4}$$

$$H_{\text{nf}}(m_{\tau_3\otimes\tau_3}) = \gamma_5(D_{\text{n}} - M_{\tau_3\otimes\tau_3}), \tag{5.5}$$

where the matrix γ_5 is regarded as a flavored one, $\gamma_5 \otimes \tau_3$ for minimally doubled fermions and $\gamma_5 \otimes (\tau_3 \otimes \tau_3)$ for two dimensional naive fermions in terms of the flavor multiplet. The flavored mass terms M_{τ_3} and $M_{\tau_3\otimes\tau_3}$ for $d = 2$ have been already given in Eq. (3.9) and (3.18) with the parameters m_{τ_3} for the minimally doubled fermion and $m_{\tau_3\otimes\tau_3}$ for the naive fermion. We here use these parameters as a mass parameter of the continuum hermitian Dirac operator in (5.2). Thus the eigenvalues are functions of m_{τ_3} and $m_{\tau_3\otimes\tau_3}$ as $\lambda(m_{\tau_3})$ and $\lambda(m_{\tau_3\otimes\tau_3})$. (These parameters correspond to the Wilson parameter r in (4.1) rather than the mass parameter since it is a parameter for the flavored-mass term.) For now we focus on the two dimensional case.

We then numerically calculate the eigenvalue flows of two dimensional minimally doubled and naive fermions. We consider background configurations proposed in [80] for the staggered case [30]: we start with a smooth $U(1)$ gauge field with topological charge Q,

$$U_{x,\hat{1}} = e^{i\omega x_2}, \qquad U_{x,\hat{2}} = \begin{cases} 1 & (x_2 = 1, 2, \cdots, L-1) \\ e^{i\omega L x_1} & (x_2 = L) \end{cases}, \tag{5.6}$$

where L is the lattice size and ω is the curvature given by $\omega = 2\pi Q$. Then, to emulate a typical gauge configuration of a practical simulation, we introduce disorder effects to link variables by random phase factors, $U_{x,\mu} \to e^{ir_{x,\mu}} U_{x,\mu}$, where $r_{x,\mu}$ is a random number uniformly distributed in $[-\delta\pi, \delta\pi]$. The parameter δ determines the magnitude of disorder.

Fig. 5.1(a) shows the eigenvalue flow of the minimally doubled Hermitean operator (5.4). It is calculated with a $Q = 1$ and $\delta = 0.25$ background configuration on a 16×16 lattice. There are two low-lying crossings around $m = 0$ with positive slopes, which correspond to would-be zero modes. With the formula (5.3), it means the index of the Dirac operator of the minimally doubled fermion in this case is -2. This result is consistent with the index theorem for the minimally doubled fermions given by

$$\text{Index}(D_{\text{md}}) = 2(-1)^{d/2} Q, \tag{5.7}$$

which contains a factor 2 reflecting two species. This relation is also satisfied by cases with other topological charges, as shown in Fig. 5.2(a) for the case for $Q = 2$. Here the net number of crossings counted with $\pm$ depending on the slopes is 4. It means the corresponding index is -4, which is consistent with (5.7). We also emphasize that there is a clear separation between low- and high-lying crossings in Fig. 5.1(a) where

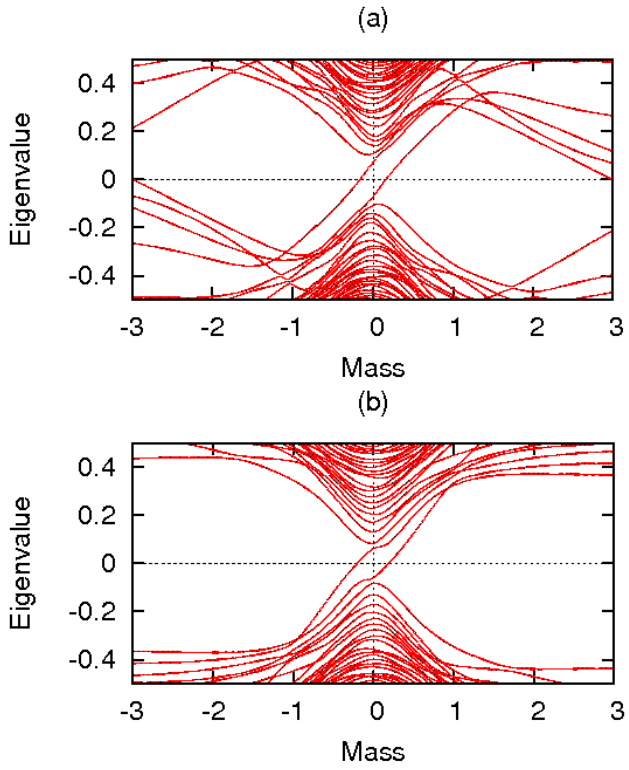

Figure 5.1: Spectral flows of (a) Minimally doubled $\lambda(m_{\tau_3})$ and (b) naive $\lambda(m_{\tau_3 \otimes \tau_3})$ Hermitean operators with a $Q = 1$, $\delta = 0.25$ background configuration on a 16×16 lattice. Two single crossings with positive slopes are seen in (a), which means the index is -2. Two doubled crossings with positive slopes are seen in (b), which means the index is -4.

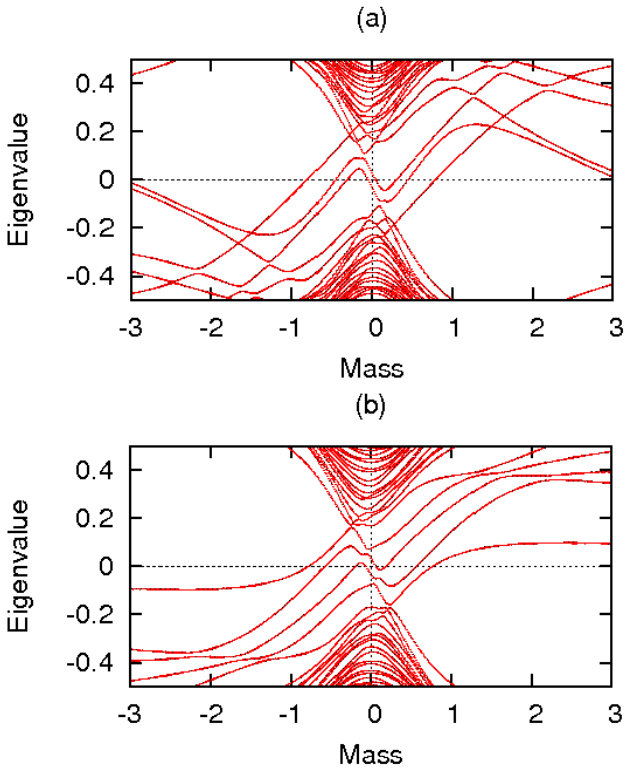

Figure 5.2: Spectral flows of (a) Minimally doubled $\lambda(m_{\tau_3})$ and (b) naive $\lambda(m_{\tau_3 \otimes \tau_3})$ Hermitean operators with a $Q = 2$, $\delta = 0.2$ background configuration on a 16×16 lattice. Six single crossings with positive slopes and two single crossings with negative slopes are seen in (a), which means the index is -4. Six doubled crossings with positive slopes and two doubled crossings with negative slopes are seen in (b), which means the index is -8.

low-lying ones are localized about $m = 0$ and high-lying ones are located at large $|m|$. It indicates the zero modes and the index tend to be robust against randomness of the gauge configuration. Now we have established the index theorem with minimally doubled fermions.

Next results for the naive fermion case are shown in Fig. 5.1(b). The calculation is done with the same background configuration as the minimally doubled case. Fig. 5.1(b) shows the eigenvalue flow of the naive Hermitean operator (5.5). There are two doubled crossings around the origin: Here we can verify they are doubled and there totally exist four crossings as shown in Fig. 5.5(a) by introducing other kinds of mass terms given in Fig. 5.5. Again with the formula (5.3) we obtain the index of the Dirac operator of the naive fermion in this case is -4. This result satisfies the index theorem for the naive fermion given by

$$\text{Index}(D_{\text{nf}}) = 2^d(-1)^{d/2}Q, \tag{5.8}$$

where it contains a factor 2^d reflecting 2^d species. The pseudo-scalar type flavored-mass term M_P totally uncovers the hidden index in between the species doublers. This theorem is also satisfied by the cases with other topological charges, as shown in Fig. 5.2(b) for $Q = 2$. Here the spectral flow is 8 since all the crossings are doubled in this case. It means the corresponding index is -8, which is consistent with (5.8). There is also large separation between low-lying and high-lying crossings. It indicates the zero modes and the index tend to be robust. Now we have established the index theorem with the naive fermion.

We remark both of the Hermitean operators, (5.4) and (5.5), satisfy a relation of $\gamma_5 H(m)\gamma_5 = -H(-m)$ where m stands for m_{τ_3} or $m_{\tau_3\otimes\tau_3}$, which improves the lower bound of $H^2(m)$ satisfying $H^2(m) = D^\dagger D + m^2$, due to the fact that the Dirac spectrum has the symmetric about the imaginary axis. Since this property enhances the stability of the index against disorder, overlap formalisms with this kind of symmetric species-splitting would be more applicable to practical simulations. We can perform the same argument for the 4-dimensional naive fermions.

For the staggered fermions, the hermitian Dirac operator appropriate for the index is Adams-type one (3.34) since it gives positive and negative mass depending on flavor-chiralities. This case was elaborated by Adams in ref. [30]. We here follow the results shown in the reference. The hermitian operator is given by

$$\begin{aligned} H_{\text{st}}(m_f) &= \Gamma_{55}\left(D_{\text{st}} - m_f M_A\right) \\ &= \Gamma_{55}\left(D_{\text{st}} - m_f \Gamma_{55}\Gamma_5\right) \\ &= \Gamma_{55} D_{\text{st}} - m_f \Gamma_5, \end{aligned} \tag{5.9}$$

where $\Gamma_{55} = \epsilon_x$ in (3.41) and $\Gamma_5 = \prod_\mu \eta_\mu C_\mu$ stand for $\Gamma_{55} = \gamma_5 \otimes \gamma_5$ and $\gamma_5 \otimes \mathbf{1}$ with discretization error $\mathcal{O}(a)$ in terms of spin-taste representation. Here we introduce a parameter m_f, thus the eigenvalues flow is given as a function of m_f as $\lambda(m_f)$. (This parameter corresponds to the Wilson parameter r in (4.5) rather than the mass parameter since it is a parameter for the flavored-mass term.) Following the same approach as naive fermions, we have shown that the index of the staggered fermion given by minus the spectral flow of this Hermitean operator (5.3) illustrates correctly the gauge topology

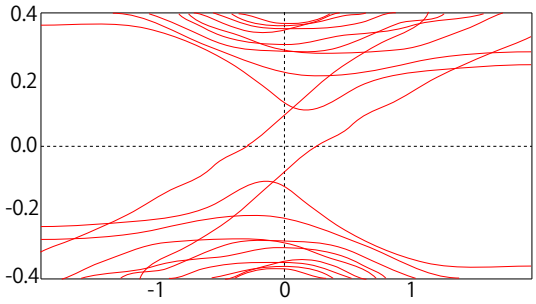

Figure 5.3: Spectral flows of staggered Hermitean operators $\lambda(m_f)$, $\delta = 0.33$ background configuration on a 16×16 lattice. The same result was shown first in [30].

up to a integer factor from the number of tastes as

$$\text{Index}(D_{\text{st}}) = 2^{d/2}(-1)^{d/2}Q \tag{5.10}$$

One of the results is shown in the figure 5.3. Here the spectral flow again means the net number of eigenvalues crossing zero at low-lying values of m, counted with signs of the slopes. Thus the theoretical foundation of the index theorem with staggered fermions is established without a renormalization depending on the gauge ensemble.

5.2 Overlap formulation

In this section we discuss overlap fermions constructed from the staggered-Wilson and generalized Wilson fermions. Firstly we show the index of exact zero modes of these overlap versions also illustrate the topological charge correctly. We now introduce overlap Dirac operators based on the staggered-Wilson and the generalized Wilson fermions as,

$$D_{\text{so}} = 1 + \epsilon \frac{H_{\text{st}}}{\sqrt{H_{\text{st}}^2}}, \qquad D_{\text{no}} = 1 + \gamma_5 \frac{H_{\text{n}}}{\sqrt{H_{\text{n}}^2}}. \tag{5.11}$$

Here we first consider only the 4-dimensional hermitian Dirac operators with M_P and M_A as in the previous section. We again note ϵ stands for $(\epsilon)_{xy} = (-1)^{x_1+\ldots+x_4}\delta_{x,y}$, which is a natural definition of γ_5 in the staggered fermions as $\gamma_5 \otimes \gamma_5$. Then we can obtain the corresponding Ginsparg-Wilson relations

$$\{\Gamma_{55}, D_{\rm so}\} = D_{\rm so}\Gamma_{55}D_{\rm so}, \qquad \{\gamma_5, D_{\rm no}\} = D_{\rm no}\gamma_5 D_{\rm no}, \tag{5.12}$$

where, as we have discussed, the γ_5 here can be identified as a flavored one in terms of the flavor multiplet, for example $\gamma_5 \to \gamma_5 \otimes \gamma_5$ for the staggered fermions and $\gamma_5 \to \gamma_5 \otimes (\tau_3 \otimes \tau_3 \otimes \tau_3 \otimes \tau_3)$ for the naive fermion. We use the dimensionless forms of the Dirac operator here. Note that, in the overlap fomulation, some of the original flavors(species) with negative mass are converted into physical massless modes in these overlap fermions while the others with positive mass become massive and decouple in the continuum limit as we discussed in 2. For example, in the case of the staggered fermion with the Adams type term M_A, two of four tastes have negative mass and the other two have positive mass if we do not consider the usual mass term. In the overlap formula it results in the two-flavor staggered-overlap fermion In the same way, the naive fermion with M_P leads to the 8-flavor staggered fermions. Here let us comment on comparison with the standard Wilson-type actions as seen in (4.1) and (4.5). Usually we regard m_f or $m_{\tau_3\otimes\tau_3}$ as Wilson parameters and introduce a mass parameter m or M as shown in (4.1) and (4.5). Therefore, the cases we discussed now correspond to $m = -r$ and $M = -r$ cases in (4.1) and (4.5) up to a trivial sign of the flavored-mass term.

Now we consider the other types of the flavored-mass term for staggered and naive fermions. For the case of the Hoelbling-type flavored-mass term (4.6), we make only the left branch cross the real axis at the negative value by adjusting the mass parameter in M. Through the overlap formula we get the one-flavor staggered-overlap fermions. In the same way, for the naive fermion with M_T in (4.3), we have the four-flavor overlap fermion by setting the mass parameter m properly. By using 4 non-trivial types of the flavored-mass terms the naive fermion, we can obtain any-flavor overlap fermions from one to 15 flavors.

Note, although the Ginsparg-Wilson relations in (5.12) seem flavored, they result in the unflavored ones since all the massless modes from the overlap formula have the same chiral charge (the same sign of γ_5). It is because the fermion modes in the same branch of the Dirac spectrum have the same chiral charge if the flavored mass terms satisfy the γ_5 hermiticity as we discussed in the chapter 3.

This reduction of flavored degrees also affects the index of the Dirac operators. Here we concentrate the Adams type for staggered and the M_P for the naive where both of them split the spectrum into two branches. We can obtain the indices of the associated staggered and naive overlap Dirac operators from the Ginsparg-Wilson relations (5.12),

$$\mathrm{Index}(D_{\rm so}) = -\frac{1}{2}\mathrm{Tr}\left(\frac{H_{\rm st}}{\sqrt{H_{\rm st}^2}}\right), \qquad \mathrm{Index}(D_{\rm no}) = -\frac{1}{2}\mathrm{Tr}\left(\frac{H_{\rm n}}{\sqrt{H_{\rm n}^2}}\right). \tag{5.13}$$

Now we can easily calculate these quantities analytically: The main part of the above equations is a sign function as $H/\sqrt{H^2} = \mathrm{sgn}(H)$. Thus the trace of this operator $\mathrm{Tr}\,(\mathrm{sgn}(H))$ gives the difference between the number of positive and negative eigenvalues at some

value of the mass parameter. It is essential to fix the mass parameter between low- and high-lying crossings in the eigenvalue flows of $H_{\rm st}$ and $H_{\rm n}$. Then the index of the above overlap Dirac operator becomes just a half of that of the original Dirac operator,

$$\text{Index}\,(D_{\rm so}) = \frac{1}{2}\text{Index}\,(D_{\rm st})\,, \qquad \text{Index}\,(D_{\rm no}) = \frac{1}{2}\text{Index}\,(D_{\rm n})\,. \tag{5.14}$$

This relation relies on the property of the Hermitean operator $\gamma_5 H(m_{\tau_3\otimes\tau_3})\gamma_5 = -H(-m_{\tau_3\otimes\tau_3})$ and $\Gamma_{55}H(m_f)\Gamma_{55} = -H(-m_f)$. These results are consistent with the fact that these overlap fermions have half of the original number of flavors as 2 for the staggered-overlap and 8 for the 4-dimensional generalized Wilson fermions. Although we consider these cases since they have such beautiful relations, we can show overlap fermions with the other flavored-mass terms also have the correct index depending on the number of flavors.

In the end of this section we play with the spectrum and the spectral flow by changing a parameter for the flavored mass terms. We consider the following flavored-mass terms for 2d naive fermion,

$$-M_{\rm n}(c) = -M_{\tau_3\otimes\tau_3} - c\,(M_{\tau_3\otimes\mathbf{1}} + M_{\mathbf{1}\otimes\tau_3})\,, \tag{5.15}$$

where c is an overall coefficient of the two extra mass terms and we take account of the convention $D - M$. We take $m_{\tau_3\otimes\tau_3} = m_{\tau_3\otimes\mathbf{1}} = m_{\mathbf{1}\otimes\tau_3} = 0$. For example, the simplest case $c = 1$ leads to single negative mass as following,

$$-M_{\rm n}(c=1) = \text{diag}(-3,1,1,1) \equiv -\tilde{M}_{\rm n}. \tag{5.16}$$

This assigns only one negative mass to the eigenvalues of the Dirac operator $D_{\rm n} - \tilde{M}_{\rm n}$. Figure 5.4(c) shows there is a single negative branch and a tripled positive branch. This means there is only one flavor with negative mass. We also depict figures for $c = 0.2$ in Fig. 5.4(a) and $c = 0.5$ in Fig. 5.4(b) to convince you that one of the branch is singled out and the others are tripled. It describes the situation that the doubled negative branch is split and one branch goes towards the the positive branch. Then for the case of $c \sim 0.5$ this branch enters a positive range. Thus it is clear that the negative branch with $c = 1$ is singled out and the positive one should be triply degenerate.

Here we also study the spectral flow of the Hermitean operator with this term (5.15). Indeed it gives us a consistency check between the number of flavors and the index: Now we have a single flavor overlap fermion, thus the associated index should be exactly equal to minus the topological charge without a flavor factor in this dimension. The eigenvalue flow of the naive Hermitean operator with $c = 0.2$, $c = 0.5$ and $c = 1$ for $Q = 1$ are depicted in Fig. 5.5. It is obvious that the doubled flows are separated in the case of $c = 0.2$, and we find two of the four flows no longer cross zeros for $c = 0.5$. Thus only two crossings remain in the case of $c = 1$. As we have discussed in Eq. (5.13), the index of the overlap version is given by minus half difference of positive and negative eigenvalues of the Hermitean version of the original Dirac operator if the Dirac spectrum has the symmetric about the imaginary axis as in this case. Thus the index of exact zero modes of the $d = 2$ the overlap fermion with $c = 1$ is given by -1 for $Q = 1$. It generally means

$$\text{Index}\left(\tilde{D}_{\rm no}\right) = -Q, \tag{5.17}$$

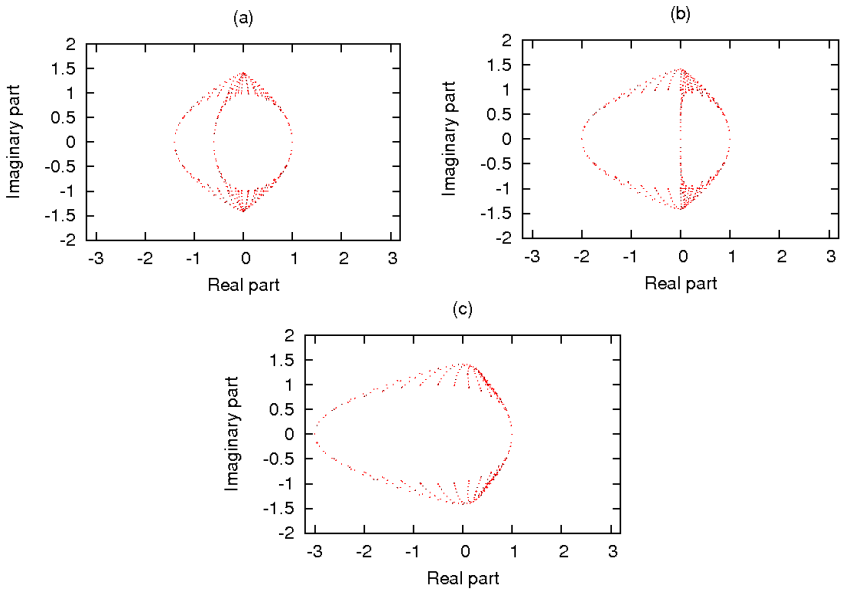

Figure 5.4: Complex spectra of the naive Dirac operators for the $d = 2$ free field case on a 36×36 lattice: (a) $c = 0.2$, (b) $c = 0.5$ and (c) $c = 1$. In (a) the doubled negative branch is lifted and one of them goes to the positive direction. In (b) this branch enters a positive range. In (c) it coincides with the positive branch.

which is a quarter of the original index of the 4-species naive fermion and there is no flavor factor. We can also check this formula for other topological charges. Thus we checked the consistency with the index. In the extension to general dimensions the theorem for the single flavor overlap fermion is given by

$$\text{Index}\left(\tilde{D}_{\text{no}}\right) = \frac{1}{2^d}\text{Index}\left(D_{\text{n}}\right) = (-1)^{d/2}Q. \tag{5.18}$$

5.3 Short summary

Let me summarize the argument in this chapter. We study the spectral flow of the Hermitean operators in these fermions. Then it is shown that the spectral flow correctly illustrates the integer index determined by gauge field topology both in the generalized Wilson and staggered-Wilson fermions reflecting the number of species. We also discuss overlap fermions composed from these fermion kernels with flavored mass terms. These fermions satisfy Ginsparg-Wilson relations instead of usual chiral symmetry. We show the topological charge can be also obtained as the index of exact zero modes of the these overlap fermions. Then we show by choosing the flavored mass term so that a desirable number of species has negative mass, the associated overlap fermion produces any number of massless fermionic modes.

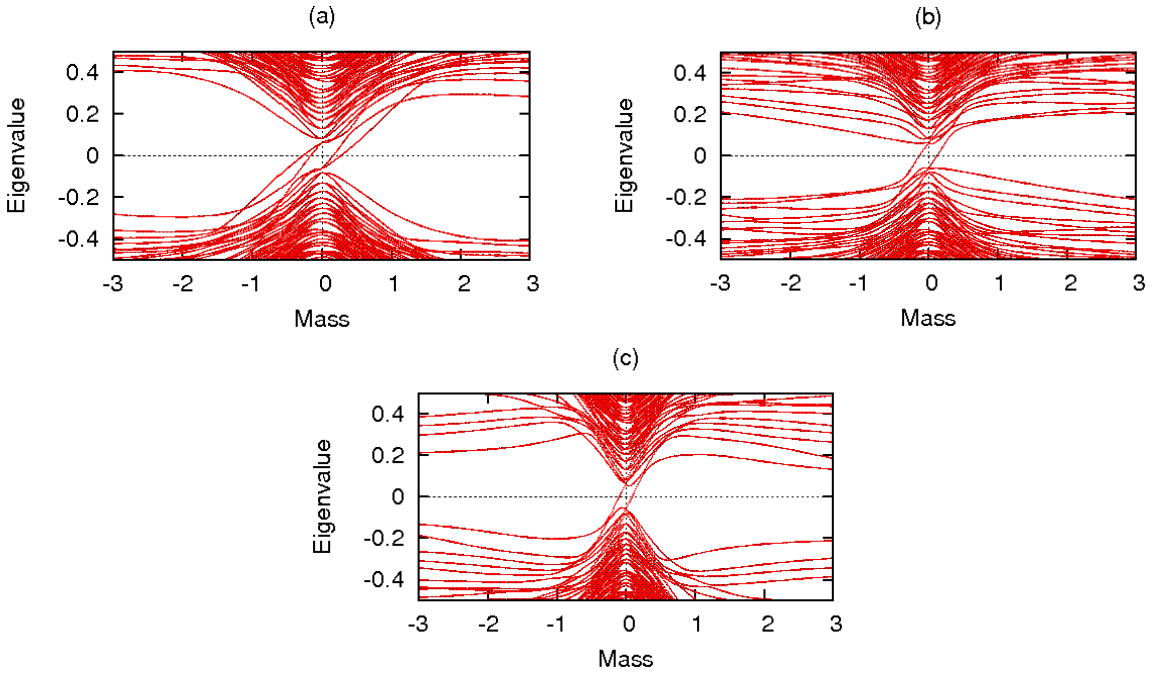

Figure 5.5: Spectral flows of the $d = 2$ naive Hermitean operators with a $Q = 1$, $\delta = 0.25$ background configuration on a 16×16 lattice: (a) $c = 0.2$, (b) $c = 0.5$ and (c) $c = 1$. The doubled flows are lifted in (a). Two of the four flows no longer cross zeros in (b). The two single crossings are shown in (c).

Chapter 6

Parity phase structure

6.1 Introduction

Since the pioneering work in Ref. [35], the rich phase structure in the lattice Wilson fermion has been extensively studied [36, 37, 38, 39, 40, 41, 42, 43, 44, 45, 86] in Fig. 2.5. As is well-known [1], Wilson fermions bypass the no-go theorem [4] and produce a single fermionic degree of freedom by breaking the chiral symmetry explicitly. This leads to an additive mass renormalization and requires fine-tuning of a mass parameter for a chiral limit. Furthermore at finite lattice spacing, there emerges a parity-broken phase (Aoki phase) [35]. The full phase diagram reflects the masses possessed by each of the original doublers. As seen from this fact, the main reason for the emergence of the parity-broken phase is that the Wilson term gives a species(taste)-sensitive mass to produce a mass splitting of species as well as breaking the chiral symmetry. The existence of the Aoki phase and the second-order phase boundary in Wilson-type lattice fermions indicates that one can apply them to lattice QCD simulations by tuning a mass parameter to take a chiral limit [46, 47, 48]. Indeed we can recover the PCAC relation near the second-order critical line, which is essential for QCD. Besides, the understanding of the parity-broken phase gives practical information for the application of its overlap [8, 9] and domain-wall versions [10, 12]. Indeed it is shown in [87] that the domain-wall fermion also possesses a complicated parity broken phase diagram for a finite size of the extra dimension.

In this chapter we elucidate the parity phase structure for the generalized WIlson and staggered-Wilson fermions in the framework of the Gross-Neveu model [91, 92, 43, 93, 94, 95] and the strong-coupling lattice QCD. We find the gap equations derived from the both theories show the pion condensate becomes nonzero in some range of the parameters and the pion becomes massless on the phase boundaries. It means the Aoki phase exists and the order of the phase transition is second-order. We also show we can take the chiral continuum limit in the Gross-Neveu model by tuning the mass and the gauge-coupling. These results indicate we can take the chiral limit by tuning the mass parameter and perform the lattice QCD simulation with these fermions as in the Wilson fermion. Especially staggered-Wilson fermions can be less expensive than Wilson fermions in lattice QCD simulations.

Note we use the simple forms of the generalized Wilson and staggered-Wilson fermions, namely the naive fermion and staggered fermion actions with the flavored-mass terms such

as (3.28) or (3.34). We do not use the standard Wilson forms with the Wilson action as shown in (4.1) and (4.5) since the purpose of this chapter is just to figure out the parity phase diagram and the related chiral limit. By shifting the phase diagram by a proper mass, we fine the usual Wilson types of the phase diagram. The other thing we want to note is that the phase diagram will be for simplicity depicted by using the dimensionless mass parameter such as $Ma \to M$. Please remember, however, in the dimensionful expression the horizontal axis has the scale of the order $1/a$ thus we need to fine-tune the parameter to give a chiral limit or the real quark mass. We will restore the lattice spacing in the discussion of the chiral and continuum limit.

Note the results in this chapter are based on the original work by the present author in Ref. [33].

6.2 Naive Gross-Neveu model

In this section we investigate the phase diagram for naive lattice fermions with flavored mass terms by using the $d = 2$ Gross-Neveu model, which has lots of common features with QCD. Let us begin with the lattice Gross-Neveu model with the flavored mass term, which is given by

$$S = \frac{1}{2}\sum_{n,\mu}\bar{\psi}_n\gamma_\mu(\psi_{n+\mu} - \psi_{n-\mu}) - \frac{g^2}{2N}\sum_n[(\bar{\psi}_n\psi_n)^2 + (\bar{\psi}_n i\gamma_5\psi_n)^2] + \sum_{n,m}\bar{\psi}_n(M\delta_{nm} + (M_f)_{n,m})\psi_m, \tag{6.1}$$

where μ stands for $\mu = 1, 2$, $n = (n_1, n_2)$ are the two dimensional coordinates and ψ_n stands for a N-component Dirac fermion field $(\psi_n)_j (j = 1, 2, ..., N)$. We note the bilinear $\bar{\psi}\psi$ means $\sum_{j=1}^N \bar{\psi}_j\psi_j$. g^2 corresponds to the 't Hooft coupling. M is a usual mass assigning the same mass to species while $(M_f)_{n,m}$ is a flavored mass assigning different masses to them. Here we define the two dimensional gamma matrices as $\gamma_1 = \sigma_1$, $\gamma_2 = \sigma_2$ and $\gamma_5 = \sigma_3$. We make all the quantities dimensionless in this equation. Here we consider scalar and pseudo-scalar four-fermi interactions which are sufficient to study the parity phase structure. By introducing auxiliary bosonic fields σ_n, π_n we remove the four-point interactions as

$$S = \frac{1}{2}\sum_{n,\mu}\bar{\psi}_n\gamma_\mu(\psi_{n+\mu} - \psi_{n-\mu}) + \sum_{n,m}\bar{\psi}_n(M_f)_{n,m}\psi_m + \frac{N}{2g^2}\sum_n((\sigma_n - M)^2 + \pi_n^2) + \sum_n\bar{\psi}_n(\sigma_n + i\gamma_5\pi_n)\psi_n. \tag{6.2}$$

By solving the equations of motion, we show the following relation between these auxiliary fields and the bilinears of the fermion fields

$$\sigma_n = M - \frac{g^2}{N}\bar{\psi}\psi, \tag{6.3}$$

$$\pi_n = -\frac{g^2}{N}\bar{\psi}i\gamma_5\psi. \tag{6.4}$$

These relations indicate how σ and π stand for the scalar and pseudo-scalar mesons. After integrating the fermion fields, the partition function and the effective action with these auxiliary fields are given by

$$Z = \int \prod_n (d\sigma_n d\pi_n) e^{-N S_{\rm eff}(\sigma,\pi)}, \tag{6.5}$$

$$S_{\rm eff}(\sigma_n, \pi_n) = \frac{1}{2g^2} \sum_n ((\sigma_n - M)^2 + \pi_n^2) - {\rm Tr}\, \log D_{n,m}, \tag{6.6}$$

with

$$D_{n,m} = (\sigma_n + i\gamma_5 \pi_n)\delta_{n.m} + \frac{\gamma_\mu}{2}(\delta_{n+\mu,m} - \delta_{n-\mu,m}) + (M_f)_{n,m}. \tag{6.7}$$

Here Tr stands for the trace both for the position and spinor spaces. As is well-known, the partition function in the Gross-Neveu model is given by the saddle point of this effective action in the large N limit. We denote as $\tilde{\sigma}_n$, $\tilde{\pi}_n$ solutions satisfying the saddle-point conditions

$$\frac{\delta S_{\rm eff}(\sigma_n, \pi_n)}{\delta \sigma_n} = \frac{\delta S_{\rm eff}(\sigma_n, \pi_n)}{\delta \pi_n} = 0. \tag{6.8}$$

Then the partition function is given by

$$Z = e^{-S_{\rm eff}(\tilde{\sigma}, \tilde{\pi})}. \tag{6.9}$$

By assuming the translational invariance we define the position-independent solutions as $\sigma_0 \equiv \tilde{\sigma}_0$ and $\pi_0 \equiv \tilde{\pi}_0$ Then we can factorize a volume factor $V = \sum_n 1$ in the effective action as

$$S_{\rm eff} = V \tilde{S}_{\rm eff}(\sigma_0, \pi_0), \tag{6.10}$$

$$\tilde{S}_{\rm eff}(\sigma_0, \pi_0) = \frac{1}{2g^2}((\sigma_0 - M)^2 + \pi_0^2) - \frac{1}{V}{\rm Tr}\, \log D. \tag{6.11}$$

We can write ${\rm Tr} \log D$ in a simple form by the Fourier transformation to momentum space

$$\begin{aligned} {\rm Tr}\, \log D &= V \int \frac{d^2k}{(2\pi)^2} \log[{\rm det}(\sigma_0 + i\gamma_5\pi_0 + M_f(k) + i\sum_\mu \gamma_\mu \sin k_\mu)] \\ &= V \int \frac{d^2k}{(2\pi)^2} \log[(\sigma_0 + M_f(k))^2 + \pi_0^2 + s^2], \end{aligned} \tag{6.12}$$

with det being the determinant in the spinor space and $s^2 = \sum_\mu \sin^2 k_\mu$. $M_f(k)$ is the flavored mass represented in momentum space. Now the saddle-point equations are written as

$$\frac{\delta \tilde{S}_{\rm eff}}{\delta \sigma_0} = \frac{(\sigma_0 - M)}{g^2} - 2\int \frac{d^2k}{(2\pi)^2} \frac{\sigma_0 + M_f(k)}{(\sigma_0 + M_f(k))^2 + \pi_0^2 + s^2} = 0, \tag{6.13}$$

$$\frac{\delta \tilde{S}_{\rm eff}}{\delta \pi_0} = \frac{\pi_0}{g^2} - 2\int \frac{d^2k}{(2\pi)^2} \frac{\pi_0}{(\sigma_0 + M_f(k))^2 + \pi_0^2 + s^2} = 0. \tag{6.14}$$

In this section we consider two types of the flavored mass for the naive fermion

$$M_f^{(1)}(k) \;=\; M_{\tau_3\otimes\tau_3} \;=\; \cos k_1 \cos k_2, \tag{6.15}$$

$$M_f^{(2)}(k) \;==\; M_{\tau_3\otimes\mathbf{1}} + M_{\mathbf{1}\otimes\tau_3} \;=\; (\cos k_1 + \cos k_2). \tag{6.16}$$

These flavored-mass terms are introduced in (3.14), (3.15) and (3.16) for the two-dimensional naive lattice fermions where we take the parameters for them as one. Studying the phase diagram with these flavored mass terms not only contributes to understanding the overlap versions but also helps to understand the staggered case in the next section. Here σ_0 and π_0 are determined as $\sigma_0(M, g^2)$, $\pi_0(M, g^2)$ from the saddle-point equations once the values of M and g^2 are fixed.

Let us look into the phase structure with respect to parity symmetry. The order parameter of this symmetry is π_0, which can take zero or non-zero values depending on values of M and g^2. Parity symmetry is spontaneously broken for the non-zero cases $\pi_0 \neq 0$. The phase boundary is determined by imposing $\pi_0 = 0$ on Eq. (6.13)(6.14) after the overall π_0 being removed in Eq. (6.14) . Then the conditions for the phase boundary, so-called gap equations, are given by

$$\frac{M_c}{g^2} \;=\; -2\int \frac{d^2k}{(2\pi)^2}\frac{M_f(k)}{(\sigma_0 + M_f(k))^2 + s^2}, \tag{6.17}$$

$$\frac{1}{g^2} \;=\; 2\int \frac{d^2k}{(2\pi)^2}\frac{1}{(\sigma_0 + M_f(k))^2 + s^2}, \tag{6.18}$$

with M_c being the critical value of M. As we will check later, this phase boundary is a second-order critical line. Here we derive the parity phase boundary $M_c(g^2)$ as a function of the coupling g^2 by getting rid of the chiral condensate σ_0 from these equations. We will calculate the parity phase boundaries for three cases of the flavored masses $M_f^{(1)}$ and $M_f^{(2)}$.

6.2.1 $M_f^{(1)}$

The lattice fermion action with this flavored mass assigns the positive mass $m = 1$ to two species with the momentum $(0,0)(\pi,\pi)$ and the negative mass $m = -1$ to the other two species with $(0,\pi)(\pi,0)$. Before calculating $M_c(g^2)$ numerically, we can anticipate the phase structure from the symmetry of the gap equations. To see this we replace k_1 by $\pi - k_1$ in (6.13) and (6.14) for $M_f^{(1)}$. Then the equations are converted into

$$\frac{-\sigma_0 + M}{g^2} = 2\int \frac{d^2k}{(2\pi)^2}\frac{-\sigma_0 + M_f^{(1)}(k)}{(-\sigma_0 + M_f^{(1)}(k))^2 + \pi_0^2 + s^2}, \tag{6.19}$$

$$\frac{\pi_0}{g^2} = 2\int \frac{d^2k}{(2\pi)^2}\frac{\pi_0}{(-\sigma_0 + M_f^{(1)}(k))^2 + \pi_0^2 + s^2}. \tag{6.20}$$

Thus, if $(\sigma_0,\, \pi_0)$ are solutions for $(M,\, g^2)$, $(-\sigma_0,\, \pi_0)$ are solutions for $(-M,\, g^2)$. It also means, if $(M_c,\, g^2)$ is a critical point, $(-M_c,\, g^2)$ too. We can anticipate the phase diagram

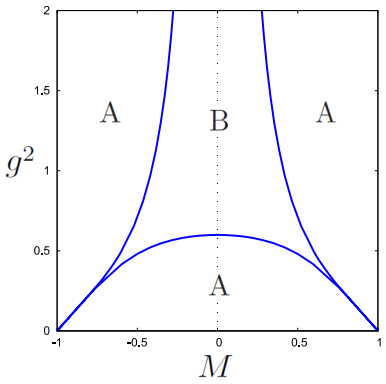

Figure 6.1: Aoki phase structure for the naive fermion with the flavored mass $M_f^{(1)}$. The left and right cusps are related to two species $(0,0)(\pi,\pi)$ with $m=1$ and the other two $(0,\pi)(\pi,0)$ with $m=-1$ respectively. A and B stands for parity-symmetric and -broken phases.

for this case is symmetric about $M=0$. Now we derive the parity phase boundary $M_c(g^2)$ numerically for $M_f^{(1)}(k) = \cos k_1 \cos k_2$. The phase diagram for this case is depicted in Fig. 6.1. A stands for the parity symmetric phase $\pi_0 = 0$ and B for Aoki phase $\pi_0 \neq 0$. In the large coupling region there are two phase boundaries while there are four phase boundaries in the weak coupling region. The left and right cusps correspond to two species $(0,0)(\pi,\pi)$ with the positive mass $(m=1)$ and the other two $(0,\pi)(\pi,0)$ with the negative mass $(m=-1)$ respectively. It reflects the mass splitting of species given by the flavored mass $M_f^{(1)}$. Here we note we obtain the same result for $-M_f^{(1)}$ except that the species $(0,0)(\pi,\pi)$ live at the right cusp and the other two live at the left. It means the sign of the this flavored mass is irrelevant for the spectrum of the Dirac operator or the associated Aoki phase.

6.2.2 $M_f^{(2)}$

The lattice fermion action with this flavored mass assigns the positive mass $(m=2)$ to one of four species with the momentum $(0,0)$, zero mass to $(0,\pi)(\pi,0)$ and the negative mass $(m=-2)$ to (π,π). To look at the symmetry of the gap equations we replace k_μ by $\pi - k_\mu$ in (6.13) and (6.14) for $M_f^{(2)}$. Then the equations are converted into

$$\frac{-\sigma_0 + M}{g^2} = 2\int \frac{d^2k}{(2\pi)^2} \frac{-\sigma_0 + M_f^{(2)}(k)}{(-\sigma_0 + M_f^{(2)}(k))^2 + \pi_0^2 + s^2}, \tag{6.21}$$

$$\frac{\pi_0}{g^2} = 2\int \frac{d^2k}{(2\pi)^2} \frac{\pi_0}{(-\sigma_0 + M_f^{(2)}(k))^2 + \pi_0^2 + s^2}. \tag{6.22}$$

Thus, if $(\sigma_0,\ \pi_0)$ are solutions for $(M,\ g^2)$, $(-\sigma_0,\ \pi_0)$ are solutions for $(-M,\ g^2)$. It also means, if $(M_c,\ g^2)$ is a critical point, $(-M_c,\ g^2)$ too. We can anticipate the phase diagram for this case is again symmetric about $M=0$. Now we derive the parity phase boundary $M_c(g^2)$ numerically for $M_f^{(2)}(k) = (\cos k_1 + \cos k_2)(1 + \cos k_1 \cos k_2)/2$. In the

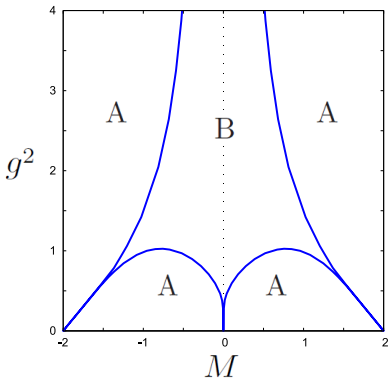

Figure 6.2: Aoki phase structure for the naive fermion with the flavored mass $M_f^{(2)}$. The three cusps correspond to $(0,0)$ with $m=2$, $(0,\pi)(\pi,0)$ with $m=0$ and (π,π) with $m=-2$ respectively from the left.

large coupling region there are two phase boundaries while there are six phase boundaries in the weak coupling region. The three cusps correspond to one of four species $(0,0)$ with $m=2$, two of them $(0,\pi)(\pi,0)$ with $m=0$ and the other one (π,π) with $m=-2$ respectively from the left. It reflects the mass splitting of species given by the flavored mass $M_f^{(2)}$.

We expect these results are qualitatively similar to the phase diagram of the $d=4$ fermion actions with the Non-abelian gauge field like QCD except for the number of species associated with each cusp. In the end of this section we check the mass of the π-meson becomes zero on the critical line $M_c(g^2)$. As is well-known, the correlation length gets infinitely large in the vicinity of the second and higher phase boundaries, which leads to massless dynamical degrees of freedom. In the case of lattice QCD with chiral-symmetry-broken fermions like Wilson fermion, the fine-tuning of the mass parameter to the 2nd order phase boundary leads to the chiral limit with massless quarks and massless pions regarded as Goldstone bosons due to the spontaneous chiral symmetry breaking. Thus it is quite important to verify it. We can show the mass of π_n becomes zero on the phase boundaries as

$$\begin{aligned} m_\pi^2 &\propto \langle \frac{\delta^2 S_{\text{eff}}}{\delta\pi_n \delta\pi_m} \rangle|_{M=M_c} = V \frac{\delta^2 \tilde{S}_{\text{eff}}}{\delta^2 \pi_0^2}|_{M=M_c} \\ &= V\Big[\frac{1}{g^2} - 2\int \frac{d^2k}{(2\pi)^2} \frac{1}{(\sigma_0 + M_f(k))^2 + \pi_0^2 + s^2} \\ &\qquad - (2\pi_0^2)\int \frac{d^2k}{(2\pi)^2} \frac{1}{((\sigma_0 + M_f(k))^2 + \pi_0^2 + s^2)^2}\Big]|_{\pi_0=0} \\ &= 0. \end{aligned} \tag{6.23}$$

The zero mass of the pion means the phase boundary we derived is the second-order critical line. We can also check the order of the phase boundaries by depicting the potential for σ_0 and π_0 as we will discuss in Sec. 6.4.

6.3 Staggered Gross-Neveu model

In this section we investigate the phase diagram for staggered fermions with the Adams-type flavored mass term (3.34) by using the $d = 2$ Gross-Neveu model. To study the parity broken phase structure we propose the generalized staggered Gross-Neveu model with the γ_5-type 4-point interaction, which is given by

$$S = \frac{1}{2}\sum_{n,\mu}\eta_\mu\bar{\chi}_n(\chi_{n+\mu}-\chi_{n-\mu}) + \sum_n \bar{\chi}_n(M+M_f^{(A)})\chi_n \\ - \frac{g^2}{2N}\sum_{\mathcal{N}}\Big[(\sum_A \bar{\chi}_{2\mathcal{N}+A}\,\chi_{2\mathcal{N}+A})^2 + (\sum_A i(-1)^{A_1+A_2}\bar{\chi}_{2\mathcal{N}+A}\,\chi_{2\mathcal{N}+A})^2\Big], \tag{6.24}$$

where we define two-dimensional coordinates as $n = 2\mathcal{N} + A$ with the sublattice $A = (A_1, A_2)$ $(A_{1,2} = 0, 1)$. χ_n is a one-component fermionic field. $(-1)^{A_1+A_2}$ corresponds to the natural definition of γ_5 for this fermion which is expressed as $\Gamma_{55} = \gamma_5 \otimes \gamma_5$ in the spinor-taste expression. $\eta_\mu = (-1)^{n_1+\ldots+n_{\mu-1}}$ corresponds to γ_μ. M is again a usual mass parameter while we take the flavored mass M_f as the Adams-type flavored-mass term, which is given by

$$M_f = M_A = \Gamma_5\Gamma_{55} \sim \mathbf{1}\otimes\gamma_5 + O(a), \tag{6.25}$$

with the following chirality matrix Γ_5

$$\Gamma_5 = -i\eta_1\eta_2\sum_{\text{sym}} C_1C_2, \tag{6.26}$$

$$C_\mu = \frac{1}{2}(T_\mu + T_{-\mu}), \tag{6.27}$$

where T_μ is the usual translation operator. (The chirality matrix in general dimensions is defined as $\Gamma_5 \equiv -(i)^{d/2}\eta_1\cdots\eta_d\sum_{\text{sym}} C_1\cdots C_d$.) This mass term assigns the positive mass $(m = +1)$ to one taste and the negative mass $(m = -1)$ to the other depending on $\pm$ eigenvalues for $\Gamma_5\Gamma_{55}$ which we call the flavor-chirality. With bosonic auxiliary fields $\sigma_{\mathcal{N}}$, $\pi_{\mathcal{N}}$, the action is rewritten as

$$S = \frac{1}{2}\sum_{n,\mu}\eta_\mu\bar{\chi}_n(\chi_{n+\mu}-\chi_{n-\mu}) + \sum_n \bar{\chi}_n M_f\chi_n \\ + \frac{N}{2g^2}\sum_{\mathcal{N}}((\sigma_{\mathcal{N}}-M)^2+\pi_{\mathcal{N}}^2) + \sum_{\mathcal{N},A}\bar{\chi}_{2\mathcal{N}+A}(\sigma_{\mathcal{N}} + i(-1)^{A_1+A_2}\pi_{\mathcal{N}})\chi_{2\mathcal{N}+A}, \tag{6.28}$$

After integrating the fermion field, the partition function and the effective action with these auxiliary fields are given by

$$Z = \int(\mathcal{D}\sigma_{\mathcal{N}}\mathcal{D}\pi_{\mathcal{N}})e^{-N\,S_{\text{eff}}(\sigma,\pi)}, \tag{6.29}$$

$$S_{\text{eff}} = \frac{1}{2g^2}\sum_{\mathcal{N}}(\sigma_{\mathcal{N}}^2+\pi_{\mathcal{N}}^2) - \text{Tr}\,\log D, \tag{6.30}$$

with

$$D_{n,m} = (\sigma_{\mathcal{N}} + i(-1)^{A_1+A_2}\pi_{\mathcal{N}})\delta_{n,m} + \frac{\eta_\mu}{2}(\delta_{n+\mu,m} - \delta_{n-\mu,m}) + (M_f)_{n,m}. \tag{6.31}$$

The process from (6.8) to (6.11) in the case of the naive fermion is common with this staggered case. We again denote as σ_0 and π_0 the position-independent solutions of the saddle-point equations. In this case, however, it is not straightforward to derive the $\mathrm{Tr}\log D$ with the Dirac operator (6.31) in the effective action Eq. (6.11). In order to estimate this trace logarithm we first obtain the determinant of the Dirac operator in the sublattice space, which means the determinant in the spinor and taste spaces. Here we express the sublattice structure as a multiplet field $\tilde{\chi}_{\mathcal{N}}$ composed of the four one-component fields as

$$\tilde{\chi}_{\mathcal{N}} = \begin{pmatrix} \chi_{\mathrm{i}} \\ \chi_{\mathrm{ii}} \\ \chi_{\mathrm{iii}} \\ \chi_{\mathrm{iv}} \end{pmatrix}, \tag{6.32}$$

where we mean $\mathrm{i} = 2\mathcal{N}$, $\mathrm{ii} = 2\mathcal{N} + (1,0)$, $\mathrm{iii} = 2\mathcal{N} + (0,1)$ and $\mathrm{iv} = 2\mathcal{N} + (1,1)$. Now let us estimate the trace term

$$\mathrm{Tr}\ \log D = V \int \frac{dk^2}{(2\pi)^2} \log\det((D(k))_{ab}, \tag{6.33}$$

where a, b stand for the index of the four sublattices running from i to iv. Here det means the determinant with respect to the sublattice. The Dirac operator is given by

$$\begin{aligned}(D(k))_{ab} = \sigma_0\delta_{ab} &+ \begin{pmatrix} + & & & \\ & - & & \\ & & - & \\ & & & + \end{pmatrix} i\pi_0 \\ &+ i \begin{pmatrix} & & & + \\ & & + & \\ & - & & \\ - & & & \end{pmatrix} \cos\frac{k_1}{2}\cos\frac{k_2}{2} \\ &+ \begin{pmatrix} 0 & i\sin\frac{k_1}{2} & i\sin\frac{k_2}{2} & 0 \\ i\sin\frac{k_1}{2} & 0 & 0 & -i\sin\frac{k_2}{2} \\ i\sin\frac{k_2}{2} & 0 & 0 & i\sin\frac{k_1}{2} \\ 0 & -i\sin\frac{k_2}{2} & i\sin\frac{k_1}{2} & 0 \end{pmatrix}.\end{aligned} \tag{6.34}$$

Then $\det D$ is given by

$$\begin{aligned}\det(D(k))_{ab} &= (\sigma_0^2 + \pi_0^2 + s^2)^2 - 2c_1^2c_2^2(\sigma_0^2 - \pi_0^2 - s^2) + c_1^4c_2^4 \\ &= ((\sigma_0 + c_1c_2)^2 + \pi_0^2 + s^2)((\sigma_0 - c_1c_2)^2 + \pi_0^2 + s^2),\end{aligned} \tag{6.35}$$

where $s_\mu = \sin k_\mu/2$, $s^2 = \sum_\mu s_\mu^2$, $c_\mu = \cos k_\mu/2$. It is notable that this determinant is expressed by the product of the two determinants of the naive fermions with the flavored

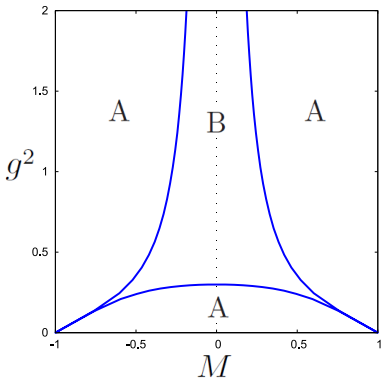

Figure 6.3: Aoki phase structure for the staggered fermion with the Adams-type flavored mass $\Gamma_5\Gamma_{55}$. The left and right cusps correspond to one of two tastes with $m = 1$ and the other with $m = -1$. A stands for a parity symmetric phase and B for Aoki phase.

mass $\pm M_f^{(1)}(k_\mu/2)$. Now we can explicitly write the saddle-point conditions satisfied by σ_0 and π_0 as

$$\frac{\sigma_0 - M}{g^2} = 4\int \frac{dk^2}{(2\pi)^2} \frac{\sigma_0(\sigma_0^2+\pi_0^2+s^2) - c_1^2c_2^2\sigma_0}{((\sigma_0+c_1c_2)^2+\pi_0^2+s^2)((\sigma_0-c_1c_2)^2+\pi_0^2+s^2)}, \tag{6.36}$$

$$\frac{\pi_0}{g^2} = 4\int \frac{dk^2}{(2\pi)^2} \frac{\pi_0(\sigma_0^2+\pi_0^2+s^2) + c_1^2c_2^2\pi_0}{((\sigma_0+c_1c_2)^2+\pi_0^2+s^2)((\sigma_0-c_1c_2)^2+\pi_0^2+s^2)}. \tag{6.37}$$

By multiplying -1 to the first equation, we see $(-\sigma_0,\ \pi_0)$ are solutions for $(-M,\ g^2)$ if $(\sigma_0,\ \pi_0)$ are solutions for $(M,\ g^2)$. It also means, if $(M_c,\ g^2)$ is a critical point, $(-M_c,\ g^2)$ too. The phase diagram will be symmetric about $M = 0$. The parity phase boundary $M_c(g^2)$ in this case is derived by imposing $\pi_0 = 0$ in (6.36)(6.37) after the overall π_0 being removed in the second one. Then the gap equations are given by

$$\frac{M_c}{g^2} = 4\int \frac{dk^2}{(2\pi)^2} \frac{2c_1^2c_2^2\sigma_0}{((\sigma_0+c_1c_2)^2+\pi_0^2+s^2)((\sigma_0-c_1c_2)^2+\pi_0^2+s^2)}, \tag{6.38}$$

$$\frac{1}{g^2} = 4\int \frac{dk^2}{(2\pi)^2} \frac{\sigma_0^2+s^2+c_1^2c_2^2}{((\sigma_0+c_1c_2)^2+\pi_0^2+s^2)((\sigma_0-c_1c_2)^2+\pi_0^2+s^2)}. \tag{6.39}$$

By removing σ_0 in these equations, we derive the phase boundary $M_c(g^2)$. The result is shown in Fig. 6.3.

Here again A stands for the parity symmetric phase ($\pi_0 = 0$) and B for Aoki phase ($\pi_0 \neq 0$). In the large coupling region there are two phase boundaries while there are four phase boundaries in the weak coupling region. The left cusp corresponds to one of two tastes with $m = 1$, and the right corresponds to the other taste with $m = -1$. Thus the phase diagram reflects the mass splitting of tastes given by the Adams-type flavored mass. We also check the pion mass becomes zero on the second order phase boundary as

$$m_\pi^2 \propto \langle \frac{\delta^2 S_{\rm eff}}{\delta\pi_n \delta\pi_m} \rangle|_{M=M_c} = V \frac{\delta^2 \tilde{S}_{\rm eff}}{\delta^2 \pi_0^2}|_{M=M_c} = 0. \tag{6.40}$$

Now let us consider the parity phase structure in the $d = 4$ QCD with the staggered fermion with this flavored mass. Considering the case of the Wilson fermion [35] where the

phase structure in the Gross-Neveu model was shown to carry over in the four dimensional QCD, we can speculate it is qualitatively similar to our result for the $d = 2$ Gross-Neveu model except the number of species associated with each cusp. In the four dimension, four tastes in the staggered fermion with the Adams-type flavored mass split into two with positive mass and the other two with negative mass depending on their flavor-chiralities. Thus each of the cusps in the phase diagram will correspond to two tastes. If we consider another type of the flavored mass term proposed in [32], the four tastes are split into one with positive mass, two with zero mass and the other with negative mass. If we can take the chiral and continuum limit around the cusps, we obtain the two- or one-flavor staggered fermions with tuning only the mass parameter, which will be numerically faster than Wilson fermion. Thus the question here is whether we can take the massless (chiral) continuum limit. We will discuss this point in the next section with starting with the case of the naive fermion.

6.4 Chiral and Continuum limit

In this section we discuss the chiral and continuum limit of the naive and staggered Gross-Neveu models with the flavored masses discussed in Sec. 6.2 and Sec. 6.3. This analysis gives us important informations on the continuum limit of the $d = 4$ QCD with these fermions. As is well-known, the chiral symmetry is realized in the effective potential of the Gross-Neveu model as the $O(2)$ rotational symmetry about σ_0 and π_0. The purpose here is to figure out the fine-tuned values of the mass and couplings to recover this symmetry for $a \to 0$. We note in order to take the chiral and continuum limit in this model, we need to introduce two independent couplings g_σ^2 and g_π^2 [43] as we will see later. The strategy is to expand the fermion determinant in the effective potential with respect to the lattice spacing a following the process in [43].

We first consider the case of the naive fermion with one of the flavored masses $M_f^{(1)} = \cos k_1 \cos k_2$. We note we restore the lattice coupling a to discuss $a \to 0$ limit. The effective potential in this case with the lattice spacing being explicit is given by

$$\tilde{S}_{\text{eff}}(\sigma_0, \pi_0) = \frac{(\sigma_0 - M)^2}{2g_\sigma^2} + \frac{\pi_0^2}{2g_\pi^2} - I, \tag{6.41}$$

$$I = \int_{-\pi/a}^{\pi/a} \frac{d^2k}{(2\pi)^2} \log[(\sigma_0 + \frac{1}{a}\cos k_1 a \cos k_2 a)^2 + \pi_0^2 + \sum_\mu \frac{\sin^2 k_\mu a}{a^2}]. \tag{6.42}$$

Now we divide the terms in the determinant I into $\mathcal{O}(1/a^2)$ and $\mathcal{O}(1/a)$ parts as

$$I(D_0, D_1) = \int_{-\pi/a}^{\pi/a} \frac{d^2k}{(2\pi)^2} \log[D_0 + D_1], \tag{6.43}$$

$$D_0 \equiv \sum_\mu \frac{\sin^2 k_\mu a}{a^2} + (\sigma_0 - \frac{\alpha}{a})^2 + \pi_0^2 + \Big(\frac{\alpha + \cos k_1 a \cos k_2 a}{a}\Big)^2, \tag{6.44}$$

$$D_1 \equiv 2(\sigma_0 - \frac{\alpha}{a})\Big(\frac{\alpha + \cos k_1 a \cos k_2 a}{a}\Big). \tag{6.45}$$

where we introduce a constant α since there is arbitrariness about how to divide the terms into $\mathcal{O}(1/a^2)$ and $\mathcal{O}(1/a)$ parts. This is determined by which cusp you choose in Fig. 6.1, or equivalently which species you want to make massless in the continuum limit. Here we fix $\alpha = -1$ which is related to the left cusp or the continuum limit with the massless species $(0,0)$ and (π,π). Here we use the shifted definition of σ_0 as $\sigma_0 + 1/a \to \sigma_0$ for simplicity for a while. Then the effective potential with this shift is given by

$$\tilde{S}_{\text{eff}}(\sigma_0,\pi_0) = \frac{(\sigma_0 - (M+1/a))^2}{2g_\sigma^2} + \frac{\pi_0^2}{2g_\pi^2} - I(D_0,D_1), \tag{6.46}$$

$$D_0 = \sum_\mu \frac{\sin^2 k_\mu a}{a^2} + \sigma_0^2 + \pi_0^2 + \Big(\frac{-1+\cos k_1 a \cos k_2 a}{a}\Big)^2, \tag{6.47}$$

$$D_1 = 2\sigma_0\Big(\frac{-1+\cos k_1 a \cos k_2 a}{a}\Big). \tag{6.48}$$

We expand I by D_1/D_0 or equivalently by the lattice spacing a,

$$I = I_0 + \sum_{n=1} I_n, \tag{6.49}$$

$$I_0 = \int_{-\pi/a}^{\pi/a} \frac{d^2k}{(2\pi)^2} \log D_0, \tag{6.50}$$

$$\begin{aligned} I_n &= -\frac{(-1)^n}{n}\int_{-\pi/a}^{\pi/a}\frac{d^2k}{(2\pi)^2}\frac{D_1^n}{D_0^n} \quad (n\geq 1), \\ &= -\frac{(-1)^n}{n}(2\sigma_0)^n a^{n-2} \\ &\quad \times \int_{-\pi}^{\pi}\frac{d^2\xi}{(2\pi)^2}\frac{(-1+\cos\xi_1\cos\xi_2)^n}{(\sum_\mu \sin^2\xi_\mu + (-1+\cos\xi_1\cos\xi_2)^2 + a^2(\sigma_0^2+\pi_0^2))^n}, \end{aligned} \tag{6.51}$$

where we introduce the dimensionless momentum $\xi_\mu = k_\mu a$. For $a \to 0$, only the I_0, I_1 and I_2 remains nonzero. $I_0(a\to 0)$, $I_1(a\to 0)$ and $I_2(a\to 0)$ are given by

$$I_0(a\to 0) = \tilde{C}_0(\sigma_0^2+\pi_0^2) - \frac{1}{2\pi}(\sigma_0^2+\pi_0^2)\log\frac{a^2(\sigma_0^2+\pi_0^2)}{e} \qquad (\tilde{C}_0 = 0.367), \tag{6.52}$$

$$I_1(a\to 0) = \frac{2\sigma_0}{a}C_1 \qquad (C_1 = -0.446), \tag{6.53}$$

$$I_2(a\to 0) = -2\sigma_0^2 C_2 \qquad (C_2 = 0.201). \tag{6.54}$$

From here we basically do not care about the $\mathcal{O}(a)$ corrections. Here we show the explicit values of $\tilde{C}_0$, C_1 and C_2 since they will be essential for the discussion later. The details of the calculations are shown in Appendix B.1. Now let us discuss the continuum limit of this theory. Including all the nonzero contributions for $a \to 0$, the effective potential is given by

$$\begin{aligned} \tilde{S}_{\text{eff}} &= -\Big(\frac{M+1/a}{g_\sigma^2} + \frac{2}{a}C_1\Big)\sigma_0 + \Big(\frac{1}{2g_\pi^2} - \tilde{C}_0 + \frac{1}{2\pi}\log a^2\Big)\pi_0^2 \\ &\quad + \Big(\frac{1}{2g_\sigma^2} - \tilde{C}_0 + 2C_2 + \frac{1}{2\pi}\log a^2\Big)\sigma_0^2 + \frac{1}{2\pi}(\sigma_0^2+\pi_0^2)\log\frac{\sigma_0^2+\pi_0^2}{e}. \end{aligned} \tag{6.55}$$

This indicates we need two independent couplings g_σ^2, g_π^2 to recover the $O(2)$ symmetry toward the continuum limit. In addition, getting rid of the σ_0 linear term leads to the massless limit. Then the natural fine-tuned parameters for the chirally symmetric limit without $\mathcal{O}(a)$ corrections are given by

$$M = -\frac{2g_\sigma^2}{a}C_1 - \frac{1}{a}, \tag{6.56}$$

$$g_\pi^2 = \frac{g_\sigma^2}{4C_2 g_\sigma^2 + 1}, \tag{6.57}$$

where Eq. (6.56) is obtained by imposing the coefficient of σ_0 and Eq. (6.57) is given by imposing the coefficients of σ_0^2 and π_0^2 coincide. To consider a renormalized theory with the chiral symmetry in the continuum limit we introduce the scale parameter (Λ-parameter) as

$$\Lambda a = \exp\left[\pi\tilde{C}_0 - 2\pi C_2 - \frac{\pi}{2g_\sigma^2}\right]. \tag{6.58}$$

With the natural fine-tuning (6.57), this definition of Λ leads to the coupling renormalization for the continuum limit including a given by

$$\frac{1}{2g_\sigma^2} = \tilde{C}_0 - 2C_2 + \frac{1}{2\pi}\log\left(\frac{1}{\Lambda^2 a^2}\right), \tag{6.59}$$

$$\frac{1}{2g_\pi^2} = \tilde{C}_0 + \frac{1}{2\pi}\log\left(\frac{1}{\Lambda^2 a^2}\right). \tag{6.60}$$

Here we need to keep Λ finite when we take the continuum limit $a \to 0$. Then the renormalized effective potential with the chiral symmetry in the continuum limit is given by

$$\tilde{S}_{\text{eff}} = \frac{1}{2\pi}(\sigma_0^2 + \pi_0^2)\log\frac{\sigma_0^2 + \pi_0^2}{e\Lambda^2}. \tag{6.61}$$

We note the fine-tuned point $(M(g_\sigma^2), g_\pi^2(g_\sigma^2))$ in (6.56)(6.57) specifies the line along which the continuum limit should be taken. At the minimum of this potential σ_0 or the VEV $\langle\sigma_0\rangle$ has a nonzero value, which corresponds to the spontaneous chiral symmetry breaking.

Let us look at the fine-tuned parameters (6.56)(6.57) in terms of the phase diagram. By this we can verify our fine-tuning yields the chiral-symmetric continuum theory. We first consider the non-zero value of g_σ^2 as $g_\sigma^2 = 0.6$ to reveal properties of the phase diagram. By hiding the lattice parameter with $a = 1$ the fine-tuned point $(M(0.6), g_\pi^2(0.6))$ is given by

$$M(g_\sigma^2 = 0.6) \;=\; -0.464, \tag{6.62}$$

$$g_\pi^2(g_\sigma^2 = 0.6) \;=\; 0.404. \tag{6.63}$$

Now we consider the M-g_π^2 phase diagram with $g_\sigma^2 = 0.6$. Before looking into this, let us review the case for the Wilson fermion. According to the case of the Wilson Gross-Neveu model [86], the phase boundary has a self-crossing point and the fine-tuned point is located slightly inside and below the self-crossing point in the parity symmetric phase.

Besides, the phase boundary naively derived from the gap equations no longer describes the true one near the self-crossing point, and we need study the effective potential to find the true critical lines including the 1st order ones. Here we will show these situations are common with our cases. The gap equations for the two couplings are given by

$$M_c = \sigma_0\Big(1 - \frac{g_\sigma^2}{g_\pi^2}\Big) - 2g_\sigma^2 \int \frac{d^2k}{(2\pi)^2} \frac{M_f^{(1)}(k)}{(\sigma_0 + M_f^{(1)}(k))^2 + s^2}, \tag{6.64}$$

$$\frac{1}{g_\pi^2} = 2\int \frac{d^2k}{(2\pi)^2} \frac{1}{(\sigma_0 + M_f^{(1)}(k))^2 + s^2}, \tag{6.65}$$

Here we come back to the unshifted definition of σ_0. In Fig. 6.4 and Fig. 6.5 we depict the $M_c(g_\pi^2)$ phase boundary derived from the gap equations (6.64)(6.65) for $g_\sigma^2 = 0.6$. The latter is an expanded one near the self-crossing point with the true phase boundaries. In the both figures a crosspoint stands for the fine-tuned point without $\mathcal{O}(a)$ corrections (6.62)(6.63). It is located slightly to the right and below the self-crossing point near the second order phase boundary. We note this region is the parity-unbroken phase. The qualitative properties of this phase diagram remain toward $g_\sigma^2 \to 0$ where the whole structure moves down to $g_\pi^2 = 0$ with the 1st-order boundaries disappearing. Here the fine-tuned point (6.56)(6.57) gets close to the endpoint of the 2nd-order phase boundary at $(M, g_\pi^2) \to (-1, 0)$, which corresponds to two species $(0,0)(\pi,\pi)$. Thus the continuum limit along this fine-tuned point yields the theory with chiral symmetry and two massless fermions, which leads to massless pions as Goldstone bosons, even though there are the 1st-order phase transitions.

Now we discuss the first order phase transition. Although it is not essential for our purpose because in the limit $g_\sigma^2 \to 0$ the 1st-order phase boundary disappears and the entire phase boundary becomes of 2nd order, we can reveal other aspects of our fermions by investigating it. As shown in [86] there are two kinds of the 1st order phase boundaries in the case of Wilson fermion. One is the parity phase boundary, across which π_0 at the minimum of the effective potential changes from zero to nonzero. The other is related to σ_0, across which the sign of σ_0 at the minimum of the potential changes discontinuously. Now we will show both of them exist also in our case. We numerically calculate the effective potential in Eq. (6.42) and search the minimum of the potential. In Fig. 6.5 we depict the appearance of the 1st order phase boundaries. Here we note the true parity phase boundary of 2nd order as a blue solid line coincides with the naively derived phase boundary as a blue dotted line at the both sides of the self-crossing. Then the 2nd-order one coming from the left converts to the 1st-order at some point, which is spilled out from the naively derived boundary. It ends at the point encountering the naively derived one again. The 1st-order phase boundary for σ_0 starts from this point, going down straight, and ends at $g_\pi^2 = 0$. In Fig. 6.6 we depict the order parameter π_0 as a function of M for some fixed values of g_π^2 around which the order changes in Fig. 6.5. Here we verify the order of the transition changes from the 2nd to the 1st about the point. In Fig. 6.7 we depict the σ_0 potential for several values of M crossing the σ_0 phase boundary. (Here we can take $\pi_0 = 0$ since it is the parity symmetric phase.) The value of σ_0 at the minimum changes from $\sigma_0 > -1$ to $\sigma_0 < -1$ in a form of the 1st-order phase transition. Indeed the potential describing these 1st-order transitions is also obtained by taking account of $\mathcal{O}(a)$

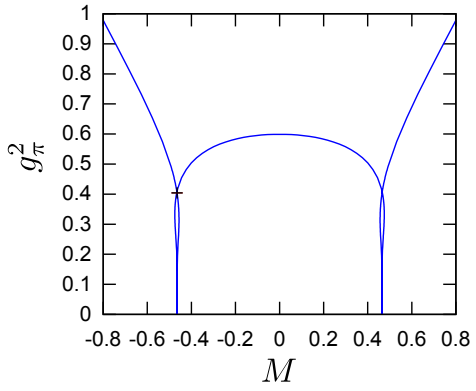

Figure 6.4: The naively derived phase boundary $M(g_\pi^2)$ for the naive fermion with $M_f^{(1)}$ with $g_\sigma^2 = 0.6$. The fine-tuned point $(-0.464, 0.404)$ as a crosspoint is located near the self-crossing point.

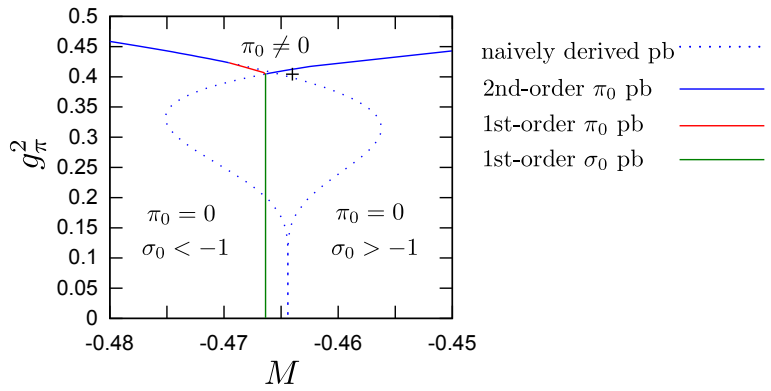

Figure 6.5: An expanded version of Fig. 6.4. A blue dotted curve is the naively derived phase boundary. The true phase boundaries are composed of the three parts. The fine-tuned point as a cross point is located slightly to the right and below the self-crossing point.

corrections. The contribution from the correction $\delta\tilde{S}_{\text{eff}}$ is given by

$$\delta\tilde{S}_{\text{eff}} = -\frac{8}{3}C_3\sigma_0^3 + 2\sigma_0(\sigma_0^2+\pi_0^2)\left(\tilde{C}_1 + \frac{1}{4\pi}\log\frac{\sigma_0^2+\pi_0^2}{e}\right), \tag{6.66}$$

with $C_3 = -0.0923$ and $\tilde{C}_1 = -0.0741$. We can qualitatively reproduce the above results from the effective potential with these corrections. We can obtain the same but reversed phase structure for the right cusp by choosing $\alpha = 1/a$ in (6.44)(6.45). We also note the sign of σ_0 continuously changes at $M = 0$. It is related with the discrete chiral symmetry ($\sigma_0 \to -\sigma_0$) of the effective action (6.42) for $M = 0$ up to a irrelevant sign. This symmetry indicates interesting possibility of another continuum limit corresponding to the case of $\alpha = 0$ in (6.44)(6.45). We will not discuss it in details here, but we note the clear argument about this topic was done by the present author in [57].

We apply the same approach to the staggered Gross-Neveu model with the Adams-type flavored mass in Eq. (6.25). As seen in Eq. (6.35), the determinant in the logarithm in

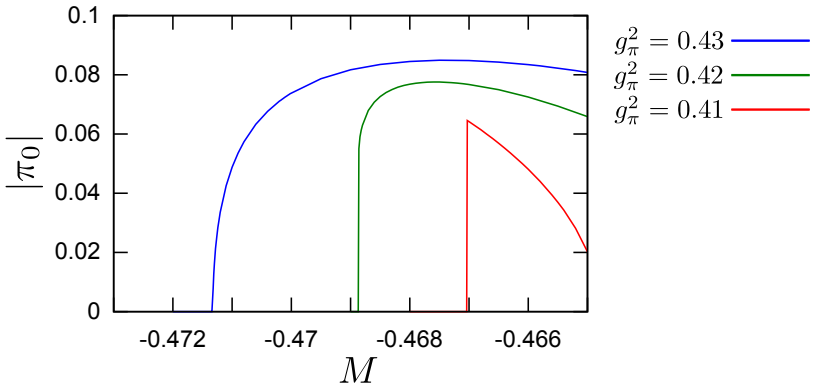

Figure 6.6: The order parameter π_0 as a function of M for $g_\pi^2 = 0.41, 0.42, 0.43$ where the order of transition changes from 1st to 2nd in Fig. 6.5.

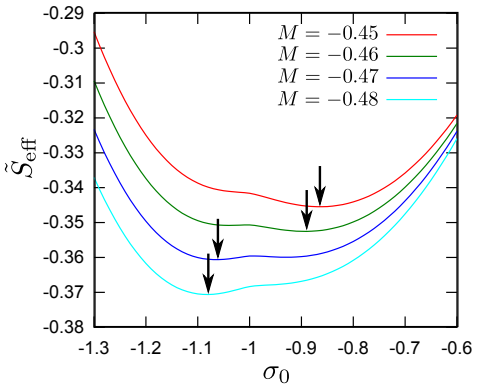

Figure 6.7: The σ_0 potential for several values of M crossing the σ_0 boundary in Fig. 6.5. The value of σ_0 at the minimum changes from $\sigma_0 > -1$ to $\sigma_0 < -1$ in a form of the 1st-order transition.

the effective action is given by the product of two determinants of the naive fermions with the mass $\pm M_f = \pm\cos(k_1/2)\cos(k_2/2)$. Thus we only have to add the contributions from the two sectors. Here we take the constant α as $\alpha = -1/a$ and redefine $\sigma_0 + 1/a \ \to \ \sigma_0$ for a while. With this choice we can discuss the left cusp related to the taste with the positive flavor-chirality. Then the effective potential with the σ_0 shift is given by

$$\tilde{S}_{\text{eff}}(\sigma_0, \pi_0) \ = \ \frac{(\sigma_0 - (M + 1/a))^2}{2g_\sigma^2} + \frac{\pi_0^2}{2g_\pi^2} - I^+ - I^-, \tag{6.67}$$

$$I^\pm = \int_{-\pi/a}^{\pi/a} \frac{d^2k}{(2\pi)^2} \log[D_0^\pm + D_1^\pm], \tag{6.68}$$

$$D_0^\pm = \sum_\mu \frac{\sin^2 \frac{k_\mu a}{2}}{a^2} + \sigma_0^2 + \pi_0^2 + \Big(\frac{-1 \pm \cos\frac{k_1 a}{2}\cos\frac{k_2 a}{2}}{a}\Big)^2, \tag{6.69}$$

$$D_1^\pm = 2\sigma_0\Big(\frac{-1 \pm \cos\frac{k_1 a}{2}\cos\frac{k_2 a}{2}}{a}\Big). \tag{6.70}$$

We expand I with respect to D_1/D_0 as

$$I^\pm = I_0^\pm + \sum_{n=1} I_n^\pm, \tag{6.71}$$

$$I_0^\pm = \int_{-\pi/a}^{\pi/a} \frac{d^2k}{(2\pi)^2} \log D_0^\pm, \tag{6.72}$$

$$I_n^\pm = -\frac{(-1)^n}{n} \int_{-\pi/a}^{\pi/a} \frac{d^2k}{(2\pi)^2} \frac{(D_1^\pm)^n}{(D_0^\pm)^n} \quad (n \geq 1). \tag{6.73}$$

For the continuum limit $a \to 0$, only the $I_0^\pm$, $I_1^\pm$ and $I_2^\pm$ remains nonzero as in the previous case.

$$I_0^+ + I_0^- = \tilde{C}_0(\sigma_0^2 + \pi_0^2) - \frac{1}{\pi}(\sigma_0^2 + \pi_0^2)\log\frac{4a^2(\sigma_0^2 + \pi_0^2)}{e} \quad (\tilde{C}_0 = 1.177), \tag{6.74}$$

$$I_1^+ + I_1^- = \frac{2\sigma_0}{a} C_1 \quad (C_1 = -0.896), \tag{6.75}$$

$$I_2^+ + I_2^- = -2\sigma_0^2 C_2 \quad (C_2 = 0.404). \tag{6.76}$$

Details of calculations are shown in Appendix B.2. The effective potential and the fine-tuned point without $\mathcal{O}(a)$ corrections $(M(g_\sigma^2), g_\pi^2(g_\sigma^2))$ are given by the equations similar to Eqs. (6.55)-(6.61) as following. The effective potential for $a \to 0$ in this case is given by

$$\begin{aligned}\tilde{S}_{\text{eff}} = &-\Big(\frac{M + 1/a}{g_\sigma^2} + \frac{2}{a}C_1\Big)\sigma_0 + \Big(\frac{1}{2g_\pi^2} - \tilde{C}_0 + \frac{1}{\pi}\log 4a^2\Big)\pi_0^2 \\ &+ \Big(\frac{1}{2g_\sigma^2} - \tilde{C}_0 + 2C_2 + \frac{1}{\pi}\log 4a^2\Big)\sigma_0^2 + \frac{1}{\pi}(\sigma_0^2 + \pi_0^2)\log\frac{\sigma_0^2 + \pi_0^2}{e}.\end{aligned} \tag{6.77}$$

Then the tuned point for the chiral limit without $\mathcal{O}(a)$ corrections is

$$M = -\frac{2g_\sigma^2}{a}C_1 - \frac{1}{a}, \tag{6.78}$$

$$g_\pi^2 = \frac{g_\sigma^2}{4C_2 g_\sigma^2 + 1}, \tag{6.79}$$

We again introduce the scale parameter (Λ-parameter) as

$$2a\Lambda = \exp\left[\frac{\pi}{2}\tilde{C}_0 - \pi C_2 - \frac{\pi}{4g_\sigma^2}\right]. \tag{6.80}$$

where we note the lattice spacing a appears with a factor 2, which is specific to the staggered fermions. The coupling renormalization for the chiral and continuum limit is given by

$$\frac{1}{2g_\sigma^2} = \tilde{C}_0 - 2C_2 + \frac{1}{\pi}\log\left(\frac{1}{4\Lambda^2 a^2}\right), \tag{6.81}$$

$$\frac{1}{2g_\pi^2} = \tilde{C}_0 + \frac{1}{\pi}\log\left(\frac{1}{4\Lambda^2 a^2}\right), \tag{6.82}$$

where we keep Λ finite when taking the continuum limit $a \to 0$. Finally the renormalized effective potential in the chiral and continuum limit is given by

$$\tilde{S}_{\text{eff}} = \frac{1}{\pi}(\sigma_0^2 + \pi_0^2)\log\frac{\sigma_0^2 + \pi_0^2}{e\Lambda^2}. \tag{6.83}$$

In this case we take $g_\sigma^2 = 0.4$ as an example, then the fine-tuned point is given by

$$M(g_\sigma^2 = 0.4) \;=\; -0.286, \tag{6.84}$$

$$g_\pi^2(g_\sigma^2 = 0.4) \;=\; 0.243. \tag{6.85}$$

The gap equations in this case are given by

$$M_c \;=\; \sigma_0\Big(1 - \frac{g_\sigma^2}{g_\pi^2}\Big) + 8g_\sigma^2\sigma_0\int\frac{dk^2}{(2\pi)^2}\frac{c_1^2c_2^2}{((\sigma_0 + c_1c_2)^2 + \pi_0^2 + s^2)((\sigma_0 - c_1c_2)^2 + \pi_0^2 + s^2)}, \tag{6.86}$$

$$\frac{1}{g_\pi^2} \;=\; 4\int\frac{dk^2}{(2\pi)^2}\frac{\sigma_0^2 + s^2 + c_1^2c_2^2}{((\sigma_0 + c_1c_2)^2 + \pi_0^2 + s^2)((\sigma_0 - c_1c_2)^2 + \pi_0^2 + s^2)}. \tag{6.87}$$

In Fig. 6.8 and Fig. 6.9 we depict the phase boundary $M(g_\pi^2)$ naively derived from the above gap equations for $g_\sigma^2 = 0.4$. The latter is an expanded one near the self-crossing point with the true phase boundaries also depicted. The fine-tuned point (6.84)(6.85) is located slightly to the right and below the self-crossing point near the true second order phase boundary in the parity symmetric phase. Toward the week-coupling limit $g_\sigma^2 \to 0$ the phase structure moves down to $g_\pi^2 = 0$, where the fine-tuned point gets close to $(M, g_\pi^2) \to (-1, 0)$ from the parity symmetric phase even though there is a 1st-order phase transition. It means our fine-tuned point leads to the continuum theory with the

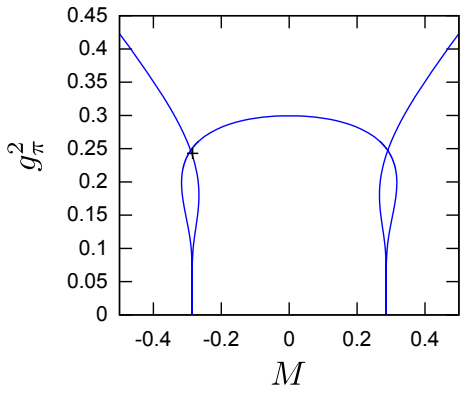

Figure 6.8: The naively derived phase boundary $M_c(g_\pi^2)$ for the staggered fermion with the Adams-type mass with $g_\sigma^2 = 0.4$. The fine-tuned point $(-0.286, 0.243)$ as a crosspoint is located near the self-crossing point.

chiral symmetry and one massless fermion corresponding to the taste with positive flavor-chirality. The situation about the first order phase boundary is the same as the naive case. In Fig. 6.9 we depict the true phase boundaries for this case. In Fig. 6.10 we depict the order parameter π_0 as a function of M. Here the order of the transition changes from the 2nd to the 1st around the order-changing point. In Fig. 6.11 we depict the σ_0 potential for several values of M crossing the σ_0 phase boundary. The value of σ_0 at the minimum changes from $\sigma_0 > -1$ to $\sigma_0 < -1$ in a form of the 1st-order phase transition.

We have shown that the chirally-symmetric continuum limit can be taken by fine-tuning a mass parameter and two coupling constants both for the naive and staggered cases. It indicates we obtain the two-flavor or one-flavor massless fermions in the chiral limit by tuning a mass parameter when we introduce the Adams-type [31] or Hoelbling-type [32] flavored masses to the $d = 4$ QCD with staggered fermions. We speculate the process to take the chiral and continuum limit could be almost the same as the case for Wilson fermion while the numerical cost will be less for the staggered fermions. The less numerical expense in the staggered fermion could make the QCD simulations with these fermions faster than Wilson fermion. We need further investigation to answer this question.

6.5 Short summary

Here let me summarize the argument on the Aoki phase from the Gross-Neveu model. In Sec. 6.2 we study the phase structure for the naive Gross-Neveu model with the flavored masses. We consider the two types of flavored mass terms for 2d naive fermions, which cause two different kinds of mass splitting in species. We solve the gap equations for the large N limit and obtain the second order phase boundaries in the M-g^2 plane. The parity broken phase diagram has some common properties with the Wilson case, and reflects the mass splitting. In Sec. 6.3 we consider the generalized staggered Gross-Neveu model including two types of four-point interactions. We take the same process as in the case of the naive fermion to obtain the phase diagram for the staggered fermion with the Adams-

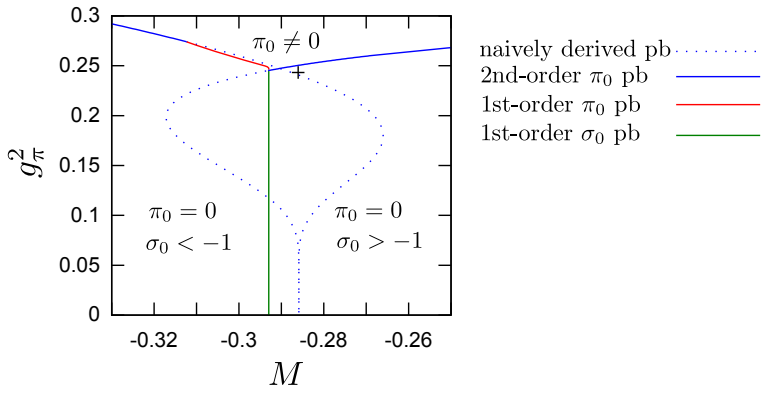

Figure 6.9: The expanded version of Fig. 6.8. A blue dotted curve is the naively derived phase boundary. The true phase boundaries are composed of the three parts. The fine-tuned point is located slightly to the right and below the self-crossing point.

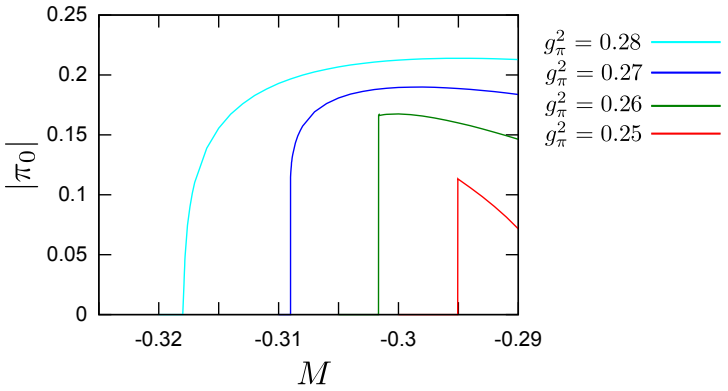

Figure 6.10: The order parameter π_0 as a function of M for $g_\pi^2 = 0.25, 0.26, 0.27, 0.28$ where the order of transition changes from 1st to 2nd in Fig. 6.9.

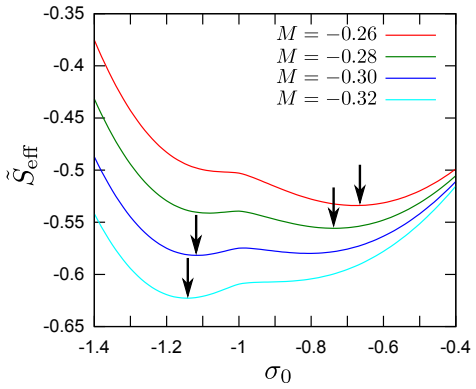

Figure 6.11: The σ_0 potential for several values of M crossing the σ_0 boundary in Fig. 6.9. The value of σ_0 at the minimum changes from $\sigma_0 > -1$ to $\sigma_0 < -1$ in a form of the 1st-order transition.

type flavored mass. We show the Aoki phase exists also in this case reflecting the mass splitting of tastes. This elucidation can contribute to the practical application of these fermions and their overlap versions. In Sec. 6.4 we discuss the continuum limit of these Gross-Neveu models around the cusps in the phase digram. We show that the chirally-symmetric continuum limit with the number of massless species associated with each of the cusps can be taken by fine-tuning a mass parameter and two coupling constants in both cases. We note the necessity of the two-coupling tuning is just a model artifact, thus we expect the continuum limit in 4d QCD will be taken by tuning the gauge coupling usually. From this we speculate the chiral limit can be taken by fine-tuning only a mass parameter in $d = 4$ lattice QCD with staggered fermions with the Adams-type [31] or Hoelbling-type [32] masses. It indicates we can obtain the one- or two-flavor massless fermions in the continuum from the staggered setup and regard massless pions as Goldstone bosons due to the spontaneous chiral symmetry breaking as in the case with Wilson fermion. These approaches avoid the use of the rooting approximation to reduce the number of tastes. We also study the first order phase boundaries peculiar to the two-coupling cases of the lattice Gross-Neveu models. We show there exist two kinds of the first order phase boundaries with respect to parity and chiral symmetry breaking.

Chapter 7

Strong-coupling QCD

In this chapter we investigate the Aoki phase structure in lattice QCD with the staggered-Wilson fermions in the strong-coupling regime [58, 98, 99, 100, 101]. One of the purposes in this analysis is to back up the results in the previous section and give a more certain evidence for the existence of the Aoki phase and the second-order phase transition. We also have another purpose, which cannot be done in the model study. One of the merit of the Gross-Neveu analysis of the Aoki phase in the previous chapter was we can solve the theory exactly and takes the exact chiral limit. However the disadvantage was we cannot consider any about the flavor since the flavor number is taken to large N limit in the 2-dimensional model. By using the strong-coupling lattice QCD, we figure out the flavor structure too. We will find the results are qualitatively similar to the case for the Wilson fermion [35]. Note the results in this chapter are based on the original work by the present author in Ref. [34].

7.1 Hopping Parameter Expansion

In this section we investigate the Aoki phase in lattice QCD with staggered-Wilson fermions in the framework of the hopping parameter expansion (HPE) in the strong-coupling regime [35]. In the hopping parameter expansion we treat mass terms as a free action while we treat kinetic terms and other terms containing transporters perturbatively. This analysis can be applied to a case that the mass is sufficiently heavy. As we have shown in the previous chapter, the parity phase transition in the staggered-Wilson fermion is likely to occur when the dimensionless mass parameter is set to be $O(1)$, or equivalently the mass is set to be $O(1/a)$. Therefore, it is suitable for study of parity phase structure. However HPE is a perturbative analysis, thus it seems that we do not know anything on vacuum and phase transition. What we can know from this analysis is whether or not the vacuum we have chosen is correct. We will start with the parity symmetric vacuum and perform perturbation. So, if we find a tachyonic behavior of the pion mass in some range of the hopping parameter, it indicates that the vacuum is wrong. This result suggests that the parity is broken in this rage of the mass parameter. Although we need to study the effective potential analysis to know about details of the vacuum in 7.2, the hopping parameter analysis gives us information on the phase transition.

We for simplicity drop the flavor indices until we discuss the two-flavor case in details

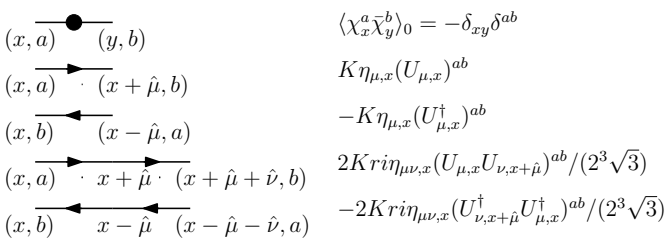

Figure 7.1: Feynman rules for hopping parameter expansion (HPE) with the Hoelbling-type staggered-Wilson fermion. a and b stand for the color indices.

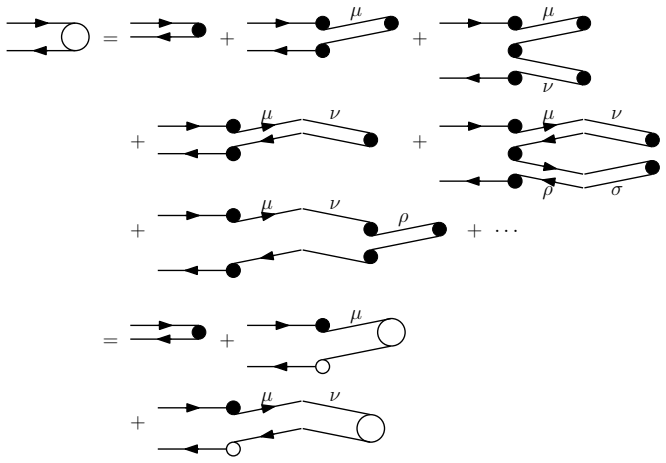

Figure 7.2: Feynman diagram for mesonic one-point functions in the $O(K^3)$ HPE with the Hoelbling fermion. Black circles stand for the leading one-point function $\langle \chi_x \bar{\chi}_x \rangle_0$ while white circles stand for $\langle \chi_x \bar{\chi}_x \rangle$ which include next-leading and higher hopping terms. By summing up higher contributions, we obtain the second equality.

in next Sec. 7.3. However it is easy to recover the flavor indices for the field χ_f, the mass parameter M_f and the condensate Σ_f $(f = 1, 2, ...)$.

7.1.1 Hoelbling type

We begin with the Hoelbling-type fermion, which contains two-hopping terms at the action level. To perform the HPE for the Hoelbling-type fermion, we rewrite the action (4.6) by redefining $\chi \to \sqrt{2K}\chi$ with $K = 1/[2(M + 2r)]$,

$$S = \sum_x \bar{\chi}_x \chi_x + 2K \sum_{x,y} \bar{\chi}_x (\eta_\mu D_\mu)_{xy} \chi_y + 2Kr \sum_{x,y} \bar{\chi}_x (M_H)_{xy} \chi_y \,, \tag{7.1}$$

where M_H is given by (3.35). The plaquette action is $1/g^2$ term and we can omit it in the strong-coupling limit. In this section we perform the hopping parameter expansion up to $O(K^3)$. It works only for a small K or a large M. However the critical mass parameter is likely to be $O(1)$, and $O(K^3)$ approximation can work well around the critical parameter.

In Fig. 7.1 we depict the Feynman rules in the HPE for this fermion. The fundamental Feynman rules contain contributions from 0-hopping (mass term), 2-hopping (kinetic term) and 4-hopping (flavored-mass term) terms. By using these Feynman rules we derive meson condensates from the one-point function of the meson operator ($\mathcal{M}_x = \bar{\chi}_x \chi_x$) in the mean-field approximation within the $O(K^3)$ HPE. The one-point function is defined as

$$\langle \chi^a_x \bar{\chi}^b_x \rangle \equiv -\delta_{ab}\Sigma_x = \frac{\int \mathcal{D}[\chi,\bar{\chi},U]\chi^a_x\bar{\chi}^b_x\ e^S}{\int \mathcal{D}[\chi,\bar{\chi},U]e^S}\ . \tag{7.2}$$

Note that we use $\mathcal{Z} = \int \mathcal{D}[\chi,\bar{\chi},U]e^S$, not $\mathcal{Z} = \int \mathcal{D}[\chi,\bar{\chi},U]e^{-S}$, following the convention for the partition function in the strong-coupling analysis [58]. The leading term in the hopping parameter expansion is given by

$$\langle \chi^a_x \bar{\chi}^b_x \rangle_0 = \frac{\int \mathcal{D}[\chi,\bar{\chi},U]\ \chi^a_x\bar{\chi}^b_x\ e^{S_0}}{\int \mathcal{D}[\chi,\bar{\chi},U]\ e^{S_0}} = -\delta^{ab}\ , \tag{7.3}$$

where $S_0 = \sum_x \bar{\chi}_x\chi_x$. By using the Feynman rules, we can evaluate the next-to-leading and next-to-next-to-leading order contributions in Fig. 7.2.

$$\begin{aligned}
\langle \chi^a_x \bar{\chi}^b_x \rangle &\equiv -\delta^{ab}\Sigma_x \\
&= \langle \chi^a_x \bar{\chi}^b_x \rangle_0 \\
&+ 2\sum_{\mu}(-1)(K\eta_{\mu,x})^2\langle(\chi^a\bar{\chi})_x\rangle_0 U_{\mu,x}\langle(\chi\bar{\chi})_{x+\hat{\mu}}\rangle_0 U^\dagger_{\mu,x}\langle(\chi\bar{\chi}^b)_x\rangle_0 \\
&+ 2\sum_{\mu,\nu}(-1)(K\eta_{\mu,x})^2(-1)(K\eta_{\nu,x})^2\langle(\chi^a\bar{\chi})_x\rangle_0 U_{\mu,x}\langle(\chi\bar{\chi})_{x+\hat{\mu}}\rangle_0 U^\dagger_{\mu,x}\langle(\chi^a\bar{\chi})_x\rangle_0 U_{\nu,x} \\
&\times \langle(\chi\bar{\chi})_{x+\hat{\nu}}\rangle_0 U^\dagger_{\nu,x}\langle(\chi\bar{\chi}^b)_x\rangle_0 \\
&+ 2\cdot 2\sum_{\mu\neq\nu}(-1)\left(2Kri\eta_{\mu\nu,x}\frac{1}{2^3\sqrt{3}}\right)^2\langle(\chi^a\bar{\chi})_x\rangle_0 U_{\mu,x}U_{\nu,x+\hat{\mu}}\langle(\chi\bar{\chi})_{x+\hat{\mu}+\hat{\nu}}\rangle_0 U^\dagger_{\mu,x}U^\dagger_{\nu,x+\hat{\mu}}\langle(\chi\bar{\chi}^b)_x\rangle_0 \\
&+ 2\cdot 2^2\sum_{\mu\neq\nu,\rho\neq\sigma}(-1)\left(2Kri\eta_{\mu\nu,x}\frac{1}{2^3\sqrt{3}}\right)^2(-1)\left(2Kri\eta_{\rho\sigma,x}\frac{1}{2^3\sqrt{3}}\right)^2 \\
&\times \langle(\chi^a\bar{\chi})_x\rangle_0 U_{\mu,x}U_{\nu,x+\hat{\mu}}\langle(\chi\bar{\chi})_{x+\hat{\mu}+\hat{\nu}}\rangle_0 U^\dagger_{\mu,x}U^\dagger_{\nu,x+\hat{\mu}}\langle(\chi\bar{\chi})_x\rangle_0 U_{\rho,x}U_{\sigma,x+\hat{\rho}} \\
&\times \langle(\chi\bar{\chi})_{x+\hat{\rho}+\hat{\sigma}}\rangle_0 U^\dagger_{\rho,x}U^\dagger_{\sigma,x+\hat{\rho}}\langle(\chi\bar{\chi}^b)_x\rangle_0 \\
&+ 2\cdot 2^2\sum_{\mu\neq\nu,\rho}(-1)\left(2Kri\eta_{\mu\nu,x}\frac{1}{2^3\sqrt{3}}\right)^2(-1)\,(K\eta_{\rho,x})\,(K\eta_{\sigma,x}) \\
&\times \langle(\chi^a\bar{\chi})_x\rangle_0 U_{\mu,x}U_{\nu,x+\hat{\mu}}\langle(\chi\bar{\chi})_{x+\hat{\mu}+\hat{\nu}}\rangle_0 U_{\rho,x+\hat{\mu}+\hat{\nu}}\langle(\chi\bar{\chi})_{x+\hat{\mu}+\hat{\nu}+\hat{\rho}}\rangle_0 U^\dagger_{\rho,x+\hat{\mu}+\hat{\nu}} \\
&\times \langle(\chi\bar{\chi})_{x+\hat{\mu}+\hat{\nu}}\rangle_0 U^\dagger_{\mu,x}U^\dagger_{\nu,x+\hat{\mu}}\langle(\chi\bar{\chi}^b)_x\rangle_0 \\
&+ \cdots\ ,
\end{aligned} \tag{7.4}$$

where $(\chi\bar{\chi})_x$ stands for $\chi_x\bar{\chi}_x$. By summing higher hopping terms, the one point function up to $O(K^3)$ is obtained as shown in Fig. 7.2, which is given by

$$-\Sigma_x \equiv -\langle \mathcal{M}_x \rangle = -\langle \mathcal{M}_x \rangle_0 + 2K^2\sum_{\mu}\Sigma_{x+\hat{\mu}}\Sigma_x - 2\cdot\frac{1}{24}(Kr)^2\sum_{\mu\neq\nu}\Sigma_x\Sigma_{x+\hat{\mu}+\hat{\nu}}. \tag{7.5}$$

The equation contains only terms up to $O(K^2)$ since $O(K^3)$ diagrams are found to vanish due to cancellation between the diagrams. Here we solve it as a self-consistent equation for the condensate Σ within the mean-field approximation. We here assume $\Sigma_x = \sigma_x + i\epsilon_x\pi_x$ as the condensate. We substitute this form of Σ_x in Eq. (7.5) and obtain the self-consistent equation

$$-(\sigma + i\epsilon_x\pi) = -1 + 2K^2 \cdot 4\left(\sigma^2 + \pi^2\right) - 2 \cdot \frac{1}{24}(Kr)^2 \cdot 4 \cdot 3\left(\sigma + i\epsilon_x\pi\right)^2, \tag{7.6}$$

which yields $-\sigma = -1 + 16K^2\pi^2$ and $-i\pi = -8K^2 \cdot 2i\sigma\pi$. For simplicity we have set $r = 2\sqrt{2}$ to make the equation(7.6) simpler. Of course we can also discuss for other values of r in a parallel way.

Now we have two solutions depending on $\pi = 0$ or $\pi \neq 0$: For $\pi = 0$ we have a trivial solution $\sigma = 1$. For $\pi \neq 0$ we have a non-trivial solution as

$$\sigma = \frac{1}{16K^2}, \qquad \pi = \pm\sqrt{\frac{1}{16K^2}\left(1 - \frac{1}{16K^2}\right)}. \tag{7.7}$$

In this solution the pion condensate is non-zero and the $\pm$ signs implies the spontaneous parity breaking. This non-trivial solution only exists for the range $\mid K \mid > 1/4$.As we will show soon later, the pion mass becomes tachyonic in this range. Thue the parity-broken phase, if it exists, appears in parameter range $\mid K \mid > 1/4$ or equivalently $-4\sqrt{2} - 2 < M < -4\sqrt{2} + 2$. The critical hopping parameter $|K_c^3| = 1/64$ indicates that the $O(K^3)$ expansion works around the critical parameter.

Here let us note on the possibility of the emergence of other condensations. The general form of the condensate is given by the sum of 16 possible condensates including the scalar, pseudo-scalar, vector, axial-vector and tensor ones. By substituting this general form into (7.5), we can show the condensates except the scalar one get zero in the parity-symmetric phase and the phase boundary $\mid K \mid \leq 1/4$ as in the usual Wilson fermion. (On the other hand, this approach cannot gives us information on the detailed condensation in the parity-broken phase.) Absence of the other condensates in the parity-symmetric phase and the phase boundary suggests that the discrete symmetry breaking in Sec. 4 does not affect the phase structure and the process of taking a chiral limit in the lattice QCD with the Hoelbling-type fermion.

We next discuss the two-point function of the meson operator $\mathcal{S}(0,x) \equiv \langle \mathcal{M}_0 \mathcal{M}_x \rangle$. From Fig. 7.3 we derive the following equation for two point function. $O(K^3)$ diagrams cancel again.

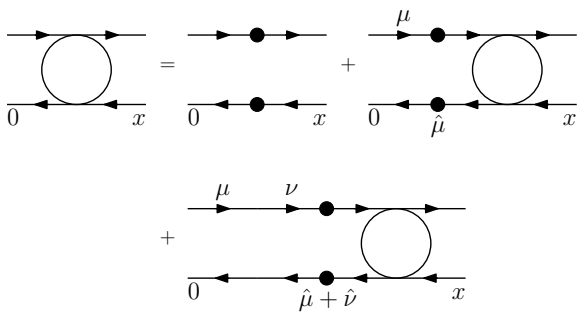

Figure 7.3: Feynman diagram for mesonic two-point functions for $O(K^3)$ HPE with the Hoelbling fermion.

$$
\begin{aligned}
\mathcal{S}(0,x) =& \langle \bar{\chi}_0^a \chi_0^a \bar{\chi}_x^b \chi_x^b \rangle \\
=& -\delta_{0x} N_c \\
& - K^2 \langle \bar{\chi}_0^a \chi_0^a \bar{\chi}_0^c (\eta_{\mu,0})^2 \Big[U_{\mu,0}^{cd} \chi_{\hat{\mu}}^d \bar{\chi}_{\hat{\mu}}^e (U_{\mu,0}^\dagger)^{ef} + (U_{\mu,-\hat{\mu}}^\dagger)^{cd} \chi_{-\hat{\mu}}^d \bar{\chi}_{-\hat{\mu}}^e U_{\mu,-\hat{\mu}}^{ef} \Big] \chi_0^f \bar{\chi}_x^b \chi_x^b \rangle \\
& - \left(2Kri \frac{1}{2^3\sqrt{3}} \right)^2 \langle \bar{\chi}_0^a \chi_0^a \bar{\chi}_0^c (\eta_{\mu\nu,0})^2 \Big[(U_{\mu,0} U_{\nu,0+\hat{\mu}})^{cd} \chi_{\hat{\mu}+\hat{\nu}}^d \bar{\chi}_{\hat{\mu}+\hat{\nu}}^e (U_{\nu,0+\hat{\mu}}^\dagger U_{\mu,0}^\dagger)^{ef} \\
& + (U_{\nu,0-\hat{\nu}}^\dagger U_{\mu,0-\hat{\mu}-\hat{\nu}}^\dagger)^{cd} \chi_{-\hat{\mu}-\hat{\nu}}^d \bar{\chi}_{-\hat{\mu}-\hat{\nu}}^e (U_{\mu,0-\hat{\mu}-\hat{\nu}} U_{\nu,0-\hat{\nu}})^{ef} \\
& + (U_{\mu,0} U_{\nu,0+\hat{\mu}-\hat{\nu}}^\dagger)^{cd} \chi_{\hat{\mu}-\hat{\nu}}^d \bar{\chi}_{\hat{\mu}-\hat{\nu}}^e (U_{\nu,0+\hat{\mu}-\hat{\nu}} U_{\mu,0}^\dagger)^{ef} \\
& + (U_{\nu,0} U_{\mu,0-\hat{\mu}+\hat{\nu}}^\dagger)^{cd} \chi_{-\hat{\mu}+\hat{\nu}}^d \bar{\chi}_{-\hat{\mu}+\hat{\nu}}^e (U_{\mu,0-\hat{\mu}+\hat{\nu}} U_{\nu,0}^\dagger)^{ef} \Big] \chi_0^f \bar{\chi}_x^b \chi_x^b \rangle .
\end{aligned} \tag{7.8}
$$

By eliminating the link variables for the strong-coupling limit, it is simplified as

$$
\begin{aligned}
\mathcal{S}(0,x) \equiv \langle \bar{\chi}_0^a \chi_0^a \bar{\chi}_x^b \chi_x^b \rangle =& -\delta_{0x} N_c + K^2 \sum_{\pm\mu} \langle \chi_{\hat{\mu}}^a \bar{\chi}_{\hat{\mu}}^a \bar{\chi}_x^b \chi_x^b \rangle \\
& + \left(2Kri \frac{1}{2^3\sqrt{3}} \right)^2 \sum_{\substack{\pm\mu,\pm\nu \\ (\mu\neq\nu)}} \langle \chi_{\hat{\mu}+\hat{\nu}}^a \bar{\chi}_{\hat{\mu}+\hat{\nu}}^a \bar{\chi}_x^b \chi_x^b \rangle .
\end{aligned} \tag{7.9}
$$

Then the self-consistent equation for $\mathcal{S}$ is given in the momentum space as

$$
\begin{aligned}
\mathcal{S}(p) = -N_c + \Bigg[& -K^2 \sum_\mu \left(e^{-ip_\mu} + e^{ip_\mu} \right) \\
& + \left(2Kr \frac{1}{2^3\sqrt{3}} \right)^2 \sum_{\mu\neq\nu} \left(e^{-i(p_\mu+p_\nu)} + e^{i(p_\mu+p_\nu)} + e^{-i(p_\mu-p_\nu)} + e^{i(p_\mu-p_\nu)} \right) \Bigg] \mathcal{S}(p).
\end{aligned} \tag{7.10}
$$

We finally obtain the meson propagator as

$$
\mathcal{S}(p) = N_c \left[-2K^2 \sum_\mu \cos p_\mu + 4 \left(2Kr \frac{1}{2^3\sqrt{3}} \right)^2 \sum_{\mu\neq\nu} \cos p_\mu \cos p_\nu - 1 \right]^{-1}. \tag{7.11}
$$

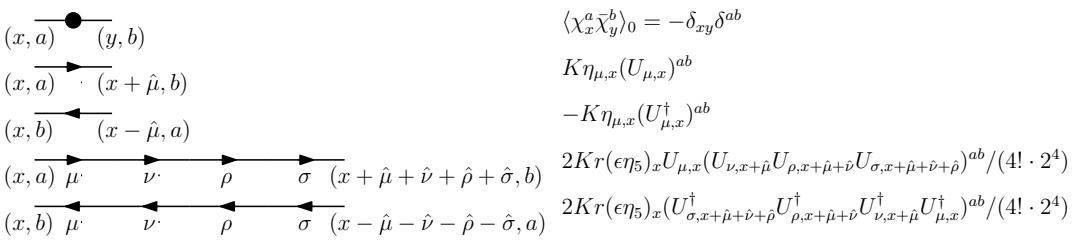

Figure 7.4: Feynman rules for the HPE with the Adams fermion.

Here the pole of $\mathcal{S}(p)$ should give mass of meson. Since χ is an one-component fermion, it may seem to be difficult to find the pion excitation from (7.11). However, as we discussed, γ_5 in the staggered fermion is given by $\epsilon_x = (-1)^{x_1+\ldots+x_4}$ and the pion operator is given by $\pi_x = \bar{\chi}_x i\epsilon_x\chi_x$. Thus we can know the momentum of pion by measuring it from the shifted origin $p = (\pi,\pi,\pi,\pi)$. Here we set $p = (im_\pi a+\pi,\pi,\pi,\pi)$ for $1/\mathcal{S}(p) = 0$ in (7.11). Then we derive the pion mass m_π as

$$\cosh(m_\pi a) = 1 + \frac{1-16K^2}{6K^2}, \tag{7.12}$$

where we again set $r = 2\sqrt{2}$ for simplicity. In this result the pion mass becomes zero at $|K| = 1/4$, then becomes tachyonic in the range $|\ K\ | > 1/4$. It indicates there occurs a phase transition between parity-symmetric and parity-broken phases at $|K| = 1/4$, which is consistent with the result from the one-point function in Eq. (7.7). We note that the massless pion at the phase boundary is compatible with the scenario that the chiral limit is taken on the second-order critical line. We can also derive the sigma meson mass by substituting $p = (im_\pi a, 0, 0, 0)$ for $1/\mathcal{S}(p) = 0$ in (7.11) as

$$\cosh(m_\sigma a) = 1 + \frac{1}{2K^2}. \tag{7.13}$$

7.1.2 Adams type

We investigate the parity phase structure for the Adams-type staggered-fermion by using the $O(K^3)$ hopping parameter expansion. The approach is basically parallel. What we need to do is consider Feynman diagrams for this case. The action (4.5) is rewritten by redefining $\chi \to \sqrt{2K}\chi$ with $K = 1/[2(M+r)]$ as,

$$S = \sum_x \bar{\chi}_x\chi_x + 2K\sum_{x,y}\bar{\chi}_x(\eta_\mu D_\mu)_{xy}\chi_y + 2Kr\sum_{x,y}\bar{\chi}_x(M_A)_{xy}\chi_y, \tag{7.14}$$

where M_A is given by (3.34). In Fig. 7.4 the Feynman rules in the HPE for this fermion are depicted. The equation for the one-point function up to $O(K^3)$ is obtained as shown in Fig. 7.5,

$$\begin{aligned} -\Sigma_x &\equiv -\langle\mathcal{M}_x\rangle \\ &= -\langle\mathcal{M}_x\rangle_0 + 2K^2\sum_\mu \Sigma_{x+\hat{\mu}}\Sigma_x - 2\cdot\frac{1}{(4!)^2\cdot 2^3}(Kr)^2\sum_{\mu\neq\nu\neq\rho\neq\sigma}\Sigma_x\Sigma_{x+\hat{\mu}+\hat{\nu}+\hat{\rho}+\hat{\sigma}}, \end{aligned} \tag{7.15}$$

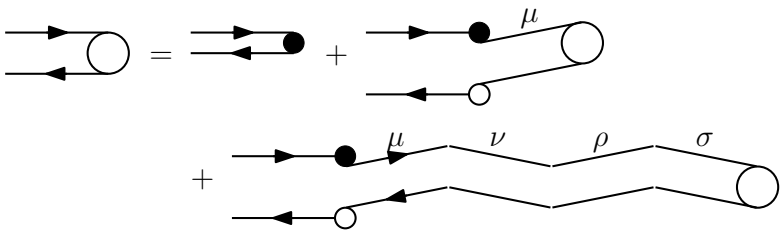

Figure 7.5: Feynman diagram for mesonic one-point functions in the $O(K^3)$ HPE with the Adams fermion. There is a 4-hopping fundamental diagram, which is peculiar to this fermion.

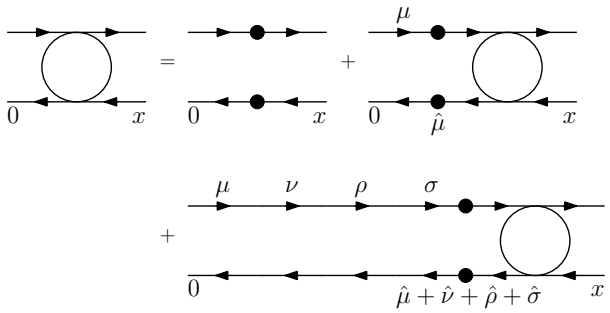

Figure 7.6: Feynman diagram for mesonic two-point functions for $O(K^3)$ HPE with the Adams fermion.

We substitute $\Sigma_x = \sigma_x + i\epsilon_x\pi_x$ form of Σ_x in Eq. (7.15) and obtain the self-consistent equation

$$-(\sigma + i\epsilon_x\pi) = -1 + 2K^2 \cdot 4\left(\sigma^2 + \pi^2\right) - 2 \cdot \frac{1}{(4!)^2 \cdot 2^3}(Kr)^2 \cdot 4!\,(\sigma + i\epsilon_x\pi)^2\,. \tag{7.16}$$

From this we obtain $-\sigma = -1 + 16K^2\pi^2$ and $-i\pi = -8K^2 \cdot 2i\sigma\pi$. Here we have set $r = 16\sqrt{3}$ to make the equation simple. We again have two solutions: For $\pi = 0$ we have a trivial solution $\sigma = 1$. For $\pi \neq 0$ we have a non-trivial solution as

$$\sigma = \frac{1}{16K^2}, \qquad \pi = \pm\sqrt{\frac{1}{16K^2}\left(1 - \frac{1}{16K^2}\right)}. \tag{7.17}$$

It indicates the parity-broken phase appears in the range of the hopping parameter as $\mid K \mid > 1/4$ or equivalently $-16\sqrt{3} - 2 < M < -16\sqrt{3} + 2$. We can show the condensates except the scalar one get zero in the parity-symmetric phase and the phase boundary $\mid K \mid \leq 1/4$. Since the Adams-type fermion possesses larger discrete symmetry than the Hoelbling-type, it is quite reasonable that there is no disease coming from the symmetry breaking.

From Fig. 7.6 we derive the following equation for two point function,

$$
\begin{aligned}
\mathcal{S}(0,x) =& \langle \bar{\chi}_0^a \chi_0^a \bar{\chi}_x^b \chi_x^b \rangle \\
=& -\delta_{0x} N_c \\
& - K^2 \langle \bar{\chi}_0^a \chi_0^a \bar{\chi}_0^c (\eta_{\mu,0})^2 \Big[U_{\mu,0}^{cd} \chi_{\hat{\mu}}^d \bar{\chi}_{\hat{\mu}}^e (U_{\mu,0}^\dagger)^{ef} + (U_{\mu,-\hat{\mu}}^\dagger)^{cd} \chi_{-\hat{\mu}}^d \bar{\chi}_{-\hat{\mu}}^e U_{\mu,-\hat{\mu}}^{ef} \Big] \chi_0^f \bar{\chi}_x^b \chi_x^b \rangle \\
& - \left(2Kr\epsilon\eta_5 \frac{1}{4! \cdot 2^4} \right)^2 \langle \bar{\chi}_0^a \chi_0^a \bar{\chi}_0^c \Big[(U_{\mu,0} U_{\nu,0+\hat{\mu}} U_{\rho,0+\hat{\mu}+\hat{\nu}} U_{\sigma,0+\hat{\mu}+\hat{\nu}+\hat{\rho}})^{cd} \times \\
& \qquad \chi_{\hat{\mu}+\hat{\nu}+\hat{\rho}+\hat{\sigma}}^d \bar{\chi}_{\hat{\mu}+\hat{\nu}+\hat{\rho}+\hat{\sigma}}^e (U_{\sigma,0+\hat{\mu}+\hat{\nu}+\hat{\rho}} U_{\rho,0+\hat{\mu}+\hat{\nu}}^\dagger U_{\nu,0+\hat{\mu}}^\dagger U_{\mu,0}^\dagger)^{ef} \\
& + (\mu \leftrightarrow -\mu \text{ or } \nu \leftrightarrow -\nu \text{ or} \rho \leftrightarrow -\rho \text{ or } \sigma \leftrightarrow -\sigma) \Big] \chi_0^f \bar{\chi}_x^b \chi_x^b \rangle
\end{aligned} \tag{7.18}
$$

By eliminating the link variables for the strong-coupling limit, it is simplified as

$$
\begin{aligned}
\mathcal{S}(0,x) \equiv \langle \bar{\chi}_0^a \chi_0^a \bar{\chi}_x^b \chi_x^b \rangle =& -\delta_{0x} N_c + K^2 \sum_{\pm\mu} \langle \chi_{\hat{\mu}}^a \bar{\chi}_{\hat{\mu}}^a \chi_x^b \bar{\chi}_x^b \rangle \\
& - \left(2Kr \frac{1}{4! \cdot 2^4} \right)^2 \sum_{\substack{\pm\mu,\pm\nu,\pm\rho,\pm\sigma \\ (\mu\neq\nu\neq\rho\neq\sigma)}} \langle \chi_{\hat{\mu}+\hat{\nu}+\hat{\rho}+\hat{\sigma}}^a \bar{\chi}_{\hat{\mu}+\hat{\nu}+\hat{\rho}+\hat{\sigma}}^a \bar{\chi}_x^b \chi_x^b \rangle .
\end{aligned} \tag{7.19}
$$

Then the self-consistent equation for $\mathcal{S}$ is given in the momentum space as

$$
\begin{aligned}
\mathcal{S}(p) = -N_c + \Bigg[& -K^2 \sum_\mu \left(e^{-ip_\mu} + e^{ip_\mu} \right) \\
& + \frac{1}{2} \left(2Kr \frac{1}{4! \cdot 2^4} \right)^2 \sum_{\substack{A=(\mu,\nu)=(+,+),(+,-) \\ B=(\rho,\sigma)=(+,+),(+,-) \\ (\mu\neq\nu\neq\rho\neq\sigma)}} \left(e^{-i(p_A+p_B)} + e^{i(p_A+p_B)} + e^{-i(p_A-p_B)} + e^{i(p_A-p_B)} \right) \Bigg].
\end{aligned} \tag{7.20}
$$

We finally obtain the meson propagator as

$$
S(p) = N_c \Bigg[-2K^2 \sum_\mu \cos p_\mu + 16 \left(2Kr \frac{1}{4! \cdot 2^4} \right)^2 \sum_{\mu\neq\nu\neq\rho\neq\sigma} \cos p_\mu \cos p_\nu \cos p_\rho \cos p_\sigma - 1 \Bigg]^{-1} \tag{7.21}
$$

Here we set $p = (im_\pi a + \pi, \pi, \pi, \pi)$ for $1/\mathcal{S}(p) = 0$ in (7.21), which gives the pion mass m_π as

$$
\cosh(m_\pi a) = 1 + \frac{1 - 16K^2}{10K^2}, \tag{7.22}
$$

where we again set $r = 16\sqrt{3}$ for simplicity. Here the pion mass becomes tachyonic in the range $\mid K \mid > 1/4$. It indicates there occurs a phase transition between parity-symmetric and broken phases at $|K| = 1/4$, which is consistent with Eq. (7.17). We can also derive the sigma meson mass by substituting $p = (im_\pi a, 0, 0, 0)$ for $1/\mathcal{S}(p) = 0$ in (7.21) as

$$
\cosh(m_\sigma a) = 1 + \frac{1}{6K^2}. \tag{7.23}
$$

7.2 Effective Potential Analysis

In this section we consider the effective potential for mesonic fields for $SU(N)$ gauge theory with the staggered-Wilson fermions. In the strong-coupling regime and the large N limit, the effective action is derived by integrating the link variables [58, 35]. By using the saddle point equation, we can investigate the vacuum and meson condensations. We will find that there is pion condensate in the range of the mass parameter, which is consistent with the results of the hopping parameter expansion.

7.2.1 Hoelbling type

In the strong-coupling limit, we can omit the plaquette action. Then the partition function for mesonic fields $\mathcal{M}_x = (\bar{\chi}\chi_x)/N$ with the source J_x is given by

$$Z(J) = \int \mathcal{D}\left[\chi, \bar{\chi}, U\right] \exp\left[N \sum_x J_x \mathcal{M}_x + S_F\right]. \tag{7.24}$$

where S_F stands for the fermion action, which is the Hoelbling-type staggered-Wilson action in this case. N stands for the number of color. In the large N limit we can perform the link integral. In this section, we consider the meson effective action up to $O(\mathcal{M}^3)$ where $\mathcal{M}$ stands for a meson field. This order corresponds to the $O(K^3)$ in the hopping parameter expansion. To perform integration of the link variable in this case, we develop a method to integrate multi-link terms. In our method, we perform the link integral by introducing two kinds of link variable measures. Now we formally rewrite the action by using this method as,

$$Z(J) = \int \mathcal{D}\left[\chi, \bar{\chi}\right] \exp\left[\sum_x N\left(J_x + \hat{M}\right)\mathcal{M}_x\right] \exp\left[\sum_x NW(\Lambda)\right], \tag{7.25}$$

where we again define $\hat{M} = M + 2r$ and

$$\exp\left[\sum_x NW(\Lambda)\right] = \prod_x Z_x$$
$$Z_x = \int \left(\prod_{\mu\neq\nu} \mathcal{D}\left[U_{\mu,x}, U_{\mu,x+\hat{\nu}}\right]\right) \exp\left[-\left(\mathrm{Tr}(VE^\dagger) - \mathrm{Tr}(V^\dagger E)\right)\right]. \tag{7.26}$$

Λ is a composite field of fermion field χ, which we will show a concrete form later. $W(\Lambda)$ is a function of Λ, which will be translated into an essential part of the effective potential of the meson fields. Now the question is how the integral in (7.26) can be perform by using the two types of the link measure. Let us consider the case of two dimensions in Fig. 7.7 for simplicity. In this case $U_{\mu,x}$ and $U_{\mu,x+\hat{\nu}}$ $(\mu \neq \nu)$ stand for link variables in a square block. Diagrams contribute to $O(\mathcal{M}^3)$ effective potential are classified into only three types: (1) 1-link μ + 1-link $-\mu$ hoppings, (2) 2-link (μ, ν) + 2-link $(-\nu, -\mu)$ hoppings, (3) 2-link (μ, ν) + 1-link $-\nu$ + 1-link $-\mu$ hoppings. The 1-link hopping comes from the

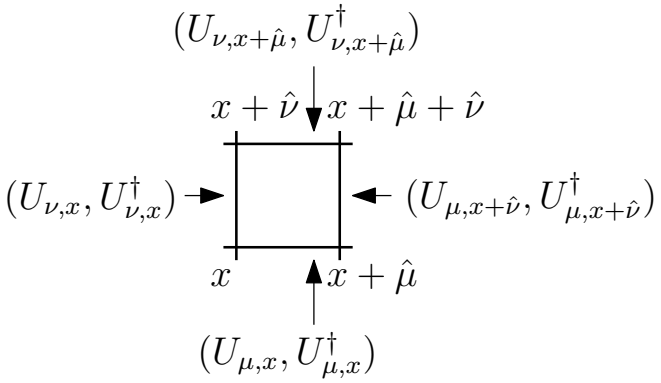

Figure 7.7: Link variables corresponding to the two kinds of measures in the partition function Eq. (7.26) in a 2 dimensional case.

usual staggered kinetic term while the 2-link hopping from the flavored-mass term. (1) and (2) are $O(\mathcal{M}^2)$ while (3) is $O(\mathcal{M}^3)$. Since one square block contains all the three diagrams. we can derive the effective potential up to $O(\mathcal{M}^3)$ by integrating link variables per each block. We note that $O(\mathcal{M}^3)$ diagrams cancel between one another, which is consistent with the case in the HPE. We can also avoid double-counting by adjusting factors for one-link and two-link terms as shown in (7.41).

In this method we need to define sets of the link variables and the fermion bilinears as V and E in Eq. (7.26) : V and E are matrices including components corresponding to 1- and 2-link terms. We call a space spanned by these matrices "the hopping space". Here we define a, b and α, β as color and hopping space indices respectively. We also denote Tr as the trace for the color and the hopping space. The concrete forms of the V and E are given by

$$V^{ab}_{\alpha\beta} = \mathrm{diag}\left(V^{ab}_1, V^{ab}_2, V^{ab}_3\right) \ , \tag{7.27}$$

with

$$\begin{aligned} V_1 &= \mathrm{diag}\left(U_{\mu,x}\right) \\ &\equiv \mathrm{diag}\underbrace{\left(U_{1,x}, U_{2,x}, \cdots, U_{4,x}\right)}_{4} \ , \end{aligned} \tag{7.28}$$

$$\begin{aligned} V_2 &= \mathrm{diag}\left(U_{\mu,x}U_{\nu,x+\hat{\mu}}\right) \\ &\equiv \mathrm{diag}\underbrace{\left(U_{1,x}U_{2,x+\hat{1}}, U_{1,x}U_{3,x+\hat{1}}, \cdots, U_{4,x}U_{3,x+\hat{4}}\right)}_{12} \ , \end{aligned} \tag{7.29}$$

$$\begin{aligned} V_3 &= \mathrm{diag}\left(U_{\mu,x+\hat{\nu}}U_{\nu,x+\hat{\mu}}\right) \\ &\equiv \mathrm{diag}\underbrace{\left(U_{1,x+\hat{2}}U^\dagger_{2,x+\hat{1}}, U_{1,x+\hat{3}}U^\dagger_{3,x+\hat{1}}, \cdots, U_{4,x+\hat{3}}U^\dagger_{3,x+\hat{4}}\right)}_{12} \ . \end{aligned} \tag{7.30}$$

$$E^{ab}_{\alpha\beta} = \mathrm{diag}\left(E^{ab}_1, E^{ab}_2, E^{ab}_3\right) \ . \tag{7.31}$$

and

$$
\begin{aligned}
E_1 &= \mathrm{diag}\,(D_{1,\mu}) \\
&\equiv \mathrm{diag}\,\underbrace{(D_{1,1}, D_{1,2}, \cdots, D_{1,4})}_{4}\ , \qquad (7.32)\\
E_i &= \mathrm{diag}\,(D_{i,\mu\nu}) \\
&\equiv \mathrm{diag}\,\underbrace{(D_{i,12}, D_{i,13}, \cdots, D_{i,43})}_{12},\ (i=2,3)\ , \qquad (7.33)
\end{aligned}
$$

where we define the operator D as the fermion bilinears,

$$
\left(D^\dagger_{1,\mu}\right)^{ab} = \frac{1}{2}\eta_{\mu,x}\bar{\chi}^a_x\chi^b_{x+\hat{\mu}}\ , \quad (D_{1,\mu})^{ab} = \frac{1}{2}\eta_{\mu,x}\bar{\chi}^a_{x+\hat{\mu}}\chi^b_x\ , \qquad (7.34)
$$

$$
\left(D^\dagger_{2,\mu\nu}\right)^{ab} = \frac{ir}{2^3\sqrt{3}}\eta_{\mu\nu,x}\bar{\chi}^a_x\chi^b_{x+\hat{\mu}+\hat{\nu}}\ , \quad (D_{2,\mu\nu})^{ab} = \frac{ir}{2^3\sqrt{3}}\eta_{\mu\nu,x}\bar{\chi}^a_{x+\hat{\mu}+\hat{\nu}}\chi^b_x\ , \qquad (7.35)
$$

$$
\left(D^\dagger_{3,\mu\nu}\right)^{ab} = \frac{ir}{2^3\sqrt{3}}\eta_{\mu\nu,x+\hat{\nu}}\bar{\chi}^a_{x+\hat{\nu}}\chi^b_{x+\hat{\mu}}\ , \quad (D_{3,\mu\nu})^{ab} = \frac{ir}{2^3\sqrt{3}}\eta_{\mu\nu,x+\hat{\nu}}\bar{\chi}^a_{x+\hat{\mu}}\chi^b_{x+\hat{\nu}}\ . \qquad (7.36)
$$

Here V_1 and E_1 are 4 diagonal matrices while V_i and E_i $(i=2,3)$ are 12×12 diagonal matrices. Now we have prepared to obtain $W(\Lambda)$. By using the relation $U^\dagger U = 1$, we obtain the Schwinger-Dyson equation,

$$
\frac{\partial^2 Z_x}{\partial E^{ab}_{\alpha\beta}\partial\left(E^\dagger\right)^{bc}_{\beta\gamma}} = -\delta_{ca}\delta^{\alpha\gamma}Z_x\ . \qquad (7.37)
$$

W is should a function of a gauge-invariant quantities as follows.

$$
\Lambda^{ab}_{\alpha\beta} = \frac{1}{N^2}\left(E^\dagger E\right)^{ab}_{\alpha\beta}\ . \qquad (7.38)
$$

We can solve the Schwinger-Dyson equation analytically and derive W as a function of Λ,

$$
W(\Lambda) = \mathrm{Tr}\left[(1-4\Lambda)^{1/2} - 1 - \ln\left[\frac{1+(1-4\Lambda)^{1/2}}{2}\right]\right]\ . \qquad (7.39)
$$

We here perform the trace for the colors and hopping spaces.

$$
\sum_x W(\Lambda) = -\sum_x\left[(1-4\Lambda_x)^{1/2} - 1 - \ln\left[\frac{1+(1-4\Lambda_x)^{1/2}}{2}\right]\right]\ , \qquad (7.40)
$$

Finally we obtain a concrete form of Λ as

$$
\Lambda_x = \frac{1}{8}\left[\sum_\mu \mathcal{M}_x\mathcal{M}_{x+\hat{\mu}} + \frac{1}{3}\sum_{\mu\neq\nu}\mathcal{M}_{x+\hat{\mu}}\mathcal{M}_{x+\hat{\mu}+\hat{\nu}}\right] - \left(\frac{r}{2^3\sqrt{3}}\right)^2\sum_{\mu\neq\nu}\left(\mathcal{M}_x\mathcal{M}_{x+\hat{\mu}+\hat{\nu}} + \mathcal{M}_{x+\hat{\nu}}\mathcal{M}_{x+\hat{\mu}}\right)\ . \qquad (7.41)
$$

The first and second terms correspond to the contribution from $D_{1,\mu}, D_{1,\mu}^\dagger$, and the third and forth terms correspond to the contribution from $D_{i,\mu}, D_{i,\mu}^\dagger$ $(i = 2, 3)$. Now we again set $r = 2\sqrt{2}$ to match the result to that of the hopping parameter expansion in Sec. 7.1. We need to change the fermion measure to the meson field measure as

$$\int \mathcal{D}\left[\chi, \bar{\chi}\right] = \int \mathcal{D}\mathcal{M} \exp\left[-N \sum_x \ln \mathcal{M}_x\right] . \tag{7.42}$$

Then the effective partition function for the meson field is given by

$$Z(J) = \int \mathcal{D}\mathcal{M} \exp\left[N\left(\sum_x J_x \mathcal{M}_x + S_{\text{eff}}(\mathcal{M})\right)\right] , \tag{7.43}$$

$$S_{\text{eff}}(\mathcal{M}) = \sum_x \left(\hat{M}\mathcal{M}_x - \ln \mathcal{M}_x\right) + \sum_x W(\Lambda). \tag{7.44}$$

where we denote $\hat{M}$ as the shifted mass parameter $\hat{M} = M + 2r$. The partition function with $J = 0$ in the large N limit is reduced to the integrant for the saddle-point values of the meson fields.

$$\begin{aligned} Z(J=0) &= \int \mathcal{D}\mathcal{M} \exp\left[N S_{\text{eff}}(\mathcal{M})\right] \\ &\sim \exp\left[N S_{\text{eff}}(\bar{\mathcal{M}})\right], \quad (N \to \infty) \ . \end{aligned} \tag{7.45}$$

Now we consider the condensates of the pion fields. As we discussed in the study of the hopping parameter expansion, we expect there emerges only the chiral condensate at least in the parity symmetric phase and the boundary. Thus, for now, we consider only the scalar σ and pseudo-scalar π fields as

$$\bar{\mathcal{M}}_x = \sigma + i\epsilon_x \pi, \tag{7.46}$$

$$= \Sigma e^{i\epsilon_x \theta}. \tag{7.47}$$

By substituting this form of the meson field into the (7.44), we derive the effective action for the Σ and θ,

$$\begin{aligned} S_{\text{eff}}(\bar{\mathcal{M}}) = \hat{M} \sum_x \Sigma \cos\theta - \sum_x \ln \Sigma \\ - \sum_x \left[\left(1 - 4 \cdot 2\Sigma^2 \sin^2\theta\right)^{1/2} - \ln\left[\frac{1 + \left(1 - 4 \cdot 2\Sigma^2 \sin^2\theta\right)^{1/2}}{2}\right]\right] . \end{aligned} \tag{7.48}$$

From the translational invariance we factorize the 4-dimensional volume from the effective action as $S_{\text{eff}}(\bar{M}) = -V_4 V_{\text{eff}}(\Sigma, \theta)$. Then the effective potential V_{eff} is given by

$$\begin{aligned} V_{\text{eff}}(\Sigma, \theta) = -\hat{M}\Sigma \cos\theta + \ln \Sigma \\ + \left[\left(1 - 4 \cdot 2\Sigma^2 \sin^2\theta\right)^{1/2} - \ln\left[\frac{1 + \left(1 - 4 \cdot 2\Sigma^2 \sin^2\theta\right)^{1/2}}{2}\right]\right] . \end{aligned} \tag{7.49}$$

Now let us look into the vacuum structure of this effective potential by solving the saddle-point condition, which are given by

$$\frac{\partial V_{\text{eff}}(\Sigma,\theta)}{\partial \Sigma} = -\hat{M}\cos\theta + \frac{1}{\Sigma} - \frac{8\Sigma\sin^2\theta}{1+\left(1-4\cdot 2\Sigma^2\sin^2\theta\right)^{1/2}} \quad = 0 \tag{7.50}$$

$$\frac{\partial V_{\text{eff}}(\Sigma,\theta)}{\partial \theta} = \Sigma\sin\theta\left[\hat{M} - \frac{8\Sigma\cos\theta}{1+\left(1-4\cdot 2\Sigma^2\sin^2\theta\right)^{1/2}}\right] \quad = 0. \tag{7.51}$$

Here we find two types of solutions for these equations depending on whether θ is zero or nonzero: For a trivial solution for θ as $\theta = 0$, we have a solution as $\Sigma = 1/\hat{M}$. For $\theta \neq 0$, the stationary conditions are written as

$$\hat{M}\Sigma - \cos\theta = 0 \tag{7.52}$$

$$1 - \frac{8\Sigma^2}{1+\left(1-4\cdot 2\Sigma^2\sin^2\theta\right)^{1/2}} = 0. \tag{7.53}$$

Then, we find a solution for $\theta \neq 0$ as

$$\Sigma = \bar{\Sigma} = \sqrt{\frac{1}{8-\hat{M}^2}} \tag{7.54}$$

$$\sin^2\theta = \sin^2\bar{\theta} = \frac{2(4-\hat{M}^2)}{8-\hat{M}^2}. \tag{7.55}$$

Now we need to figure out which solution is realized as the vacuum of the theory by comparing the potentials for the two solutions. We easily show for $\hat{M}^2 < 4$,

$$V_{\text{eff}}(1/\hat{M},0) - V_{\text{eff}}(\bar{\Sigma},\bar{\theta}) > 0. \tag{7.56}$$

while $V_{\text{eff}}(1/\hat{M},0) - V_{\text{eff}}(\bar{\Sigma},\bar{\theta}) < 0$ for $\hat{M}^2 > 4$. Thus the vacuum of the strong-coupling QCD with the Hoelbling-type staggered-Wilson fermion is given by the following: For $\hat{M}^2 > 4$ or equivalently $M > -4\sqrt{2}+2$, $M < -4\sqrt{2}-2$, there is only the chiral condensate as

$$\frac{1}{N}\langle\bar{\chi}\chi\rangle = \Sigma\cos\theta \quad = \frac{1}{\hat{M}} \tag{7.57}$$

$$\frac{1}{N}\langle\bar{\chi}i\epsilon_x\chi\rangle = \Sigma\sin\theta \quad = 0. \tag{7.58}$$

For $\hat{M}^2 < 4$ or equivalently $-4\sqrt{2}-2 < M < -4\sqrt{2}+2$, there emerge the pion condensate which breaks the parity symmetry.

$$\frac{1}{N}\langle\bar{\chi}\chi\rangle = \bar{\Sigma}\cos\bar{\theta} \quad = \frac{\hat{M}}{8-\hat{M}^2} \tag{7.59}$$

$$\frac{1}{N}\langle\bar{\chi}i\epsilon_x\chi\rangle = \bar{\Sigma}\sin\bar{\theta} \quad = \pm\frac{\sqrt{2(4-\hat{M}^2)}}{8-\hat{M}^2}. \tag{7.60}$$

The critical mass $M_c = -4\sqrt{2} \pm 2$ and the range for the Aoki phase $-4\sqrt{2} - 2 < M < -4\sqrt{2} + 2$ is consistent with those of the hopping parameter expansion shown below (7.7). The sign of the pion condensate (7.60) reflects the parity symmetry of the theory. This result results strongly suggest the existence of the parity-broken phase in the lattice QCD with the Hoelbling-type fermion although it is just a strong-coupling limit.

We can also derive the mass spectrum of mesons by expanding the effective potential (7.49) up to the quadratic terms of the mesonic excitation field $\Pi_x = \mathcal{M}_x - \bar{\mathcal{M}}_x$. Since we are interested in the chiral limit which is taken from the parity-symmetric phase to the critical line, we here concentrate on the pion mass in the parity-symmetric phase. The masses of other mesons in the phase or those in the parity-broken phase are out of the scope of this study. For the parity symmetric phase ($\hat{M}^2 > 4$) the quadratic part of the effective action is given by

$$\begin{aligned} S_{\rm eff}(\mathcal{M}) - S_{\rm eff}(\bar{\mathcal{M}}) &= \sum_{x,y} S^{(2)}_{\rm eff}(x,y)\Pi_x\Pi_y \\ &= \int_{-\pi}^{\pi} \frac{d^4p}{(2\pi)^4}\Pi(-p)\mathcal{D}\Pi(p) \ , \end{aligned} \tag{7.61}$$

where $\Pi(p)$ is the Fourier component of Π_x, and

$$\mathcal{D} = \frac{1}{2\Sigma^2} + \left[\frac{1}{4}\sum_{\mu}\cos p_\mu - \frac{1}{24}\sum_{\mu\neq\nu}(\cos p_{\mu+\nu} + \cos p_{\mu-\nu})\right] \ . \tag{7.62}$$

with $p_{\mu\pm\nu} \equiv p_\mu \pm p_\nu$. Then we obtain the pion mass by solving $\mathcal{D} = 0$ at $p = (im_\pi a + \pi, \pi, \pi, \pi)$. The pion mass for the parity symmetric phase is given by

$$\cosh(m_\pi a) = 1 + \frac{2\hat{M}^2 - 8}{3}. \tag{7.63}$$

By using the definition $K = 1/2\hat{M}$ with $\hat{M} = M + 2r$ and $r = 2\sqrt{2}$, we find $\cosh(m_\pi a) = 1 + (1 - 16K^2)/6K^2$ which is consistent with the result of the hopping parameter expansion (7.12): The pion mass becomes zero at the critical mass $\hat{M}^2 = 4$, which indicates there occurs a 2nd-order phase transition between parity-symmetric and broken phases in the strong-coupling limit. By defining quark mass as $m_q a = \hat{M} - \hat{M}_c$, we find PCAC relation near the critical mass as

$$(m_\pi a)^2 = \frac{8}{3} m_q a + O(a^2). \tag{7.64}$$

We note we can also study the case for non-zero spacial momenta by considering $p = (iEa + \pi, p_1 a + \pi, p_2 a + \pi, p_3 a + \pi)$ in (7.62). By using the pion mass (7.64) and re-normalizing the Dirac operator as $-\frac{8}{3}\mathcal{D} \to \mathcal{D}$, we show (7.62) results in the Lorentz-covariant form with the correct dispersion relation in the continuum as,

$$\mathcal{D} = (E^2 - \mathbf{p}^2 - m_\pi^2)a^2 + O(a^3) \tag{7.65}$$

with $\mathbf{p}^2 = p_1^2 + p_2^2 + p_3^2$. Although this analysis contain large lattice artifacts, this result indicates that the Lorentz symmetry will be recovered in the continuum limit.

Now we confirm no other condensation appears in this analysis as in the hopping parameter expansion in Sec. 7.1. For this purpose we consider a general form of the meson field as

$$\bar{\mathcal{M}}_x = \sigma + i\epsilon_x\pi + \sum_\mu (-1)^{x_\mu} v_\mu + \sum_\mu i\epsilon_x (-1)^{x_\mu} a_\mu + \sum_{\mu>\nu} (-1)^{x_\mu + x_\nu} t_{\mu\nu} \tag{7.66}$$

where we define the vector, axial-vector and tensor meson fields as v_μ, a_μ and t_μ. We can easily show there is no other condensates in the parity symmetric phase $\hat{M}^2 > 4$ by substituting this general form of the meson fields (7.66) into the meson action (7.44). We find the saddle-point equations give nonzero condensate only for σ here. Thus we conclude the vacuum we obtained in the parity symmetric phase is a true one. It suggests the breaking of the discrete symmetry does not lead to any problematic influence on the vacuum structure in this phase at least in the strong-coupling limit. Thus the strong-coupling vacuum structure is qualitatively the same as the case of the Wilson fermion, where the pion mass gets zero for the critical mass or on the 2nd-order phase boundary. Since the lattice QCD simulation is performed by tuning the mass parameter from the parity-symmetric phase to the phase boundary, we expect we can take the chiral limit by mass tuning toward the second-order critical line in the lattice QCD with this fermion as in the Wilson fermion.

7.2.2 Adams type

We next investigate the case for the Adams fermion. We again consider the effective pontential up to $O(\mathcal{M}^3)$ The derivation is almost the same as the Hoelbling case in Subsec. 7.2.1. The main difference between them is the number of the multi-links. The fermion of the Adams type includes the four-hopping terms while the Hoelbling one has the two-hopping terms. The appendix C is devoted to the details of the calculation of the strong-coupling effective potential for the Adams-type fermion. Here we only mention to the results from the effective potential analysis for the Adams case.

In this case we again set $r = 16\sqrt{3}$ to match the result to that of the hopping parameter expansion in Sec. 7.1. We can derive the effective potential for the scalar and pi meson fields by assuming the condensation as $\mathcal{M}_x = \Sigma e^{i\epsilon_x\theta}$. We note the functional form of the effective action is the same as Eq. (7.49). By solving the saddle-point equations in the same way as the Hoelbling case, we find the critical mass is given by $\hat{M}_c^2 = 4$ or equivalently $M_c = -16\sqrt{3} \pm 2$ with $\hat{M} = M + r$ and $r = 16\sqrt{3}$. Then the vacuum of the strong-coupling QCD with the Adams-type staggered-Wilson fermion is also derived in a parallel way: For $\hat{M}^2 > 4$ or $M > -16\sqrt{3} + 2,\ M < -16\sqrt{3} - 2$, there is the chiral condensate as

$$\frac{1}{N}\langle\bar{\chi}\chi\rangle = \Sigma\cos\theta \quad = \frac{1}{\hat{M}} \tag{7.67}$$

$$\frac{1}{N}\langle\bar{\chi} i\epsilon_x\chi\rangle = \Sigma\sin\theta \quad = 0. \tag{7.68}$$

For $\hat{M}^2 < 4$ or $-16\sqrt{3} - 2 < M < -16\sqrt{3} + 2$, there emerge the pion condensate which

breaks the parity symmetry.

$$\frac{1}{N}\langle\bar{\chi}\chi\rangle = \bar{\Sigma}\cos\bar{\theta} \quad = \frac{\hat{M}}{8-\hat{M}^2} \tag{7.69}$$

$$\frac{1}{N}\langle\bar{\chi}i\epsilon_x\chi\rangle = \bar{\Sigma}\sin\bar{\theta} \quad = \pm\frac{\sqrt{2(4-\hat{M}^2)}}{8-\hat{M}^2}. \tag{7.70}$$

We note the critical mass and the parameter range of the Aoki phase are consistent with those of the hopping parameter expansion shown below (7.17). This result supports the existence of the parity-broken phase in the lattice QCD with the Adams fermion again.

The mass of the pion is derived from the quadratic parts of the effective potential in a parallel way to the Hoelbling type. The pion mass for this case is given by

$$\cosh(m_\pi a) = 1 + \frac{2\hat{M}^2 - 8}{5}, \tag{7.71}$$

for the parity symmetric phase ($\hat{M}^2 > 4$). By using the definition $K = 1/2\hat{M}$ with $\hat{M} = M + r$ and $r = 16\sqrt{3}$, we find $\cosh(m_\pi a) = 1 + (1 - 16K^2)/10K^2$ which is consistent with the result of the hopping parameter expansion (7.22): The pion mass becomes zero at the critical mass $\hat{M}^2 = 4$, which indicates there occurs a 2nd-order phase transition between parity-symmetric and broken phases in the strong-coupling limit. The PCAC relation holds near the critical mass also in this case. As in the Hoelbling type (7.65) we can also show the Lorentz-covariant dispersion relation recovers in the continuum limit in the Adams-type formalism as $\mathcal{D} = (E^2 - \mathbf{p}^2 - m_\pi^2)a^2 + O(a^3)$.

The argument on the possibility of other condensations is also done in the same way: We can show there is no other condensates in the parity symmetric phase $\hat{M}^2 > 4$ by substituting a general form of the meson fields (7.66) into the mesonic action for this case. We find no symptom manifesting the breaking of the essential physical symmetry for the vacuum structure in this phase in the strong-coupling limit. We emphasize that this vacuum structure is qualitatively the same as the case of the Wilson fermion, where the pion mass is getting zero as being close to the critical mass from the parity-symmetric phase. It suggests we can take the chiral limit by tuning the mass parameter toward the second-order critical line from the parity symmetric phase in the lattice QCD with this fermion.

7.3 Two-flavor case

In this section we discuss the phase structure for two-flavor staggered-Wilson fermions. we first consider the two-flavor case for the Hoelbling-type fermion action. In this case the situation is quite similar to the Wilson fermion [35]. We here consider the case that mass parameters for two flavors M_f ($f = 1, 2$) are equal. The chiral and parity condensates are given by

$$\frac{1}{N}\langle\bar{\chi}_f\chi_f\rangle = \Sigma_f\cos\theta_f = \frac{1}{\hat{M}_f}, \tag{7.72}$$

$$\frac{1}{N}\langle\bar{\chi}_f i\epsilon_x\chi_f\rangle = \Sigma_f\sin\theta_f = 0, \tag{7.73}$$

for $\hat{M}_f^2 \geq 4$ (Parity-symmetric phase) while they are given by

$$\frac{1}{N}\langle\bar{\chi}_f\chi_f\rangle = \bar{\Sigma}_f \cos\bar{\theta}_f = \frac{\hat{M}_f}{8-\hat{M}_f^2}, \tag{7.74}$$

$$\frac{1}{N}\langle\bar{\chi}_f i\epsilon_x\chi_f\rangle = \bar{\Sigma}_f \sin\bar{\theta}_f = \pm\frac{\sqrt{2(4-\hat{M}_f^2)}}{8-\hat{M}_f^2}, \tag{7.75}$$

for $\hat{M_f}^2 < 4$ (Aoki phase). Here we remind you of $\hat{M}_f = M_f + 2r$ with $r = 2\sqrt{2}$. For the parity symmetric phase, we do not need a special care in (7.72)(7.73). The whole $SU(2)$ chiral symmetry for the two-flavor QCD is just explicitly broken. On the phase boundary there appear three massless pions due to the divergence of the correlation length on the second-order critical line. (We here assume the phase transition is second-order.) When we perform the two-flavor lattice QCD simulation with this formulation, the chiral limit is taken toward the critical line and the three massless pions are regarded as the NG bosons associated with the spontaneous breaking of $SU(2)$ chiral symmetry. In the parity-broken phase, the question which parity condensate becomes nonzero depends on whether θ_1 has the same sign as θ_2 in (7.75). For $\theta_1 = \theta_2$,

$$\begin{aligned}
&\langle\bar{\chi}i\epsilon_x\chi\rangle \neq 0, \\
&\langle\bar{\chi}i\epsilon_x\tau_i\chi\rangle = 0, \quad (i=1,2,3)
\end{aligned} \tag{7.76}$$

where τ_i is the Pauli matrix and χ stands for the doublet $\chi = (\chi_1, \chi_2)^{\mathrm{T}}$. For $\theta_1 = -\theta_2$,

$$\begin{aligned}
&\langle\bar{\chi}i\epsilon_x\chi\rangle = 0, \\
&\langle\bar{\chi}i\epsilon_x\tau_1\chi\rangle = 0, \\
&\langle\bar{\chi}i\epsilon_x\tau_2\chi\rangle = 0, \\
&\langle\bar{\chi}i\epsilon_x\tau_3\chi\rangle \neq 0.
\end{aligned} \tag{7.77}$$

Here we remind ourselves of the statement of the Vafa-Witten's theorem [104]; in the vector-like theory (QCD), the parity is not spontaneously broken. However, if we look into the presuppositions of this theorem carefully, we find this theorem only states that the flavor-singlet pion condensate cannot exist in QCD. We know nothing about the flavor-non-singlet pion condensation or parity-flavor symmetry breaking. The only thing we know is the flavor-singlet pion condensate is likely to be forbidden in QCD. Thus we expect the latter case ($\theta_1 = -\theta_2$) is chosen as the true vacuum of the theory. We expect this should be also confirmed by studying $1/N$ or $1/g^2$ expansion of our analysis. The flavored pion condensate (7.77) indicates, besides the parity symmetry, the $SU(2)$ flavor symmetry is spontaneously broken to its $U(1)$ subgroup. Thus in the Aoki phase there emerge two massless pions as NG bosons associated with the breaking of the flavor symmetry. To summarize, we have three massless pions on the phase boundary while two of them remain massless in the parity broken phase. In this case the flavor-singlet meson, which corresponds to η meson, has nothing to do with the parity-flavor symmetry breaking since $\langle\bar{\chi}i\epsilon_x\chi\rangle = 0$. Thus there is no reason that the mass of this meson is light. In this formalism the so-called $U(1)$ problem is automatically resolved. This situation is qualitatively the same as the case of Wilson fermion [35].

The Adams-type staggered-Wilson fermion has degeneracy of two tastes for each branch, thus we can consider the two-flavor case automatically with a single Adams-type fermion. In this case there is no flavor symmetry which can be spontaneously broken in the Aoki phase except for the $U(1)$ baryon symmetry. It is because we have the taste breaking of the two species in each branch of Adams-type Dirac spectrum. Therefore we just have one massless pion on the phase boundary as long as we work on a finite lattice spacing while there is no massless excitation in the Aoki phase. However, what is special here is that the SU(2) flavor symmetry will recover in the continuum limit. Thus we expect three massless pions appear when we take the chiral and continuum limit.

For both the staggered-Wilson fermions, the two-flavor massless QCD is likely to be realized on the phase boundary, where we perform QCD simulations through the chiral limit. We also expect the PCAC relation holds near the critical line, which is essential for QCD simulations.

7.4 Short summary

Let me summarize the argument on the strong-coupling QCD. In Sec. 7.1 we analyze the staggered-Wilson fermions by using the hopping parameter expansion. The vacuum expectation value of the pion field (pion condensate) gets nonzero in some range of the hopping parameter. We also show the square pion mass is zero on the phase boundary and negative in the range where the pion condensate is nonzero. These results suggest there is a parity-broken phase and a second-order phase boundary for these fermions. In Sec. 7.2 we study the effective potential for meson fields in strong-coupling regime and large N limit to elaborate the phase structure in more details. Here we develop a method to obtain the effective potential for the fermion action with multiple hopping terms. The gap equations from the effective potential exhibit the nonzero pion condensate in the same parameter range as with the hopping parameter expansion. This range corresponds to the parity broken phase (Aoki phase). The effective potential analysis also shows the pion becomes massless on the phase boundary, which means the order of the phase transition is second-order at least in this regime. We can speculate this property carries over in the weak-coupling limit, then we can take the chiral limit by tuning the mass parameter in lattice QCD with the staggered-Wilson fermions as with Wilson fermion. In Sec. 7.3 We discuss the two-flavor cases. The case for the Hoelbling fermion is similar to the original Wilson fermion: We detect the three massless pions on the second-order phase boundary while two of them remain massless in the Aoki phase because of the parity-flavor symmetry breaking due to the flavored pion condensate $\langle \bar{\chi} i\epsilon\tau_3\chi\rangle$. The Adams-type staggered-Wilson fermion, which has degeneracy of two tastes for each branch, automatically contains two flavors. Although the taste-mixing breaks the flavor symmetry to the U(1) subgroup in the finite lattice spacing, the SU(2) flavor symmetry is expected to recover in the continuum limit. Thus three massless pions emerge if we tune the mass parameter to the phase boundary and take the continuum limit. Both the cases have possibility that we perform the two-flavor QCD simulations by tuning the mass parameter. Note that the results shown in this chapter are based on the analysis in approximation up to $O(K^3)$ or $O(\mathcal{M}^3)$. To conclude existence of the Aoki phase, we need full-order results with further

calculation. However we note that our results are qualitatively consistent with those for Wilson fermions, and we expect it implies the parity phase structure with the second-order phase transition. We also speculate that the qualitative results carry over to the full-order analysis.

Our results on the Aoki phase diagram in the strong-coupling regime exhibit no diseases due to discrete symmetry breaking in the parity-symmetric phase and on the phase boundary. It suggests the requisite continuum symmetry will recover in the QCD simulation with the staggered-Wilson fermion, which is consistent with the results in the lattice perturbation in [59, 31, 32]. All of these results indicate that we can apply the staggered-Wilson fermions to the lattice QCD simulations by the mass parameter tuning.

Chapter 8

Conclusion

In this thesis I have studied new formulations of lattice fermions which enable us to perform lattice simulations more efficiently; this will result in progress in the understanding of hadron physics, physics of quark-gluon-plasma, etc. We can classify the new formulations into two classes: 1. Generalized Wilson and overlap fermions (based on naive fermions) and 2. Staggered-Wilson and staggered-overlap fermions (based on staggered fermions). The key point for both formulations is the introduction of the flavored-mass term as a generalization of the Wilson term.

Regarding the first formulation, we have shown that the generalized Wilson terms, or flavored-mass terms for naive fermions, give more possibilities of species splitting that lead to generalized Wilson fermions with any number of flavors. We have shown that the index theorem holds for them, and correctly detects the gauge topology through the index of the associated Dirac operators. We also study the parity phase structure in the lattice QCD with these generalized Wilson fermions, to elaborate if they could be successfully applicable to practical calculations through the mass parameter tuning. Our results indicate that one can perform the lattice QCD simulation with a desirable number of flavors, including the physical two-flavor or three-flavor cases, by using only one generalized Wilson or overlap fermion. In the introduction in Chapter 1, we note one of the hardships in the doubling problem is that we cannot control the number of fermions on the lattice. The generalized Wilson fermions brilliantly resolve this problem.

The second formulation, or the formulation of staggered-Wilson and staggered-overlap fermions, was first proposed by D. Adams who introduced the flavored-mass terms for staggered fermions. We gives a theoretical foundation to these novel fermions by pointing out that the flavored-mass terms for staggered fermions are related through the spin diagonalization to those for the naive fermions . This indicates that the generalized Wilson fermion can be decomposed into four staggered-Wilson fermions. We also show the applicability of the new staggered-Wilson fermions to lattice QCD simulations. As is the case with the Wilson fermions based on the naive fermion, the parity phase structure with the second-order phase transition also exists in the lattice QCD with the staggered-Wilson fermion. Our results on the parity phase diagram in the Gross-Neveu model and the strong-coupling lattice QCD with staggered-Wilson fermions are qualitatively similar to those for usual Wilson fermions. It indicates the PCAC relation holds around the second-order critical line, which is essential for the simulation of QCD. Since the existence

of the Aoki phase also indicates the applicability of the overlap fermions to lattice QCD calculations, we conclude that we can perform lattice QCD simulations with these new formulations including staggered-Wilson and staggered-overlap fermions in a similar way to the original Wilson and overlap fermions.

Here let us summarize the contents of each chapter. In Chapter 3 we have constructed the flavored-mass terms for naive fermions by using the point-splitting fields. Imposing the γ_5 hermiticity on the Dirac operator with flavored-mass terms allows one to classify the flavored-mass terms for physical fermions into four non-trivial types which we call vector, axial-vector, tensor and pseudo-scalar types. These four types give various kinds of 16 species-splitting, which leads to various types of generalized Wilson fermions with any number of flavors from 1 to 15. We also show that two of these flavored-mass terms correspond to the two types of staggered flavored-mass terms for the staggered-Wilson fermions. In Chapter 4 we summarize the generalized Wilson fermion action and the staggered-Wilson fermion, with emphasis on the symmetries possessed by them. We show that the staggered-Wilson fermion possesses basic symmetries of QCD including the parity and Lorentz symmetries. In Chapter 5 we study the index theorem for these new fermions with flavored-mass terms by looking into the spectral flow of the hermitean versions of Dirac operators. We find that both naive and staggered fermions with flavored-mass terms correctly detect the gauge topology through the Dirac index. We also construct the overlap versions of these fermions, which lead to the generalized overlap fermions based on the naive fermion and the staggered-overlap fermions. In particular the latter has the possibility of reducing the notorious numerical expense for lattice QCD simulations with the usual overlap fermions. In Chapter 6 and 7 we discuss the applicability of the staggered-Wilson fermions to lattice QCD simulations. Special attention paid to the parity broken phase structure and the second-order phase transition in the lattice QCD with these novel fermions, and we show that we can perform numerical QCD simulations by taking a chiral limit through the mass parameter tuning. We first consider the two-dimensional Gross-Neveu model and show the presence of the Aoki (parity) phase structure. We also investigate the chiral limit of this theory, and we show that one can take the chiral and continuum limit by tuning the parameters as with the Wilson fermion. We next study the strong-coupling QCD analysis in four dimensions, which is believed to describe the infrared physics correctly at least. This analysis also shows the existence of the Aoki phase and the second-order critical lines.

To summarize, our results on the novel lattice fermions strongly suggest that we can perform lattice QCD simulations with these fermions in the same way as the usual Wilson or overlap fermions. The generalized Wilson and overlap fermions based on naive fermions can yield lattice fermions with any number of flavors from 1 to 15. Thus we can study two or three-flavor QCD only with one generalized Wilson or overlap fermion while we normally need two or three usual Wilson fermions. This would reduce the cost of numerical tasks. On the other hand, the staggered-Wilson and staggered-overlap fermions obviously have the advantage over the usual formulations. Since the matrix size of the Dirac operator for the staggered-based fermions, the CPU time required for calculation of the fermion propagator should be reduced by factor 1/4 at least. In particular, in the case of staggered-overlap fermions, the simulation costs will be reduced greatly since the sign function in the overlap Dirac operator is derived through the Lanczos process where multiplication of

the matrix and the vector are repeated several times until the Dirac operator converges to the solution. I believe that our theoretical study on the new lattice fermions is not only valuable in understanding of the pure-theoretical aspects of the lattice field theory, but also essential for improving practical application of them to the numerical simulations.

Acknowledgement

The author is grateful to his supervisor, Prof. Ken-ichi Shizuya, for guiding him and giving useful advice on this thesis. He is thankful to his host researcher in Brookhaven National Laboratory, Prof. Michael Creutz for guiding him to exciting topics and collaborating with him. He thanks his collaborators on the present study, Taro Kimura, Shota Komatsu, Toshifumi Noumi, Shingo Torii in the University of Tokyo, Prof. Sinya Aoki in the University of Tsukuba Takashi Nakano and Prof. Akira Ohnishi in Yukawa Institute for Theoretical Physics. He also thanks to the collaborators on the other works, Mitsutoshi Fujita, Prof. Kenji Fukushima, Toru Kikuchi and Masaki Murata. He appreciates hearty encouragement by his parents during he has been enrolled in the graduate school.

Appendix A

Spin-flavor representation of fermion actions

Let us first describe the case of naive fermions. The action of the naive fermion, expressed by χ as in (2.38), can be recast in the following form.

$$\begin{aligned} S_{\rm nf} =& \frac{1}{2} \sum_{N,\,\mu,\,A,\,B} \eta_\mu(A) \bar{\chi}_A(N) \Big((\delta_{A+\hat{\mu},\,B} + \delta_{A-\hat{\mu},\,B}) \nabla_\mu \chi_B(N) - (\delta_{A+\hat{\mu},\,B} - \delta_{A-\hat{\mu},\,B}) \nabla_\mu^2 \chi_B(N) \Big) \\ & + m \sum_{N,\,A} \bar{\chi}_A(N) \chi_A(N) \,, \end{aligned} \tag{A.1}$$

where A_μ and B_μ take zero or one, and the definitions of ∇_μ and ∇_μ^2 are given in (A.12) and (A.13). In order to further rewrite the above action using the field Ψ, defined in (A.8) and (A.9), the following formulas are useful;

$$\begin{aligned} & \sum_{A,\,B} \eta_\mu(A) (\delta_{A+\hat{\mu},\,B} + \delta_{A-\hat{\mu},\,B}) \left(\frac{\gamma_A}{2} \right)_{\alpha,\,f_1} \left(\frac{\bar{\gamma}_B}{2} \right)_{\alpha',\,f_1'} = \sum_A \left(\frac{\gamma_A}{2} \right)_{\alpha,\,f_1} \left(\gamma_\mu^{\rm T} \, \frac{\bar{\gamma}_A}{2} \right)_{\alpha',\,f_1'} \\ & = (\gamma_\mu)_{\alpha,\,\alpha'} \, \delta_{f_1,\,f_1'} \,, \end{aligned} \tag{A.2}$$

and

$$\begin{aligned} & \sum_{A,\,B} \eta_\mu(A) (\delta_{A+\hat{\mu},\,B} - \delta_{A-\hat{\mu},\,B}) \left(\frac{\gamma_A}{2} \right)_{\alpha,\,f_1} \left(\frac{\bar{\gamma}_B}{2} \right)_{\alpha',\,f_1'} = \sum_A \left(\gamma_5 \, \frac{\gamma_A}{2} \, \gamma_5 \right)_{\alpha,\,f_1} \left(\frac{\bar{\gamma}_A}{2} \, \gamma_\mu^{\rm T} \right)_{\alpha',\,f_1'} \\ & = (\gamma_5)_{\alpha,\,\alpha'} \, (\gamma_5^{\rm T} \gamma_\mu^{\rm T})_{f_1,\,f_1'} \,. \end{aligned} \tag{A.3}$$

To derive (A.2) and (A.3), it is convenient to first consider the cases when $A_\mu = 0$ and $A_\mu = 1$ separately and put them together at the end. Using these formulas one obtains the expression (A.10) for the naive fermion.

In the case of Wilson fermions, we also need to re-express the Wilson term, which can

be represented in terms of $\chi_A(N)$ as

$$S_W = -\frac{r}{2}\sum_{N,\,\mu,\,A,\,B}\tilde{\eta}_\mu(A)\bar{\chi}_A(N)\gamma_\mu\Big[2(\delta_{A+\hat{\mu},\,B}+\delta_{A-\hat{\mu},\,B})\chi_B(N)-(\delta_{A+\hat{\mu},\,B}-\delta_{A-\hat{\mu},\,B})\nabla_\mu\chi_B(N) + (\delta_{A+\hat{\mu},\,B}+\delta_{A-\hat{\mu},\,B})\nabla_\mu^2\chi_B(N)\Big] + 4r\sum_{N,A}\bar{\chi}_A(N)\chi_A(N)\,. \tag{A.4}$$

To derive the expression in terms of Ψ, this time one needs the variants of (A.2) and (A.3);

$$\sum_{A,\,B}\tilde{\eta}_\mu(A)(\delta_{A+\hat{\mu},\,B}+\delta_{A-\hat{\mu},\,B})\left(\frac{\gamma_A}{2}\right)_{\alpha,\,f_1}\left(\frac{\bar{\gamma}_B}{2}\right)_{\alpha',\,f_1'} = \sum_A\left(\frac{\gamma_A}{2}\right)_{\alpha,\,f_1}\left(\frac{\bar{\gamma}_A}{2}\,\gamma_\mu^{\mathrm{T}}\right)_{\alpha',\,f_1'} = \delta_{\alpha,\,\alpha'}\,(\gamma_\mu^{\mathrm{T}})_{f_1,\,f_1'}\,, \tag{A.5}$$

and

$$\sum_{A,\,B}\tilde{\eta}_\mu(A)(\delta_{A+\hat{\mu},\,B}-\delta_{A-\hat{\mu},\,B})\left(\frac{\gamma_A}{2}\right)_{\alpha,\,f_1}\left(\frac{\bar{\gamma}_B}{2}\right)_{\alpha',\,f_1'} = \sum_A\left(\gamma_5\,\frac{\gamma_A}{2}\,\gamma_5\right)_{\alpha,\,f_1}\left(\gamma_\mu^{\mathrm{T}}\,\frac{\bar{\gamma}_A}{2}\right)_{\alpha',\,f_1'} = (\gamma_5\gamma_\mu)_{\alpha,\,\alpha'}\,(\gamma_5^{\mathrm{T}})_{f_1,\,f_1'}\,. \tag{A.6}$$

Applying these formulas one can re-express the Wilson term and obtain (A.18).

A.1 Spin-flavor representation of the naive fermion

We reconsider the naive fermion by using the results in the previous subsection. As in the case of the staggered fermion, it is useful to introduce the field $\Psi(N)$ as

$$\Psi(N)_{\alpha,\,f_1,\,f_2} = \sum_A\left(\frac{\gamma_A}{2}\right)_{\alpha,\,f_1}\chi_A(N)_{f_2}\,,\quad \bar{\Psi}(N)_{\alpha,\,f_1,\,f_2} = \sum_A\left(\frac{\bar{\gamma}_A}{2}\right)_{\alpha,\,f_1}\bar{\chi}_A(N)_{f_2}\,, \tag{A.7}$$

where $A_\mu = 0$ or 1, $\chi_A(N) = \chi_{2N+A}$, $\gamma_A = \gamma_1^{A_1}\gamma_2^{A_2}\gamma_3^{A_3}\gamma_4^{A_4}$, and $\bar{\gamma}_A$ denotes the complex conjugate of γ_A. The relation between the fields ψ and Ψ is given by

$$\Psi(N)_{\alpha,\,f_1,\,f_2} = \sum_A\left(\frac{\gamma_A}{2}\right)_{\alpha,\,f_1}(\bar{\gamma}_A)_{\beta,\,f_2}\,(\psi_{2N+A})_\beta\,, \tag{A.8}$$

$$\bar{\Psi}(N)_{\alpha,\,f_1,\,f_2} = \sum_A\left(\frac{\bar{\gamma}_A}{2}\right)_{\alpha,\,f_1}(\gamma_A)_{\beta,\,f_2}\,(\bar{\psi}_{2N+A})_\beta\,. \tag{A.9}$$

In terms of $\Psi(N)$, the naive fermion action (2.21) can be written as

$$S_{\mathrm{nf}} = \frac{1}{2}\sum_{N,\mu}\left[\bar{\Psi}(N)\,(\gamma_\mu\otimes\mathbf{1}_4\otimes\mathbf{1}_4)\,\nabla_\mu\Psi(N) + \bar{\Psi}(N)\left(\gamma_5\otimes\gamma_\mu^{\mathrm{T}}\gamma_5^{\mathrm{T}}\otimes\mathbf{1}_4\right)\nabla_\mu^2\Psi(N)\right] + m\sum_N\bar{\Psi}(N)\,(\mathbf{1}_4\otimes\mathbf{1}_4\otimes\mathbf{1}_4)\,\Psi(N)\,, \tag{A.10}$$

where

$$\bar{\Psi}(A\otimes B\otimes C)\Psi = \sum_{\alpha,\alpha',f_1,f_1',f_2,f_2'} \bar{\Psi}_{\alpha,f_1,f_2}(A)_{\alpha\alpha'}(B)_{f_1f_1'}(C)_{f_2f_2'}\Psi_{\alpha',f_1',f_2'}, \quad \text{(A.11)}$$

$$\nabla_\mu\Psi(N) = \frac{\Psi(N+\hat{\mu})-\Psi(N-\hat{\mu})}{2}, \quad \text{(A.12)}$$

$$\nabla_\mu^2\Psi(N) = \frac{\Psi(N+\hat{\mu})-2\Psi(N)+\Psi(N-\hat{\mu})}{2} \quad \text{(A.13)}$$

and the superscript T denotes transposition.

Now let us discuss the structure of the expression (A.10). The first and the third term in the right-hand side of (A.10) can be interpreted as the kinetic term and the mass term for each doubler by identifying the index α as a spinor index and the indices f_1, f_2 as flavor indices. We can see that the first term in (A.10) is invariant under the U(16) $\times$ U(16) transformations generated by $(\mathbf{1}_4\otimes\mathfrak{u}(4)\otimes\mathfrak{u}(4))$ and $(\gamma_5\otimes\mathfrak{u}(4)\otimes\mathfrak{u}(4))$, which correspond to the vector and the axial-vector symmetries among sixteen doublers. On the other hand the third term is invariant only under the diagonal U(16) transformations generated by $(\mathbf{1}_4\otimes\mathfrak{u}(4)\otimes\mathfrak{u}(4))$, which correspond to the vector (flavor) symmetries. These symmetries among doublers are partially broken by the presence of the second term, which mixes different doublers. A closer look at the structure of the second term shows that they are invariant under the U(4) $\times$ U(4) symmetry, which are expressed as

$$\Psi(N)\to\Psi'(N) = \exp\left[\mathrm{i}\,(\mathbf{1}_4\otimes\mathbf{1}_4\otimes\widetilde{T}^+)+\mathrm{i}\,(\gamma_5\otimes\gamma_5^{\mathrm{T}}\otimes\widetilde{T}^-)\right]\Psi(N), \quad \text{(A.14)}$$

$$\bar{\Psi}(N)\to\bar{\Psi}'(N) = \bar{\Psi}(N)\exp\left[-\mathrm{i}\,(\mathbf{1}_4\otimes\mathbf{1}_4\otimes\widetilde{T}^+)+\mathrm{i}\,(\gamma_5\otimes\gamma_5^{\mathrm{T}}\otimes\widetilde{T}^-)\right], \quad \text{(A.15)}$$

where $\widetilde{T}^+$ and $\widetilde{T}^-$ are 4×4 Hermitian matrices, given by

$$\widetilde{T}^+,\widetilde{T}^-\in\mathrm{span}\left\{\mathbf{1}_4\,,\ \gamma_5\,,\ \ \gamma_\mu\,,\mathrm{i}\gamma_\mu\gamma_5\,,\frac{\mathrm{i}\,[\gamma_\mu\,,\gamma_\nu]}{2}\right\}. \quad \text{(A.16)}$$

These transformations turn out to coincide respectively with the transformations generated by $\mathcal{M}^+$ and $\mathcal{M}^-$. Therefore, from the discussion in this subsection, we can identify the U(4) $\times$ U(4) symmetries of the kinetic term of the naive fermion as a part of the U(16) $\times$ U(16) vector and axial-vector symmetries of sixteen doublers and the $\mathrm{U}(4)^+$ symmetries as a part of the U(16) vector symmetries. We also note that Eq. (A.10) clearly indicates the U(4) $\times$ U(4) symmetries come from the rotation of four copies of staggered fermions in the naive fermion as we discussed in the previous subsection.

A.2 Wilson fermion

In this section we will discuss the symmetry and its breaking in the Wilson fermion. As is well-known, the Wilson term splits sixteen doublers into five branches. Since simulation almost exclusively uses the "physical" branches, which contain only one massless fermion mode, the symmetry and the structure in other branches have not been fully investigated so far. Therefore, here we will clarify the continuous symmetries and their spontaneous

breaking in all the branches including "unphysical" ones. As a consequence, we will find an unexpected symmetry enhancement and its spontaneous breaking in the central branch. The action for Wilson fermion [1] is given by

$$S = S_{\rm nf} + S_W \quad \text{with} \quad S_W = -\frac{r}{2}\sum_{n,\mu}\bar{\psi}_n\left(\psi_{n+\hat{\mu}} - 2\psi_n + \psi_{n-\hat{\mu}}\right) . \tag{A.17}$$

In terms of the spin-flavor representation, the Wilson term S_W is written as

$$\begin{aligned} S_W &= -\frac{r}{2}\sum_{N,\mu}\Big[2\bar{\Psi}(N)\left(\mathbf{1}_4\otimes\gamma_\mu^{\rm T}\otimes\gamma_\mu\right)\Psi(N) + \bar{\Psi}(N)\left(\mathbf{1}_4\otimes\gamma_\mu^{\rm T}\otimes\gamma_\mu\right)\nabla_\mu^2\Psi(N) \\ &\quad +\bar{\Psi}(N)\left(\gamma_\mu\gamma_5\otimes\gamma_5^{\rm T}\otimes\gamma_\mu\right)\nabla_\mu\Psi(N)\Big] + 4r\sum_N\bar{\Psi}(N)\left(\mathbf{1}_4\otimes\mathbf{1}_4\otimes\mathbf{1}_4\right)\Psi(N) \end{aligned} \tag{A.18}$$

The first three terms in (A.18) are invariant under the ordinary U(1) vector transformation, $\mathrm{U}(1)_V$, which is defined by

$$\Psi(N) \to \Psi'(N) = \exp\left[{\rm i}\theta(\mathbf{1}_4\otimes\mathbf{1}_4\otimes\mathbf{1}_4)\right]\Psi(N) , \tag{A.19}$$

$$\bar{\Psi}(N) \to \bar{\Psi}'(N) = \bar{\Psi}(N)\exp\left[-{\rm i}\theta(\mathbf{1}_4\otimes\mathbf{1}_4\otimes\mathbf{1}_4)\right] , \tag{A.20}$$

$$\psi_n \to \psi'_n = e^{{\rm i}\theta}\psi_n , \quad \bar{\psi}_n \to \bar{\psi}'_n = e^{-{\rm i}\theta}\bar{\psi}_n , \tag{A.21}$$

and the site-dependent U(1) vector transformation, $\mathrm{U}(1)_V^-$, defined by

$$\Psi(N) \to \Psi'(N) = \exp\left[{\rm i}\theta(\gamma_5\otimes\gamma_5^{\rm T}\otimes\mathbf{1}_4)\right]\Psi(N) , \tag{A.22}$$

$$\bar{\Psi}(N) \to \bar{\Psi}'(N) = \bar{\Psi}(N)\exp\left[{\rm i}\theta(\gamma_5\otimes\gamma_5^{\rm T}\otimes\mathbf{1}_4)\right] , \tag{A.23}$$

$$\psi_n \to \psi'_n = e^{{\rm i}(-1)^{n_1+\cdots+n_4}\theta}\psi_n , \quad \bar{\psi}_n \to \bar{\psi}'_n = e^{{\rm i}(-1)^{n_1+\cdots+n_4}\theta}\bar{\psi}_n . \tag{A.24}$$

By contrast the last term in (A.18) is invariant only under the $\mathrm{U}(1)_V$ transformation. Therefore, the total Wilson fermion action possesses only the $\mathrm{U}(1)_V$ symmetry for general values of m and r. Interestingly enough, however, the additional $\mathrm{U}(1)_V^-$ symmetry appears if m and r satisfy $m + 4r = 0$, at which the on-site terms cancel out between the mass term and the Wilson term. As shown in the reference [], this symmetry is spontaneously broken by the pion condensate, $\langle\bar{\psi}\gamma_5\psi\rangle$ where the associated NG boson appears.

Appendix B

Derivation of the effective potentials in GN models

In this appendix we evaluate the integrals which are required for the effective potentials for the cases with the naive and staggered fermions.

B.1 Naive fermion

We have to evaluate the integrals of (6.50) and (6.51) to obtain the effective potential of the model with the naive fermion. Let us first study the following integral,

$$I_0 = \int_{-\pi/a}^{\pi/a} \frac{d^2k}{(2\pi)^2} \log\left[\frac{s^2}{a^2} + \sigma_0^2 + \pi_0^2 + \left(\frac{-1+M_f}{a}\right)^2\right], \tag{B.1}$$

where we denote $s^2 = \sum_\mu \sin^2(k_\mu a)$ and $M_f = \cos(k_1 a)\cos(k_2 a)$. If we omit a constant term which is not involving σ_0 and π_0, it can be rewritten in an integral representation as

$$I_0 \simeq \int_0^{\sigma_0^2+\pi_0^2} d\rho\ F_0(\rho), \tag{B.2}$$

$$F_0(\rho) = \int_{-\pi/a}^{\pi/a} \frac{d^2k}{(2\pi)^2} \frac{1}{s^2/a^2 + (-1+M_f)^2/a^2 + \rho}. \tag{B.3}$$

We pick up the divergent part in the limit of $a \to 0$,

$$F_0(\rho) \xrightarrow{a\to 0} \int_{-\pi/(2a)}^{3\pi/(2a)} \frac{d^2k}{(2\pi)^2} \left(\frac{1}{\sum_\mu k_\mu^2 + \rho} + \frac{1}{\sum_\mu (k_\mu - \pi)^2 + \rho}\right) + c_0, \tag{B.4}$$

$$c_0 = \int_{-\pi/2}^{3\pi/2} \frac{d^2\xi}{(2\pi)^2} \left(\frac{1}{s^2 + (-1+M_f)^2} - \frac{1}{\sum_\mu \xi_\mu^2} - \frac{1}{\sum_\mu (\xi_\mu - \pi)^2}\right) (= 0.0421\cdots) \tag{B.5}$$

Here we shift the Brillouin zone to treat the divergent part, which originates from two massless modes around $k = (0,0)$ and (π,π). We then find the following expression by

comparing the first term with the corresponding integral in the continuum theory,

$$\int_{-\pi/(2a)}^{3\pi/(2a)} \frac{d^2k}{(2\pi)^2}\left(\frac{1}{\sum_\mu k_\mu^2+\rho}+\frac{1}{\sum_\mu (k_\mu-\pi)^2+\rho}\right)=\frac{1}{2\pi}\log\frac{1}{a^2\rho}+c_0' \quad (c_0'=0.325)\,. \tag{B.6}$$

Therefore the integral is given by

$$F_0(\rho)=\frac{1}{2\pi}\log\frac{1}{a^2\rho}+\tilde{C}_0 \quad \left(\tilde{C}_0=0.367\right), \tag{B.7}$$

where $\tilde{C}_0 = c_0 + c_0'$ is the constant used in (6.52). By substituting this into (B.2), we obtain the expression in (6.52)

$$I_0(a\to 0)=\tilde{C}(\sigma_0^2+\pi_0^2)-\frac{1}{2\pi}(\sigma_0^2+\pi_0^2)\log\frac{a^2(\sigma_0^2+\pi_0^2)}{e}. \tag{B.8}$$

Next we show the integral expressions of (6.53) and (6.54). They are given by

$$C_1 = \int_{-\pi}^{\pi}\frac{d^2\xi}{(2\pi)^2}\frac{-1+M_f}{s^2+(-1+M_f)^2} \quad (=-0.446), \tag{B.9}$$

$$C_2 = \int_{-\pi}^{\pi}\frac{d^2\xi}{(2\pi)^2}\left(\frac{-1+M_f}{s^2+(-1+M_f)^2}\right)^2 \quad (=0.201). \tag{B.10}$$

These integrals are sufficient to consider the continuum limit of the model, but not to discuss the 1st-order phase transition. The $\mathcal{O}(a)$ corrections come from the following integrals,

$$I_3(a\to 0)=\frac{8}{3}\sigma_0^3 a C_3, \quad C_3=\int_{-\pi}^{\pi}\frac{d^2\xi}{(2\pi)^2}\left(\frac{-1+M_f}{s^2+(-1+M_f)^2}\right)^3 \quad (=-0.0923), \tag{B.11}$$

$$\begin{aligned}
\delta I_1 &= I_1-\frac{2\sigma_0}{a}C_1 \\
&= 2\sigma_0\int_{-\pi/a}^{\pi/a}\frac{d^2k}{(2\pi)^2}\left(\frac{(-1+M_f)/a}{s^2/a^2+(-1+M_f)^2/a^2+\sigma_0^2+\pi_0^2}-\frac{(-1+M_f)/a}{s^2/a^2+(-1+M_f)^2/a^2}\right) \\
&= -2\sigma_0 a\int_0^{\sigma_0^2+\pi_0^2} d\rho\; F_1(\rho),
\end{aligned} \tag{B.12}$$

$$F_1(\rho) = \frac{1}{a}\int_{-\pi/a}^{\pi/a}\frac{d^2k}{(2\pi)^2}\frac{(-1+M_f)/a}{(s^2/a^2+(-1+M_f)^2/a^2+\rho)^2}. \tag{B.13}$$

We can evaluate the second one in a similar way by splitting into a divergent part and a finite constant,

$$F_1(\rho) \overset{a\to 0}{\longrightarrow} -\frac{1}{2}\int_{-\pi/(2a)}^{3\pi/(2a)}\frac{d^2k}{(2\pi)^2}\left(\frac{\sum_\mu k_\mu^2}{\left(\sum_\mu k_\mu^2+\rho\right)^2}+\frac{\sum_\mu (k_\mu-\pi)^2}{\left(\sum_\mu (k_\mu-\pi)^2+\rho\right)^2}\right)+c_1 \tag{B.14}$$

$$c_1 = \int_{-\pi/2}^{3\pi/2}\frac{d^2\xi}{(2\pi)^2}\left(\frac{(-1+M_f)}{(s^2+(-1+M_f)^2)^2}+\frac{1}{2\sum_\mu \xi_\mu^2}+\frac{1}{2\sum_\mu(\xi_\mu-\pi)^2}\right)(=0.00912)\,. \tag{B.15}$$

The divergent part is given by

$$\int_{-\pi/(2a)}^{3\pi/(2a)} \frac{d^2k}{(2\pi)^2} \left(\frac{\sum_\mu k_\mu^2}{\left(\sum_\mu k_\mu^2 + \rho\right)^2} + \frac{\sum_\mu (k_\mu - \pi)^2}{\left(\sum_\mu (k_\mu - \pi)^2 + \rho\right)^2} \right) = \frac{1}{2\pi} \log \frac{1}{a^2\rho} + c_1' \quad (c_1' = 0.166). \tag{B.16}$$

Thus we obtain

$$F_1(\rho) = -\frac{1}{4\pi} \log \frac{1}{a^2\rho} + \tilde{C}_1 \quad \left(\tilde{C}_1 = c_1 - \frac{c_1'}{2} = -0.0741 \right). \tag{B.17}$$

By substituting this expression into (B.12), we obtain

$$\delta I_1 = -2\sigma_0 a \left[\tilde{C}_1(\sigma_0^2 + \pi_0^2) + \frac{1}{4\pi}(\sigma_0^2 + \pi_0^2) \log \frac{a^2(\sigma_0^2 + \pi_0^2)}{e} \right]. \tag{B.18}$$

These integrals contribute to the $\mathcal{O}(a)$ corrections to the effective potential (6.66).

B.2 Staggered fermion

We evaluate the integrals required for the effective potentials with the staggered fermion. Explicit forms of the finite constants in (6.75) and (6.76) are simply given by

$$C_1 = \int_{-\pi}^{\pi} \frac{d^2\xi}{(2\pi)^2} \left[\frac{-1 + M_f}{s^2 + (-1 + M_f)} + \frac{-1 - M_f}{s^2 + (-1 - M_f)} \right] \quad (= -0.896), \tag{B.19}$$

$$C_2 = \int_{-\pi}^{\pi} \frac{d^2\xi}{(2\pi)^2} \left[\left(\frac{-1 + M_f}{s^2 + (-1 + M_f)} \right)^2 + \left(\frac{-1 - M_f}{s^2 + (-1 - M_f)} \right)^2 \right] \quad (= 0.404), \tag{B.20}$$

where we use similar symbols as the naive fermion case, $s^2 = \sum_\mu \sin^2(k_\mu a/2)$, $M_f = \cos(k_1 a/2)\cos(k_2 a/2)$.

The integral (6.74) is slightly complicated, but can be evaluated in a similar manner. Omitting a constant term independent on σ_0 and π_0, it can be written as

$$I_0^+ = \int_{-\pi/a}^{\pi/a} \frac{d^2k}{(2\pi)^2} \log \left[\frac{s^2}{a^2} + \sigma_0^2 + \pi_0^2 + \left(\frac{-1 + M_f}{a} \right)^2 \right]$$

$$\simeq \int_0^{\sigma_0^2 + \pi_0^2} d\rho \; F(\rho), \tag{B.21}$$

$$F(\rho) = \int_{-\pi/a}^{\pi/a} \frac{d^2k}{(2\pi)^2} \frac{1}{s^2/a^2 + (-1 + M_f)^2/a^2 + \rho}. \tag{B.22}$$

We can split this integral into a divergent part and a finite constant in the limit of $a \to 0$,

$$F(\rho) \overset{a\to 0}{\longrightarrow} \int_{-\pi/a}^{\pi/a} \frac{d^2k}{(2\pi)^2} \frac{1}{\sum_\mu k_\mu^2/4 + \rho} + c_0^+,$$

$$c_0^+ = \int_{-\pi}^{\pi} \frac{d^2\xi}{(2\pi)^2} \left(\frac{1}{s^2 + (-1 + M_f)^2} - \frac{1}{\sum_\mu \xi_\mu^2/4} \right) \quad (= 0.0440). \tag{B.23}$$

The divergent part is given by

$$\int_{-\pi/a}^{\pi/a} \frac{d^2k}{(2\pi)^2} \frac{1}{\sum_\mu k_\mu^2/4 + \rho} = \frac{1}{\pi} \log \frac{1}{4a^2\rho} + C_0^{+\prime} \quad \left(C_0^{+\prime} = 0.798\right). \tag{B.24}$$

Thus we obtain

$$F(\rho) = \frac{1}{\pi} \log \frac{1}{4a^2\rho} + \tilde{C}_0^{+} \quad \left(\tilde{C}_0^{+} = C_0^{+} + C_0^{+\prime} = 0.842\right). \tag{B.25}$$

The corresponding integral becomes

$$I_0^+(a \to 0) = \tilde{C}_0^+(\sigma_0^2 + \pi_0^2) - \frac{1}{\pi}(\sigma_0^2 + \pi_0^2) \log \frac{4a^2(\sigma_0^2 + \pi_0^2)}{e}. \tag{B.26}$$

The other integral is written as

$$I_0^- \simeq C_0^-(\sigma_0^2 + \pi_0^2) + \mathcal{O}(a), \tag{B.27}$$

$$C_0^- = \int_{-\pi}^{\pi} \frac{d^2\xi}{(2\pi)^2} \frac{1}{s^2 + (1 + M_f)^2} \quad (= 0.333) \tag{B.28}$$

where we again omit a constant independent on σ_0 and π_0. As a result we obtain the expression of (6.74),

$$I_0^+ + I_0^- = \tilde{C}_0(\sigma_0^2 + \pi_0^2) - \frac{1}{\pi}(\sigma_0^2 + \pi_0^2) \log \frac{4a^2(\sigma_0^2 + \pi_0^2)}{e} \quad \left(\tilde{C}_0 = \tilde{C}_0^+ + C_0^- = 1.177\right). \tag{B.29}$$

Appendix C

Strong-coupling analysis for Adams-type

In this chapter we show the derivation of the effective potential for the Adams-type fermion in the strong-coupling limit. To derive the effective potentiail for the Adams type, we replace Eq. (7.26) by Eq. (C.1) in the Adams type.

$$\exp\left[\sum_x NW(\Lambda)\right] = \prod_x Z_x,$$
$$Z_x = \int \left(\prod_{\mu\neq\nu\neq\rho\neq\sigma} \mathcal{D}\left[U_{\mu,x}, U_{\mu,x+\hat{\nu}}, U_{\rho,x+\hat{\mu}+\hat{\nu}}, U_{\sigma,x+\hat{\mu}+\hat{\nu}+\hat{\rho}}\right] \right) \exp\left[-\left(\mathrm{Tr}(VE^\dagger) - \mathrm{Tr}(V^\dagger E)\right)\right]. \tag{C.1}$$

Here we represent the partition function as 4 link integrals with $U_{\mu,x}$, $U_{\nu,x+\hat{\mu}}$, $U_{\rho,x+\hat{\mu}+\hat{\nu}}$, $U_{\sigma,x+\hat{\mu}+\hat{\nu}+\hat{\rho}}$. V and E in Eq. (C.1) are the matrices which include components corresponding to 1-, 2-, 3-, and 4-link terms. The components of V and E consist of link variables and fermion fields respectively. The concrete forms of the V and E for this case are given by

$$V^{ab}_{\alpha\beta} = \mathrm{diag}\left(V^{ab}_1, V^{ab}_2, \cdots, V^{ab}_{11}\right) \ , \tag{C.2}$$

with

$$V_1 = \mathrm{diag}\left(U_{\mu,x}\right) \ , \tag{C.3}$$
$$V_2 = \mathrm{diag}\left(U_{\mu,x}U_{\nu,x+\hat{\mu}}U_{\rho,x+\hat{\mu}+\hat{\nu}}U_{\sigma,x+\hat{\mu}+\hat{\nu}+\hat{\rho}}\right) \ , \tag{C.4}$$
$$V_3 = \mathrm{diag}\left(U^{\dagger}_{\mu,x}U_{\nu,x}U_{\rho,x+\hat{\nu}}U_{\sigma,x+\hat{\nu}+\hat{\rho}}\right) \ , \tag{C.5}$$
$$V_4 = \mathrm{diag}\left(U_{\mu,x+\hat{\nu}}U^{\dagger}_{\nu,x+\hat{\mu}}U_{\rho,x+\hat{\mu}}U_{\sigma,x+\hat{\mu}+\hat{\rho}}\right) \ , \tag{C.6}$$
$$V_5 = \mathrm{diag}\left(U_{\mu,x+\hat{\rho}}U_{\nu,x+\hat{\mu}+\hat{\rho}}U^{\dagger}_{\rho,x+\hat{\mu}+\hat{\nu}}U_{\sigma,x+\hat{\mu}+\hat{\nu}}\right) \ , \tag{C.7}$$
$$V_6 = \mathrm{diag}\left(U_{\mu,x+\hat{\sigma}}U_{\nu,x+\hat{\mu}+\hat{\sigma}}U_{\rho,x+\hat{\mu}+\hat{\nu}+\hat{\sigma}}U^{\dagger}_{\sigma,x+\hat{\mu}+\hat{\nu}+\hat{\rho}}\right) \ , \tag{C.8}$$
$$V_7 = \mathrm{diag}\left(U_{\mu,x+\hat{\rho}+\hat{\sigma}}U_{\nu,x+\hat{\mu}+\hat{\rho}+\hat{\sigma}}U^{\dagger}_{\rho,x+\hat{\mu}+\hat{\nu}+\hat{\sigma}}U^{\dagger}_{\sigma,x+\hat{\mu}+\hat{\nu}}\right) \ , \tag{C.9}$$
$$V_8 = \mathrm{diag}\left(U_{\mu,x+\hat{\nu}+\hat{\sigma}}U^{\dagger}_{\nu,x+\hat{\mu}+\hat{\sigma}}U_{\rho,x+\hat{\mu}+\hat{\sigma}}U^{\dagger}_{\sigma,x+\hat{\mu}+\hat{\rho}}\right) \ , \tag{C.10}$$
$$V_9 = \mathrm{diag}\left(U_{\mu,x+\hat{\nu}+\hat{\rho}}U^{\dagger}_{\nu,x+\hat{\mu}+\hat{\rho}}U^{\dagger}_{\rho,x+\hat{\mu}}U_{\sigma,x+\hat{\mu}}\right) \ , \tag{C.11}$$
$$V_{10} = \mathrm{diag}\left(U^{\dagger}_{\mu,x+\hat{\nu}}U^{\dagger}_{\nu,x}U_{\rho,x}U_{\sigma,x+\hat{\rho}}\right) \ , \tag{C.12}$$
$$V_{11} = \mathrm{diag}\left(U_{\mu,x+\hat{\nu}+\hat{\sigma}}U^{\dagger}_{\nu,x+\hat{\mu}+\hat{\rho}}U_{\rho,x+\hat{\mu}+\hat{\rho}}U^{\dagger}_{\sigma,x+\hat{\mu}+\hat{\rho}}\right) \ . \tag{C.13}$$

$$E^{ab}_{\alpha\beta} = \mathrm{diag}\left(E^{ab}_1, E^{ab}_2, \cdots, E^{ab}_{11}\right) \ , \tag{C.14}$$

and

$$E_1 = \mathrm{diag}\left(D_{1,\mu}\right) \ , \tag{C.15}$$
$$E_i = \mathrm{diag}\left(D_{i,\mu\nu\rho\sigma}\right), \ (i = 2, 3, \cdots, 11) \ , \tag{C.16}$$

where we define the operator D as the fermion bilinears,

$$\left(D^{\dagger}_{1,\mu}\right)^{ab} = \frac{1}{2}\eta_{\mu,x}\bar{\chi}^{a}_{x}\chi^{b}_{x+\hat{\mu}} \ , \quad (D_{1,\mu})^{ab} = \frac{1}{2}\eta_{\mu,x}\bar{\chi}^{a}_{x+\hat{\mu}}\chi^{b}_{x} \ , \tag{C.17}$$

$$\left(D^{\dagger}_{2,\mu\nu\rho\sigma}\right)^{ab} = -k\bar{\chi}^{a}_{x}\chi^{b}_{x+\hat{\mu}+\hat{\nu}+\hat{\rho}+\hat{\sigma}} \ , \quad (D_{2,\mu\nu})^{ab} = k\bar{\chi}^{a}_{x+\hat{\mu}+\hat{\nu}+\hat{\rho}+\hat{\sigma}}\chi^{b}_{x} \ , \tag{C.18}$$

$$\left(D^{\dagger}_{3,\mu\nu\rho\sigma}\right)^{ab} = -k_{\mu}\bar{\chi}^{a}_{x+\hat{\mu}}\chi^{b}_{x+\hat{\nu}+\hat{\rho}+\hat{\sigma}} \ , \quad (D_{3,\mu\nu})^{ab} = k_{\mu}\bar{\chi}^{a}_{x+\hat{\nu}+\hat{\rho}+\hat{\sigma}}\chi^{b}_{x+\hat{\mu}} \ , \tag{C.19}$$

$$\left(D^{\dagger}_{4,\mu\nu\rho\sigma}\right)^{ab} = -k_{\nu}\bar{\chi}^{a}_{x+\hat{\nu}}\chi^{b}_{x+\hat{\mu}+\hat{\rho}+\hat{\sigma}} \ , \quad (D_{4,\mu\nu})^{ab} = k_{\nu}\bar{\chi}^{a}_{x+\hat{\mu}+\hat{\rho}+\hat{\sigma}}\chi^{b}_{x+\hat{\nu}} \ , \tag{C.20}$$

$$\left(D^{\dagger}_{5,\mu\nu\rho\sigma}\right)^{ab} = -k_{\rho}\bar{\chi}^{a}_{x+\hat{\rho}}\chi^{b}_{x+\hat{\mu}+\hat{\nu}+\hat{\sigma}} \ , \quad (D_{5,\mu\nu})^{ab} = k_{\rho}\bar{\chi}^{a}_{x+\hat{\mu}+\hat{\nu}+\hat{\sigma}}\chi^{b}_{x+\hat{\rho}} \ , \tag{C.21}$$

$$\left(D^{\dagger}_{6,\mu\nu\rho\sigma}\right)^{ab} = -k_{\sigma}\bar{\chi}^{a}_{x+\hat{\sigma}}\chi^{b}_{x+\hat{\mu}+\hat{\nu}+\hat{\rho}} \ , \quad (D_{6,\mu\nu})^{ab} = k_{\sigma}\bar{\chi}^{a}_{x+\hat{\mu}+\hat{\nu}+\hat{\rho}}\chi^{b}_{x+\hat{\sigma}} \ , \tag{C.22}$$

$$\left(D^{\dagger}_{7,\mu\nu\rho\sigma}\right)^{ab} = -k_{\rho+\sigma}\bar{\chi}^{a}_{x+\hat{\rho}+\hat{\sigma}}\chi^{b}_{x+\hat{\mu}+\hat{\nu}} \ , \quad (D_{7,\mu\nu})^{ab} = k_{\rho+\sigma}\bar{\chi}^{a}_{x+\hat{\mu}+\hat{\nu}}\chi^{b}_{x+\hat{\rho}+\hat{\sigma}} \ , \tag{C.23}$$

$$\left(D^{\dagger}_{8,\mu\nu\rho\sigma}\right)^{ab} = -k_{\hat{\nu}+\hat{\sigma}}\bar{\chi}^{a}_{x+\hat{\nu}+\hat{\sigma}}\chi^{b}_{x+\hat{\mu}+\hat{\rho}} \ , \quad (D_{8,\mu\nu})^{ab} = k_{\hat{\nu}+\hat{\sigma}}\bar{\chi}^{a}_{x+\hat{\mu}+\hat{\rho}}\chi^{b}_{x+\hat{\nu}+\hat{\sigma}} \ , \tag{C.24}$$

$$\left(D^{\dagger}_{9,\mu\nu\rho\sigma}\right)^{ab} = -k_{\hat{\nu}+\hat{\rho}}\bar{\chi}^{a}_{x+\hat{\nu}+\hat{\rho}}\chi^{b}_{x+\hat{\mu}+\hat{\sigma}} \ , \quad (D_{9,\mu\nu})^{ab} = k_{\hat{\nu}+\hat{\rho}}\bar{\chi}^{a}_{x+\hat{\mu}+\hat{\sigma}}\chi^{b}_{x+\hat{\nu}+\hat{\rho}} \ , \tag{C.25}$$

$$\left(D^{\dagger}_{10,\mu\nu\rho\sigma}\right)^{ab} = -k_{\hat{\mu}+\hat{\nu}}\bar{\chi}^{a}_{x+\hat{\mu}+\hat{\nu}}\chi^{b}_{x+\hat{\rho}+\hat{\sigma}} \ , \quad (D_{10,\mu\nu})^{ab} = k_{\hat{\mu}+\hat{\nu}}\bar{\chi}^{a}_{x+\hat{\rho}+\hat{\sigma}}\chi^{b}_{x+\hat{\mu}+\hat{\nu}} \ , \tag{C.26}$$

$$\left(D^{\dagger}_{11,\mu\nu\rho\sigma}\right)^{ab} = -k_{\hat{\nu}+\hat{\sigma}}\bar{\chi}^{a}_{x+\hat{\nu}+\hat{\sigma}}\chi^{b}_{x+\hat{\mu}+\hat{\rho}} \ , \quad (D_{11,\mu\nu})^{ab} = k_{\hat{\nu}+\hat{\sigma}}\bar{\chi}^{a}_{x+\hat{\mu}+\hat{\rho}}\chi^{b}_{x+\hat{\nu}+\hat{\sigma}} \ . \tag{C.27}$$

Note that $k = r\left(\epsilon\eta_5\right)_x/(4!\cdot 16), k_\mu = r\left(\epsilon\eta_5\right)_{x+\mu}/(4!\cdot 16)$, and $k_{\mu+\nu} = r\left(\epsilon\eta_5\right)_{x+\mu+\nu}/(4!\cdot 16)$. Here V_1 and E_1 are 4 diagonal matrices while V_i and E_i $(i = 2, 3, \cdots, 11)$ are 24×24 diagonal matrices. Here we note the situation of the cancellation between the diagrams crossing the different blocks is basically the same as the case for the Hoelbling type although there is difference between the 2-link and 4-link hoppings. We can derive W as a function of Λ by using the Schwinger-Dyson equation in a similar way to the Hoelbling type. Λ is

$$\Lambda_x = \frac{1}{16}\Bigg[\sum_{\mu}\mathcal{M}_x\mathcal{M}_{x+\hat{\mu}} + \frac{1}{3}\sum_{\mu\neq\nu}\mathcal{M}_{x+\hat{\mu}}\mathcal{M}_{x+\hat{\mu}+\hat{\nu}} \tag{C.28}$$

$$+ \frac{1}{6}\sum_{\mu\neq\nu\neq\rho}\mathcal{M}_{x+\hat{\mu}+\hat{\nu}}\mathcal{M}_{x+\hat{\mu}+\hat{\nu}+\hat{\rho}} + \frac{1}{6}\sum_{\mu\neq\nu\neq\rho\neq\sigma}\mathcal{M}_{x+\hat{\mu}+\hat{\nu}+\hat{\rho}}\mathcal{M}_{x+\hat{\mu}+\hat{\nu}+\hat{\rho}+\hat{\sigma}}\Bigg] \tag{C.29}$$

$$- \left(\frac{r}{4!\cdot 16}\right)^2\sum_{\mu\neq\nu\neq\rho\neq\sigma}\left(2\mathcal{M}_x\mathcal{M}_{x+\hat{\mu}+\hat{\nu}+\hat{\rho}+\hat{\sigma}} + 4\mathcal{M}_{x+\hat{\mu}}\mathcal{M}_{x+\hat{\nu}+\hat{\rho}+\hat{\sigma}} + 2\mathcal{M}_{x+\hat{\mu}+\hat{\nu}}\mathcal{M}_{x+\hat{\rho}+\hat{\sigma}}\right) \ . \tag{C.30}$$

Bibliography

[1] K. G. Wilson, Phys. Rev. D **10**, 2445 (1974).

[2] M. Creutz, Phys. Rev. D **21**, 2308 (1980).

[3] L. H. Karsten and J. Smit, Nucl. Phys. B **183**, 103 (1981).

[4] H. B. Nielsen and M. Ninomiya, Nucl. Phys. B **185**, 20 (1981); Nucl. Phys. B **193** 173 (1981); Phys. Lett. B **105** 219 (1981).

[5] J. W. Milnor, "Topology from the differential viewpoint", The University Press of Virginia, Charlottesville, (1965).

[6] K. G. Wilson, "Quarks and Strings on a Lattice", MIT Press, Cambridge, (1975).

[7] K. G. Wilson, "Quarks and Strings on a Lattice", Plenum Press, New York, (1977).

[8] P. H. Ginsparg and K. G. Wilson, Phys. Rev. D **25**, 2649 (1982).

[9] N. Neuberger, Phys. Lett. B **427**, 353 (1998) [arXiv:hep-lat/9801031].

[10] D. B. Kaplan, Phys. Lett. B **288**, 342 (1992).

[11] Y. Shamir, Nucl. Phys. B **406**, 90 (1993) [arXiv:hep-lat/9303005].

[12] V. Furman and Y. Shamir, Nucl. Phys. B **439**, 54 (1995) [arXiv:hep-lat/9405004].

[13] J. B. Kogut and L. Susskind, Phys. Rev. D **11**, 395 (1975).

[14] L. Susskind, Phys. Rev. D **16**, 3031 (1977).

[15] H. S. Sharatchandra, H. J. Thun and P. Weisz, Nucl. Phys. B **192**, 205 (1981).

[16] L. H. Karsten, Phys. Lett. B **104**, 315 (1981).

[17] F. Wilczek, Phys. Rev. Lett. **59**, 2397 (1987).

[18] M. Creutz, JHEP 0804, 017 (2008) [arXiv:0712.1201];

[19] A. Boriçi, Phys. Rev. D **78**, 074504 (2008) [arXiv:0712.4401].

[20] M. Creutz and T. Misumi, Phys. Rev. D **82**, 074502 (2010) [arXiv:1007.3328].

[21] P. F. Bedaque, M. I. Buchoff, B. C. Tiburzi and A. Walker-Loud, Phys. Lett. B **662**, 449 (2008) [arXiv:0801.3361].

[22] P. F. Bedaque, M. I. Buchoff, B. C. Tiburzi and A. Walker-Loud, Phys. Rev. D **78**, 017502 (2008) [arXiv:0804.1145].

[23] K. Cichy, J. Gonzalez Lopez, K. Jansen, A. Kujawa and A. Shindler, Nucl. Phys. B **800**, 94 (2008) [arXiv:0802.3637].

[24] S. Capitani, J. Weber, H. Wittig, Phys. Lett. B **681**, 105 (2009) [arXiv:0907.2825].

[25] T. Kimura and T. Misumi, Prog. Theor. Phys. **124**, 415 (2010) [arXiv:0907.1371];

[26] T. Kimura and T. Misumi, Prog. Theor. Phys. **123**, 63 (2010) [arXiv:0907.3774].

[27] S. Capitani, M. Creutz, J. Weber, H. Wittig, JHEP 1009, 027 (2010) [arXiv:1006.2009].

[28] T. Misumi, M. Creutz and T. Kimura, PoS Lattice2010 (2010) 260 [arXiv:1010.3713].

[29] M. Creutz, T. Kimura and T. Misumi, JHEP 1012, 041 (2010) [arXiv:1011.0761].

[30] D. H. Adams, Phys. Rev. Lett. **104**, 141602 (2010) [arXiv:0912.2850].

[31] D. H. Adams, Phys. Lett. B **699**, 394 (2011) [arXiv:1008.2833].

[32] C. Hoelbling, Phys. Lett. B **696**, 422 (2010) [arXiv:1009.5362].

[33] M. Creutz, T. Kimura and T. Misumi, Phys. Rev. D **83**, 094506 (2011) [arXiv:1101.4239].

[34] T. Misumi, M. Creutz, T. Kimura, T. Z Nakano and A. Ohnishi, PoS Lattice2011 (2011) 108 [arXiv:1110.1231].

[35] S. Aoki, Phys. Rev. D **30**, 2653 (1984).

[36] S. Aoki, Phys. Lett. B **190**, 140 (1987).

[37] S. Aoki and A. Gochshh, Phys. Lett. B **190**, 140 (1987).

[38] S. Aoki and A. Gochshh, Phys. Lett. B **243**, 409 (1990).

[39] S. Aoki, Phys. Rev. D **33**, 2377 (1986).

[40] S. Aoki, Phys. Rev. D **34**, 3170 (1986).

[41] S. Aoki, Phys. Rev. Lett. **57** 3136 (1986).

[42] S. Aoki, Nucl. Phys. B **314**, 79 (1989).

[43] S. Aoki and K. Higashijima, Prog. Theor. Phys. **76**, 521 (1986).

[44] M. Creutz, (1996) [arXiv:hep-lat/9608024].

[45] S. Sharpe and R. Singleton. Jr, Phys. Rev. D **58**, 074501 (1998). [arXiv:hep-lat/9804028].

[46] S. Aoki, A. Uehara and T. Umemura, Phys. Rev. Lett. **76**, 873 (1996).

[47] S. Aoki, T. Kaneda and A. Ukawa, Phys. Rev. D **56**, 1808 (1997).

[48] S. Aoki, Prog. Theor. Phys. Supplement **122**, 179 (1999).

[49] P. de Forcrand, A. Kurkela and M. Panero, PoS Lattice2010 (2011) 080, [arXiv:1102.1000].

[50] B. Svetitsky, S. D. Drell, H. R Quinn and M. Weinstein, Phys. Rev. D **22**, 490 (1980).

[51] J. M. Blairon, B. Brout, F. Englert and J. Greensite, Nucl. Phys. B **180**, 439 (1981).

[52] H. Kluberg-Stern, A. Morel, O. Napoly and B. Petersson, Nucl. Phys. B **190**, 504 (1981).

[53] H. Kluberg-Stern, A. Morel, O. Napoly and B. Petersson, Nucl. Phys. B **220**, 447 (1983).

[54] F. Gliozzi, Nucl. Phys. B **204**, 419 (1982).

[55] H. Kluberg-Stern, A. Morel and B. Petersson, Nucl. Phys. B . 215, 527 (1983).

[56] T. Jolicoeur, H. Kluberg-Stern, M. Lev, A. Morel and B. Petersson, Nucl. Phys. B **235**, 455 (1984).

[57] T. Kimura, S. Komatsu, T. Misumi, T. Noumi, S. Torii and S. Aoki, JHEP **01 (2012)** 048 [arXiv:1111.0402].

[58] N. Kawamoto and J. Smit, Nucl. Phys. B**192**, 100 (1981).

[59] M. F. L. Golterman and J. Smit, Nucl. Phys. B **245**, 61 (1984).

[60] C. van den Doel and J. Smit, Nucl. Phys. B **228**, 122 (1983).

[61] M. F. L. Golterman and J. Smit, Nucl. Phys. B **255**, 328 (1985).

[62] M. F. L. Golterman, Nucl. Phys. B **273**, 663 (1986).

[63] G. W. Kilcup and S. Sharpe, Nucl. Phys. B **283**, 493 (1987).

[64] CP-PACS collaboration, S. Aoki et.al., Phys. Rev. Lett. **84**, 238 (2000).

[65] CP-PACS collaboration, S. Aoki et.al., Phys. Rev. D **66**, 077501 (2002).

[66] T. Appelquist, G. T. Fleming and E. T. Neil, Phys. Rev. Lett. **100**, 171607 (2008).

[67] T. Appelquist, G. T. Fleming, M. F. Lin, E. T. Neil and D. A. Schaich, Phys. Rev. D **84**, 054501 (2011) [arXiv:1106.2148].

[68] A. Deuzeman, M. P. Lombardo and E. Pallante, Phys. Rev. D **82**, 074503 (2010) [arXiv:0904.4662].

[69] E. Bilgici, A. Flachi, E. Itou, M. Kurachi, C. -J D. Lin, H. Matsufuru, H. Ohki and T. Onogi *et al.*, Phys. Rev. D **80**, 034507 (2009) [arXiv:0902.3768];

[70] T. Aoyama, H. Ikeda, E. Itou, M. Kurachi, C. -J. D. Lin, H. Matsufuru, K. Ogawa and H. Ohki *et al.*, [arXiv:1109.5806].

[71] A. Hasenfratz, Phys. Rev. D **82**, 014506 (2010) [arXiv:1004.1004].

[72] M. Hayakawa, K. -I. Ishikawa, Y. Osaki, S. Takeda, S. Uno and N. Yamada, Phys. Rev. D **83**, 074509 (2011) [arXiv:1011.2577].

[73] T. DeGrand, [arXiv:1109.1237].

[74] L. Del Debbio, [arXiv:1102.4066].

[75] T. Kimura, M. Creutz and T. Misumi, PoS Lattice2011 (2011) [arXiv:1110.2482].

[76] P. de Forcrand, Aleksi Kurkela and Marco Panero, [arXiv:1102.1867].

[77] R. G. Edwards, U. M. Heller and R. Narayanan, Nucl. Phys. B **522**, 285 (1998) [arXiv:hep-lat/9801015].

[78] D. H. Adams, Annals Phys. **296** (2002) 131-151 [arXiv:hep-lat/9812003].

[79] D. H. Adams, J. Math. Phys. **42** (2001) 5522-5533 [arXiv:hep-lat/0009026].

[80] J. Smit and J. C. Vink, Nucl. Phys. B **286**, 485 (1987).

[81] J. Smit and J. C. Vink, Nucl. Phys. B **298**, 557 (1988).

[82] B. C. Tiburzi, Phys. Rev. D **82**, 034511 (2010) [arXiv:1006.0172].

[83] D. Chakrabarti, S. Hands and A. Rago, JHEP 0906, 060 (2009) [arXiv:0904.1310].

[84] M. Creutz, (2010) [arXiv:1007.5502].

[85] J. Smit and J. C. Vink, Nucl. Phys. B **303**, 36 (1988); Phys. Lett. B **194**, 433 (1987); J.C. Vink, Phys. Lett. B **210**, 211 (1988); B **212**, 483 (1988).

[86] T. Izubuchi, J. Noaki and A. Ukawa, Phys. Rev. D **58**, 114507 (1998) [arXiv:hep-lat/9805019].

[87] T. Izubuchi and K. Nagai, Phys. Rev. D**61**, 094501 (2000) [arXiv:hep-lat/9906017].

[88] JLQCD collaboration: H. Fukaya, et.al., Phys. Rev. D **74**, 094505 (2006) [arXiv:hep-lat/0702003].

[89] JLQCD collaboration: H. Fukaya, et.al., Phys. Rev. Lett **98**, 172001 (2007) [arXiv:hep-lat/0702003].

[90] M. Creutz, PoS Lattice2010 (2010) 078 [arXiv:1009.3154].

[91] D. J. Gross and A. Neveu, Phys. Rev. D **10**, 3235 (1974).

[92] T. Eguchi and R. Nakayama, Phys. Lett. B **126**, 89 (1983).

[93] B. Leder, Ph.D. Thesis, [arXiv:0707.1939].

[94] T. Korzec, Ph.D. Thesis, http://edoc.hu-berlin.de/docviews/abstract.php?id=28045 .

[95] B. Leder, JHEP 0804, 044 (2008) [arXiv:0711.1072].

[96] M. Creutz, Phys. Rev. Lett. **92**, 201601 (2004) [arXiv:hep-lat/0312018].

[97] M. Creutz, Phys. Rev. Lett. **92**, 162003 (2004) [arXiv:hep-ph/0312225].

[98] N. Kawamoto, Nucl. Phys. B **190**, 617 (1981).

[99] J. Hoek, N. Kawamoto and J. Smit, Nucl. Phys. B **199**, 495 (1982).

[100] I. Ichinose, Phys. Lett. B **135**, 148 (1984).

[101] I. Ichinose, Nucl. Phys. B **249**, 715 (1985).

[102] V. Azcoiti, G. Di Carlo, A. Vaquero, Phys. Rev. D **79**, 014509 (2009) [arXiv:0809.2972].

[103] S. R. Sharpe, Phys. Rev. D **79**, 054503 (2009) [arXiv:0811.0409].

[104] C. Vaffa and E. Witten, Phys. Rev. Lett **53**, 535 (1984).